KIT SCIENTIFIC REPORTS 7612

Modelling of PFC life-time in tokamak fusion reactor

Y. Igitkhanov, B. Bazylev, I. Landman

KIT Scientific Publishing

Y. Igitkhanov, B. Bazylev, I. Landman

Modelling of PFC life-time in tokamak fusion reactor

Karlsruhe Institute of Technology
KIT SCIENTIFIC REPORTS 7612

Modelling of PFC life-time in tokamak fusion reactor

by
Y. Igitkhanov
B. Bazylev
I. Landman

KIT Scientific Publishing

Report-Nr. KIT-SR 7612

Impressum

Karlsruher Institut für Technologie (KIT)
KIT Scientific Publishing
Straße am Forum 2
D-76131 Karlsruhe
www.ksp.kit.edu

KIT – Universität des Landes Baden-Württemberg und nationales
Forschungszentrum in der Helmholtz-Gemeinschaft

KIT Scientific Publishing 2012
Print on Demand

Forschungszentrum Karlsruhe
In der Helmholtz-Gemeinschaft
Wissenschaftliche Berichte

Modelling of PFC life-time in tokamak fusion reactor

Yu. Igitkhanov, B. Bazylev and I. Landman

Karlsruhe Institute of Technology

Institute for Pulsed Power and Microwave Technology,
Programm Fusion
Post Box 3640, 76021 Karlsruhe, Germany

PREPRINT

No: /IHM

Januar 2012

Table of content

Introduction		3
I.	Calculation of runaway electrons stopping power in ITER	5
II.	On the generation of Runaway Electrons during Massive Gas Injection	10
III.	CFC and W Monoblock Blanket Concepts for Fusion Reactor	15
IV.	The PFC erosion in DEMO due to runaway electrons	20
V.	Effect of Off-Normal Events on Reactor First Wall	25
VI.	Plasma facing material lifetime in DEMO reactor	30
VII.	Sputtering yield for the PF components under reactor plasma edge conditions	39
VIII.	Numerical Simulation of Tungsten Melt Layer Erosion caused by JxB force at TEXTOR	46
IX.	Erosion simulation of FW Be armour after ITER transient heat loads and RE action	50
X.	Modeling of Runaway Electron Beams for JET and ITER	55
XI.	Resume	60
Appendix I	Calculation of sputtering yield	63
Appendix II	Comparison of Water and Helium collant efficiency	65

Introduction

One of the main challenges for fusion reactors is the compatibility between reactor-grade plasma and the materials facing the plasma. The ITER design guidance is to apply a beryllium layer onto the plasma-facing chamber surface. For the DEMO condition, the Be or carbon layers will not be suitable due to radiation damage of the material or high physical and chemical sputtering rates and potential large retention of tritium. We are analyzing here two designs of the first wall (FW) based on the bear materials (stainless steel or tungsten) and on materials, covered with some scarifying (protecting) layers. The thermal designs of Demo blanket dictated by two heat sources: a volumetric heat associated to the neutron wall load (~2.5 MW/m^2 in DEMO according to usual specifications) and surface heat coming directly from the plasma in steady-state operation ~0.5MW/m^2. While the volumetric heating is not particularly demanding for the FW design (but the neutrons should be taken into account for the irradiation damage), the surface heating dictated the lay-out in term of allowable temperatures and stresses. From the plasma side it is particularly demanding to keep the bulk plasma contamination below the critical level. The possible damage of the FW materials due to the plasma erosion/sputtering is estimated. We found that the bare materials cannot be used under DEMO conditions. The plasma-facing surface has to be protected with a layer of another material or a sacrificial layer of the same material. In the presented here, design the oxide dispersion strengthened EUROFER steel is considered. The thickness of the wall is 3mm before the Helium cooling channels with surface temperatures already around 550°C, which is the limit for EUROFER steel. Effect of transients (VDE, ELMs and runaways) on the FW erosion is discussed further.

The performance of materials in fusion reactor DEMO has long been recognized as fundamental issue affecting the ultimate technological and economic feasibility of fusion power. Many factors influence the choice of a functional and structural material in a fusion reactor. Component lifetime in the steady-state is limited by three effects: radiation damage, disruptions, and sputtering erosion. Our design strategy is to determine the structure and coating thicknesses, which maximize component lifetime against all life limitations. At present, the stainless steel modifications (EUROFER) remain the primary choice for a structural material because of the large existing data-base and industrial capability. Tungsten alloys are the primary materials for the plasma-facing surface in DEMO. Although W/EUROFER bound is compatible with high neutron fluencies to minimize the necessary replacement of the in-vessel components and is “low-activation” type, the loss of creep strength at relatively low temperatures could be the main drawback of EUROFER as a structural material. That is why the realization of the FW sandwich-type blanket with W as a armour material and EUROFER as a structural material must be investigated as a most promising combination. Moreover, the reinforcement by SiC fibers or oxide dispersion strengthened (ODS) steels may potentially improve the high temperature creep resistance of EUROFER steel. Analysis of another FW blanket configuration made from W alloy mono-block with imbedded cooling water tube is also After calculating disruption damage (vaporization, melting) for candidate materials we present the lifetime analysis for different structures suitable for DEMO reactor.

Here we investigate thermal resistance and erosion of PFC materials against plasma energy and particles affect under reactor plasma conditions. Two codes employed for calculation of energy deposition into materials, corresponding erosion (melting and evaporation and melting). Benchmarking with exsisting experiments servs for improving physics in the codes and increases the credibility of results in predictive calculations for ITER and DEMO reactor conditions.

Below we present the collection of papers submitted or published during 2011, which mostly where also reported on different conferences during the 2010-2011 years. We begin in chapter I with the discusson of the penetration of relativistic runaway electrons into the FW blanket layer and in chapter II will discusse the generation of runaway electrons during massive gas injection. In chapter III two concepts of monoblock blanket moduls, made from CFC and W are discussed. The PFC erosion in DEMO due to runaway electrons is considered in chapter IV. Effect of off-normal events on reactor first wall is described in chapter V. Chapter VI contains essesments of the plasma facing material lifetime in DEMO reactor. Sputtering yields for the PF components under reactor plasma-edge conditions are discussed in chapter VII. Chapter VIII contains the results of numerical

simulation of tungsten melt layer erosion caused by JxB force at TEXTOR. Finaly, we present some conclusive remarks.

I. Calculation of runaway electrons stopping power in ITER

Yu. Igitkhanov, B. Bazylev, I. Landman Journal of Nuclear Materials 415 (2011) S845–S848, presented in PSI-19, san Diego 2010,

The energy loss rate of runaway electrons (RE) was analysed for ITER plasma facing components materials (Be and W). The stopping power, the energy deposition profiles, and the material erosion are estimated by using the codes MEMOS and ENDEP. The latter has been updated by including the effect of the target's polarizability. Our calculations show that this effect is significant for high RE energies and low Z materials such as Be. We also find that the conversion of the RE's magnetic energy into heat can explain the temperature rise on dump plate in JET. In the case of ITER, the calculated heat deposition due to RE is almost two times the melting threshold energy of Be but well below that of W.

1.Introduction

The runaway electrons (RE) in ITER will be generated by the dominant avalanche phenomenon and will carry a magnetic energy significantly higher than their kinetic energy, in contrast to present experiments [1]. In order to optimize the plasma facing components (PFC) in the ITER design, it is essential to predict the power deposition and the lifetime of the PFC materials [2,3]. In this paper, we analyse the energy loss rate of relativistic ITER RE by calculating their stopping power (SP) and the energy deposition (ED) in Be and W targets. We consider for that purpose three aspects: (1) the secondary electron generation (SEG) in solid media, (2) the effect of the magnetic field B on the beam's incidence angles α, and (3) a electron-density effect that accounts for the polarizability of the media and hence reduces the energy deposition length. We estimate also the RE heat deposition on JET's dump limiter. Numerical simulations are performed with the Monte Carlo Energy Deposition code ENDEP together with the fluid Melt Motion on Surface code MEMOS [4] to calculate (1) the energy deposition of the RE into Be and W targets and (2) the level of erosion caused by the RE, respectively. We have upgraded the ENDEP code so that it includes the effects mentioned above. The simulations were performed assuming a Gaussian distribution of RE in momentum space with an average energy E_d. Variations in a are caused by drifts and thus depend on the magnetic pitch angle or, alternatively, on the energy E_{tr} that derives from the component of the RE velocity that is perpendicular to B. For instance, while α is only~1° for $E_{tr}/E = 0$ (where E is the total kinetic energy), it increases up to 20 for E_{tr}/E~0.5% [3,4].

We first assess the kinetic and magnetic energies stored in ITER RE, then analyse the density effect correction on the energy deposition of the RE in Be and W targets, and finally discuss the results of MEMOS and ENDEP calculations.

2. Kinetic and magnetic energy stored in the RE

In ITER one expects E_d=12.5 MeV [5]. Therefore, the relativistic scaling factor, $\gamma \equiv (1-\beta^2)^{1/2} \equiv E_d/mc^2$, is ~24.5 and β = 0.9992, where the average velocity of the RE is β c and m is the rest mass of the electron. Since it is expected that at most 70% of the plasma current is carried by RE [1], I_{RE}~10.5 MA, their kinetic energy Wkin can be estimated by knowing the density of RE, which can estimated as $n_{RE}=I_{RE}/ec\beta$ S~1.2 10^{16} m^{-3}, for a plasma surface area S ~21.9 m^2. The total number of RE in the entire plasma volume is then $N_{RE}=V\ n_{RE}$~10^{19}, where V~837 m^3; therefore, $W_{kin}=N_{RE}$ (E_d-mc^2)~20 MJ. The magnetic energy carried by a RE beam can be estimated as W_{REmag}~W_{mag} $(I_{RE}/I_{pl})^2$ and, alternatively, from the Alfven current I_A = 0:017$\beta\gamma$~0:415 MA as W_{REmag}~W_{kin} (I_{RE}/I_A) [6]. Thus, in ITER, WREmag can be up to 25 times higher thanW_{kin}, i.e., W_{REmag}=0.5 GJ. In the case of JET, E_d~10 MeV and I_{RE}~1.0 MA [7]. Consequently is, I_A~0.33 MA and W_{REmag}~3W_{kin}. In general, losses in Wkin eventually trigger the deposition of W_{mag} into the first wall (FW) owing to the dissipation of induced currents in the structure. The stemming dissipation of W_{kin} is due to collisions of the RE with either the PFC or impurities in the plasma.

3. Heat loads to the first wall due to the RE impact.

It has been shown in JET that a localized impact of the RE onto the upper dump plate leads to an increase of the surface temperature ΔT with an increase of the RE current I_{RE}[7]. The RE beam hits the plate where some portion μ of the incident energy converts into heat. The energy Q released within some thin layer Δ in the surface area *S* during the time $\tau \leq \tau_{skin}$ can be written as:

$$Q = \frac{1}{S}\cdot\left(\frac{\tau\cdot\varepsilon}{e}\cdot I_{RE} + \frac{L\cdot I_{RE}^2}{2}\right) \propto \eta\cdot\frac{\tau}{S}\cdot R\cdot I_{eff}^2 \qquad (1)$$

where the first term is the kinetic energy, ε is the average RE energy and the second term is the magnetic energy and *L* is the total inductance. The RE beam deposition time τ ~ 0.2 ms >> $t_{skin} >> \tau_{skin} \sim 4\pi\Delta^2/c^2\rho$, where Δ~0.2–0.15mm is the penetration length, ρ ~ 1.2μΩ m for CFC target [7]. In this case, the magnetic flux penetrates the plate inducing an ohmic current that reinforces the dissipating RE current. Eventually, the magnetic energy of the RE beam becomes thermal, so that $I_{eff} \sim I_{RE}\ (L_i/2R)^{1/2}$ Here, the resistance of the CFC target is $R \sim 1.8\ 10^{-9}\ \Omega$ for the penetration length Δ ~0.2mm and $R \sim 1.3\ 10^{-9}\ \Omega$ for Δ ~0.15mm and the spot area S~0.03m^2 [7]. The energy deposition of RE into the CFC target was evaluated by the MEMOS code for RE with E_d ~*8-10*MeV, the deposition time τ ~ 0.2 ms ms and α ≈ 5°-20° [3]. The calculations show an almost linear dependence of surface temperature increase ΔT with an increase of heat energy *Q*:

$$Q_{MJ/m^2} \approx \left(\Delta T^{\circ}K - 34\right)/234 \qquad (2)$$

By substituting *Q* in (1), one gets the variation of surface temperature on the RE current:

$$\Delta T^{\circ}K \approx 34 + 234\cdot\eta\cdot R\cdot\frac{I_{eff}^2}{\Delta S} \qquad (3)$$

In **Fig. 1**, the solid curves show the deposition of the RE current energy into heat. They fit the experimental data (read scuares) fairly well both in shape and quantitatively, if the conversion efficiency η assumed ≤ 50 %.

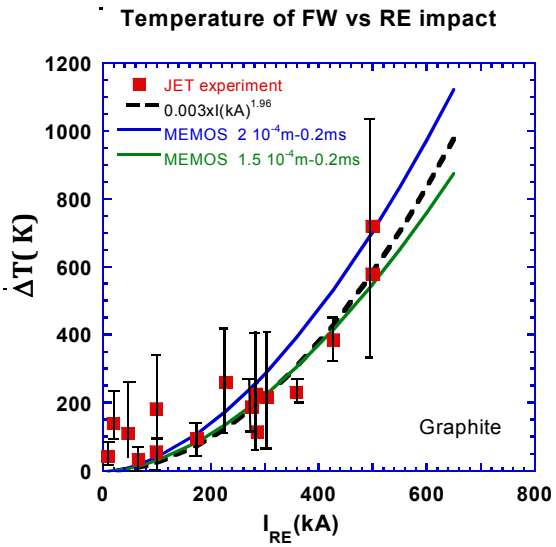

Fig.1 Surface temperature increase at the JET upper dump plate vs. the RE current increase measured in JET (red squares) [7]; the blue and green curves correspond to ~ 50% of the RE energy conversion into heat. Heat release on the plate due to RE impact calculated by MEMOS.

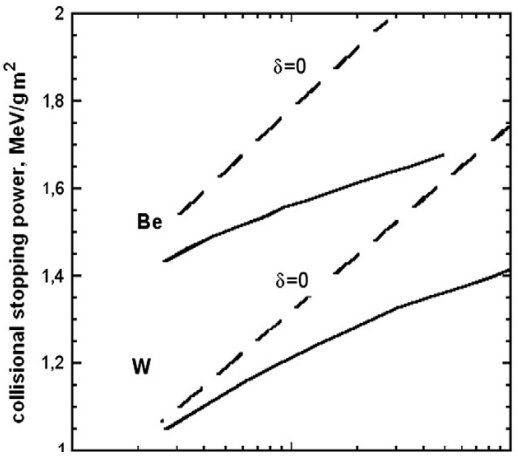

Fig.2 The SP of RE in Be and W in MW/g m^{-2}. The sraight curves show the values of mass-collisional SP calculated with the density effect correction.

The MEMOS calculation shows that for the CFC and at shallow incidence angle about half of the RE energy dissipates while the rest reflects back with particles and radiation. Hence, our assesmets

show that the magnetic energy, stored in the RE current can be converted into heat at the FW structure.

4. Collisional stopping power and the density effect correction.

The energy loss of RE passing through matter occurs mainly due to ionization and radiation and can be expressed in terms of the collisional and radiative SPs [8-10]. To assess the density effect on the energy loss we consider here only the collisional SP. For relativistic electrons the mass collisional SP defines the average energy, transferred from the incident RE electrons to bound atomic electrons [9]:

$$\left.\frac{1}{\rho}\frac{\partial E}{\partial s}\right|_{Coll} = \frac{A}{\beta^2}\left[B + 2\ln(\beta\gamma) + \ln\frac{mc^2}{2}(\gamma-1) + 1 - \beta^2 - \delta\right] \qquad (4)$$

$$A = 2\pi n r_e^2 mc^2/\rho, \qquad B = \ln(mc^2/I)$$

Here, s is the penetration depth normal to in the target, $E=(\gamma-1)mc^2$ is the kinetic energy and βc is the velocity of the runaways, Z is the atomic number and n is the density of the target, $I=9.4\,Z$ eV is the mean excitation energy of the target atoms [9], r_e is the classical radius of the electron $r_e = e^2/mc^2$. The coefficie nts A and B are listed in the **Table 1** for different target materials and the term δ describes the density effect correction, which decreases the SP owing to the polarizability of the target medium, which reduces the effectiveness of distant collisions.

Table 1

Material	Be	Graphite	Fe	W
A	0.0678	0.0765	0.0713	0.0615
B	18.8	18.3	16	13.9
C	-2.7	-2.82	-3.97	-5.33
a	0.26	0.318	0.088	0.214
m	3.38	3.15	3.47	2.93
x1	2	2	3	3
x0	0	0.04	0	0.21

This effect was inmplemented into the MEMOS code, following the prescriptions from [9]. The correction factor δ depends on $\beta\gamma$ and can be fitted as:

$$\delta(x) = \begin{cases} 4.606x - C, & x0 > x > x1 \\ 4.606x - C + a\cdot(x1 - x)^m, & x < x1 \end{cases} \qquad (5)$$

where x=log(βγ) and the constants $xo, x1, m, a$ are given in the Table I [9].

In **Fig.2** the mass collisional SP is calculated from equation (4) with and without density effect correction. The dashed curves give the values of the SP without taking into account the density effect. The density effect is more significant for high RE energies and low Z materials like Be, amounting to as much as 15% of the mass collisional SP at energies of 10 MeV (see **Fig.2**). In the case of high Z materials like W the density effect is smaller because electrons are more strongly bound and hence less effective in polarizing the medium. The ENDEP calculations of the SP with and without density effect correction show a somewhat smaller effect due to SEG and radiation losses, not accounted for in equation (4).

5. The results of ENDEP and MEMOS calculations for RE in ITER

The SP and scattering angle calculations were performed by the ENDEP code for impinging RE on sandwich type PFC structures, resembling the ITER FW. **Figs. 3a** and **3b** show the SP (both

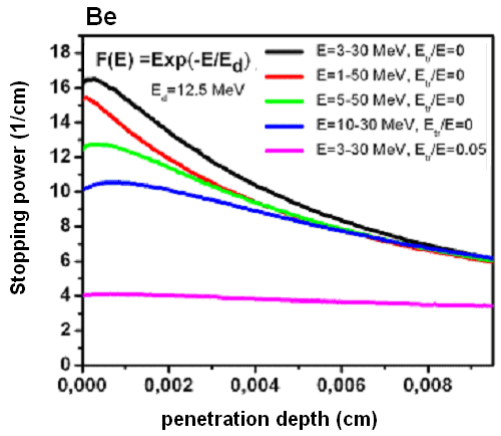

Fig.3a The SP for RE in Be plates shown as a function of the penetration depth. The incident electrons have a Gaussian distribution with $E_d=12.5eV$. The five incident energy ranges indicated with different colours. The RE beam strikes the plate along the magnetic field line at ~1° for E_{tr}=0 and at ~20°for E_{tr}/E~0.05.

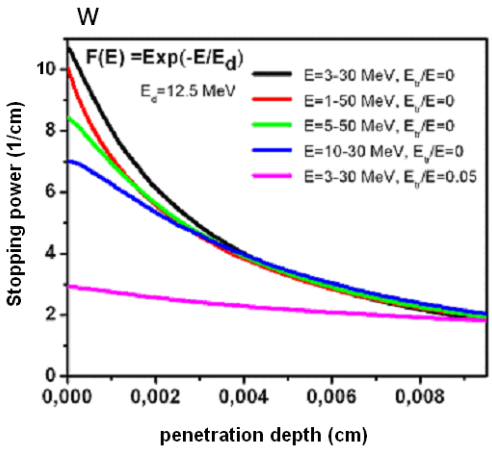

Fig.3b The SP for RE in W plates shown as a function of the penetration depth. The incident electrons have a Gaussian distribution with $E_d=12.5eV$. The five incident energy ranges indicated with different colours. The RE beam strikes the plate along the magnetic field line at ~1° for E_{tr}=0 and at ~20°for E_{tr}/E~0.05.

collisional and radiative) as a function of penetration depth normal to the material surface for Be and W, respectively. The RE strike the plate with α in the range of 1° to 20° (depending on E_{tr}) and $E_d=12.5$MeV. Five incident energy ranges have been chosen arbitrarily in our Monte Carlo computations (indicated with different colors). **Fig. 3a** shows that the SP is smallest for the highest energy RE and also for those with steepest incidence angle (α~20°). Note also that the SP in W is

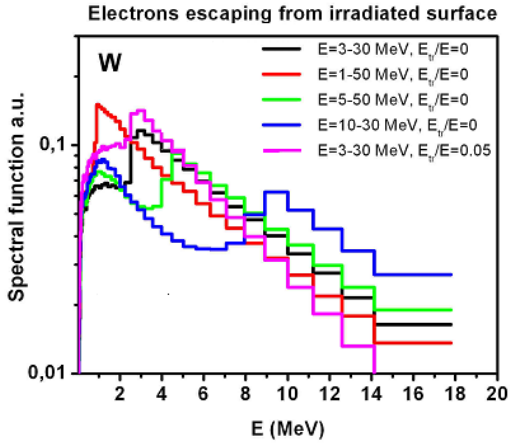

Fig.4 The distribution function of the back sattered electrons for a W plate, plotted for different energy ranges. The two peaks corresponding to primary and secondary electrons can be seen.

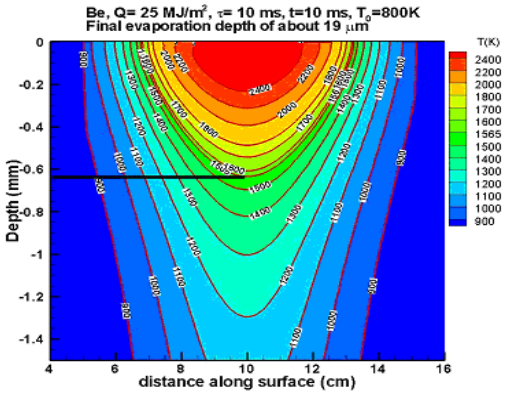

Fig.5 The temperature contours on a plane normal to the Be target that contains the RE incidence point; the RE beam exposition time is 10 ms at an energy of 25MJ/m^2. Almost a half of this energy is transferred to heat. The temperature on Be plate exceeds the melting temperature. The critical energy for Be surface melting is about 5MJ/m^2

larger than that in Be. Balance calculations at α~ 1° indicate that only half of RE energy is absorbed in Be while the rest is mainly reflected off by back-scattered electrons (~48%) and photons (~2%). The fraction of back-scattered electrons is ~77% of the incident number but accounts for primary and secondary electrons. In W, the fraction of absorbed energy is ~30% while the rest is reflected off by back-scattered electrons (~55%) and photons (~15%). In this case, ~82% of the incident number of electrons is back-scattered. For α ~20°, the ratio of absorbed energy reaches 80% in Be and 50% in W. We find an enhanced SEG in W and a strong increase in radiation production, which is one

order of magnitude larger than that in Be. In general, the fraction of back scattered electrons plus that of transmitted ones through the plate is different from 1 because of SEG. Calculations show that collisional SP dominates over radiative (mainly bremsstrahlung) SP and is almost independent of the kinetic energy for highly relativistic electrons [8]. The mean square inclination angle of RE undergoing the scattering in the material is very small. **Fig. 4** shows the distribution function of reflected back electrons for a W plate, plotted for different energy ranges. Two peaks, corresponding to primary and secondary electrons can be clearly seen. **Fig. 5** shows the temperature contours on the plane normal to the Be plate as a result of the RE beam impact (from the top) after 10 ms of exposure to 25MJ/m^2. About half of this energy, as it mentioned above, is converted into heat. The MEMOS calculation shows that the temperature on the Be plate T~ 2400 K exceeds the melting temperature (1560 K), whereas for the W plate the same RE power heats the plate surface up to T~2100 K and remains below the melting temperature (3695 K). It has been found, that the critical energy for surface melting is about 5MJ/m^2 for Be and~65MJ/m^2 for W.

6. Conclusions

1) The observed increase of temperature in a spot on the JET dump plate upon increasing the RE current can be explained by assuming that the magnetic energy of the RE converts into heat.
2) The density effect correction in the SP is significant for the higher RE energies and low Z materials like Be, amounting to as much as 15% of the mass collisional SP at energies of 10 MeV. In the case of high Z materials like W the density effect is smaller, because the electrons are more strongly bound and hence are less effective in polarizing the medium.
3) Calculations of the RE SP onto the ITER FW Be bulk armour predict a strong erosion. The threshold energy for Be melting is about 5MJ/m^2, whereas the RE heat deposition is expected to be almost twice as large.
4) Deposition of the RE does not melt W, since the threshold energy for W melting is about 65MJ/m^2. The W surface temperature Tmax ~ 2100 K remains much below the melting temperature (~3600K).

References

[1] ITER Physics Basis, 1999, *Nucl. Fusion* 39, 2137
[2] A. Loarte et al. Physica Scripta T128, p 222, (2007);
[3] B. Bazylev, I. Landman G. Arnoux, at al. PSI 2010, P1-98.
[4] B. Bazylev et al Physica Scripta, T128 (2007) 229-233;
[5] M. Sugihara, RE specification for ITER, 2009
[6] R. Miller, Introduction to the Physics of Strong-Current Beams of Charged Particles, Plenum press, (1982).
[7] G. Arnoux, B. Basylev, M. Lehnen et al., PSI 2010, O-31;
[8] M. Berger, M. Inokuti et al., Journal of the ICRU, v.9, issue 2, report 37, (1984)
[9] R. Sternheimer, Phys.Rev.88, 851 (1952);
[10] M. Inokuti, Rev. of Modern Phys., v.43, n.3, (1971), p.297

II. On the generation of Runaway Electrons during Massive Gas Injection

Yu. Igitkhanov, presented on PET-13 Conference in Suites Lake Tahoe 2011, submitted to Contribution to Plasma Physics, (2011)
Received 1 November 2011; Published online 1 December 2012

Highly energetic runaway electrons are able to penetrate the electron shell of partly ionized heavy ions during collisions, for which reason they may be scattered by a positive charge effectively larger than that of a shielded nucleus. This effect increases the Coulomb cross section and can be treated via an effective ion charge $Z_{eff}(\varepsilon_{kin})$that depends on the energy of the incident electrons ε_{kin}. The increase of effective charge number with increasing electron energy in multi-component plasmas renders qualitatively the same result as high Z_{eff} Coulomb plasmas. Since the generation rate of runaways depends on Z_{eff}, its production during the mitigation of disruptions by massive gas injection could in some cases decrease owing to a heavy impurity concentration in the boundary tokamak plasma. This may explain why it has been observed that the runaway's avalanche is suppressed at electron densities below the so-called "Rosenbluth density".

1 Introduction

The multiplication of runaway electrons (RE) in fusion reactor plasmas represents one of the greatest potential threats for plasma-facing components [1]. RE in tokamak plasmas usually appear during start-up or shut-down operation phases but, particularly, during the suppression of disruption by massive gas injection (MGI) [2,3]. Injecting a considerable amount of heavy noble gas atoms like Ar, Ne, etc. cools down the boundary plasma, yet this causes RE acceleration and avalanches.
In the case of multi-component plasmas, it has been recognized that energetic electrons could penetrate through the electronic shell of partly ionized heavy ions thus experiencing a non-Coulomb scattering with the bound electrons as well as a Coulomb scattering with the atomic core. Investigations on supra-thermal (non-relativistic) electrons in multi-component plasmas have shown that non-Coulomb collisions contribute significantly to the plasma resistance and affect other transport coefficients [4,5]. The pitch-angle scattering of supra-thermal ions by partly ionized impurities has been considered in [6]. Here, it is shown that non-Coulomb-like scattering also takes place for highly energetic relativistic electrons in multi-component tokamak plasmas. This effect provides a rationale for the hindrance of further RE generation in tokamak plasmas during the mitigation of thermal disruption by MGI.

2 Non-Coulomb collision of RE

As shown in Refs.[1,6], non-Coulomb scattering implies an increase of the cross section for the electron-ion collision. The problem was treated as that of a Coulomb plasma collision with an effective $Z_I(\varepsilon_{kin})$ (where ε_{kin} is the kinetic energy of the incident electrons), which in general is larger than that of the actual Z_I. At low energies, $Z_I(\varepsilon_{kin})$ is equal to Z_I, but at energies of the order of mega-electron-volts, the range of interest here, $Z_I(\varepsilon_{kin})$ may reach the charge of the bare nucleus ξ_I. In the following, it is shown that the model developed in Ref. [4] for the cross section of supra-thermal electron collisions with partially ionized atoms can be generalized to the scattering of highly relativistic electrons within the multi-component plasma and used to find an expression for $Z_I(\varepsilon_{kin})$ over the entire energy range of ε_{kin}. Namely,

$$Z_I^2(\varepsilon) = \xi_I^2 \cdot A_I^2 \left[1 + \frac{(1 - A_I^2)}{4 A_I^2 \lambda_I} \ln\left(1 + \frac{\varepsilon^2}{\beta_I^2 T_e^2} \right) \right] \qquad (1)$$

where $A \equiv Z_I/\xi_I$, is the degree of ionization, ξ_I is the nuclear charge, Z_I is the net, or "shielded" charge of the impurity ion, $\lambda_I = \lambda_i - \ln(Z_I)$ is the Coulomb logarithm for collisions of electrons with impurity ions in the charge state Z_I, λ_i is the Coulomb logarithm for collisions of electrons with background ions, ε is ε_{kin} normalized on electron temperature, T_e and the parameter β is:

$$\beta_I = \frac{6}{T_{e[eV]}} \cdot \left(\frac{\sqrt{\xi_I}}{1-A} \right)^{4/3} \tag{2}$$

For a bare nucleus, $A=1$ and $Z_I(\varepsilon)=\xi_I$, whereas for a neutral atom, $A=0$ ($\varepsilon \to 0$). Hence, the effective scattering depends only on two parameters, A and ε. Our aim here is to calculate the effective charge value,

$$Z_{eff}(\varepsilon) = \sum_I n_I Z_I^2(\varepsilon) \cdot \lambda_I / \lambda_i \cdot n_e \tag{3}$$

which represents the ion charge in the case of a multi-component plasma. Substituting $Z_I(\square)$ from (1), one can write the energy dependent effective charge as:

$$Z_{eff}(\varepsilon) = \sum_I Z_I^2 \frac{\lambda_I}{\lambda} \cdot \frac{n_i}{n_e} \cdot \left[1 + \frac{(\xi_I^2 - Z_I^2)}{4 Z_I^2 \lambda_I} \ln\left(1 + \frac{\varepsilon^2}{\beta_I^2 T_e^2} \right) \right] \tag{4}$$

If we assume for simplicity that only one ion species contributes to the energy dependent $Z_{\text{eff}}(\varepsilon)$, while the other ions are fully ionized, we find the following expression for $Z_{\text{eff}}(\varepsilon)$:

$$Z_{eff}(\varepsilon) = Z_{eff}(0) \cdot \left[1 + \alpha_I \ln\left(1 + \frac{\varepsilon^2}{\beta_I^2 T_e^2} \right) \right] \tag{5}$$

where

$$\alpha_I = \frac{(\xi_I^2 - Z_I^2)}{4 Z_{eff}(0) \lambda} \frac{n_I}{n_e} \tag{6}$$

Here n_I and Z_I are the most representative impurity ion density and charge state for a given temperature T_e [7]. At high energies, $Z_{\text{eff}}(\varepsilon)$ can exceed both the charge of impurity ions in the plasma, Z_I, and the nuclear charges of these ions, ξ_I. Indeed, for a plasma with a single ion species, with $Z_{\text{eff}}(\varepsilon) \sim \xi_I$, we have $Z_{\text{eff}}(\varepsilon) \sim (\xi_I)^2/Z_I \geq \xi_I$ [5]. The representative argon charge state Z_I as a function of temperature is taken from [8] and plotted on Fig. 1 together with the presently calculated $\alpha_I(T_e)$ and $\beta_I(T)$ for the case of Ar impurities (ξ_I=40, λ=15). One can see that he parameters α_I and β drop with increasing plasma temperature for impure plasmas when $n_e Z_{eff} \sim n_I Z_I^2$. Moreover, α_I becomes independent on impurity concentration $\alpha_I(T_e) \sim (\xi_I/Z_I(T_e))^2$-1..

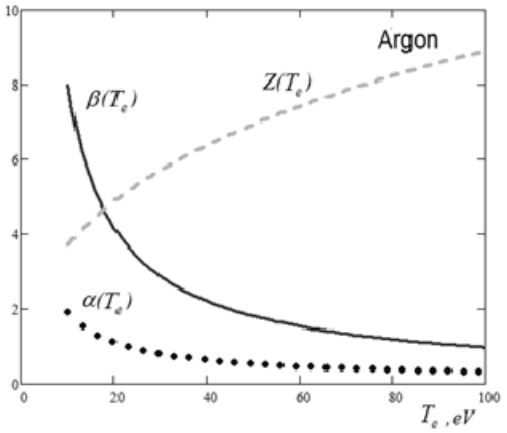

Fig. 1 Dependence of the α, β parameters and the charge state Z_I on the electron temperature for Ar plasma.

The dependence of $Z_{\text{eff}}(\varepsilon)$ on the RE energy was calculated for different electron temperatures. The Argon impurity concentration and the representative charge state are determined from coronal equilibrium [7]. As shown in Fig.2, we find that the increase of $Z_{\text{eff}}(\varepsilon)$ due to non-Coulomb

collisions is more pronounce at low temperatures when the impurity ions are slightly ionized. In this case, the difference between the nuclear charge and ion charge is large.

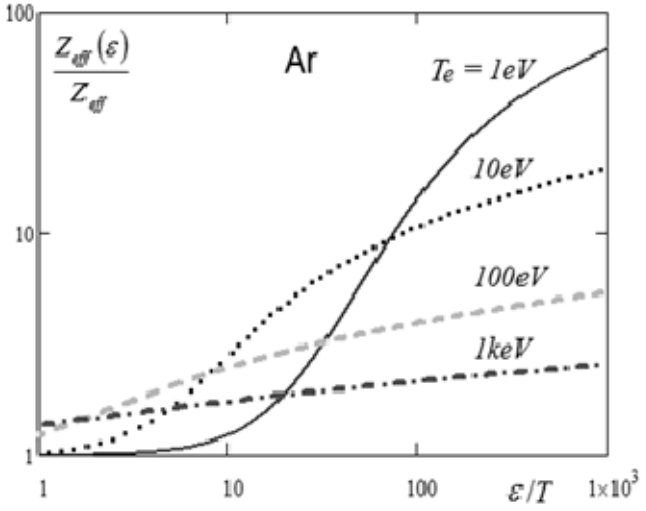

Fig. 2. $Z_{\text{eff}}(\varepsilon)$ (normalized to $Z_{\text{eff}}(\varepsilon=0)$) as a function of RE energy (normalized to the electron temperature) for different plasma temperatures. The Argon impurity concentration and the representative charge state are determined from coronal equilibrium [7].

The penetration of supra-thermal electrons (non-relativistic) into the electron shells of the partially ionized impurities may reduce the plasma transport coefficients (e.g. electron electric conductivity) [4,5]. This, in principle, could cause an unfavorable increase of the required Rosenbluth's suppression density. However, in the cases that we are considering, the number of RE is usually several orders of magnitude smaller than the concentration of thermal electrons in the dense plasma and, therefore, the transport coefficients are determined mainly by thermal electrons. In ITER one expects the average kinetic energy of RE to be E = 12.5 MeV [5], therefore, the relativistic scaling factor, $\gamma = (1-\beta^2)^{-1/2} = E/mc^2$, is ~24 and $\beta \sim 0.99916$, where the average velocity of the RE is βc and m is the rest mass of the electron. By assuming that the plasma current is carried mainly by RE, I_{RE}~10MA, the density of RE can be estimated as $n_{\text{RE}} = I_{\text{RE}}/\text{ec}\beta\cdot\text{S} \sim 10^{16}\text{m}^{-3}$, which is almost 3-4 orders of magnitude smaller than the thermal density. This indicates that RE will not affect the thermal conductivity and the value of the "Rosenbluth density" will remain unchanged. However, as it will be shown below, the production rate of RE electrons is strongly affected by non-Coulomb collisions of RE.

3 Reduction of runaway production in the case of a non-Coulomb collision

The main population of RE in fusion plasma arises due to multiplication of energetic electrons by close Coulomb collisions with plasma electrons when the electric field exceeds some critical value $E \geq E_{\text{crit}}$. The growth rate of secondary RE can be written as [1]:

$$\gamma_{\text{sec}}(\varepsilon) \equiv -\frac{1}{n_{re}^{I}}\frac{\partial n_{re}^{II}}{\partial t} = \gamma_0 \cdot \sqrt{\frac{\pi\cdot\phi}{Z_{eff}(\varepsilon)+5}}\cdot(\eta-1)F(\eta,\varepsilon) \qquad (7)$$

$$\gamma_0 = eE_{crit}/m_e c\ln\Lambda$$

where Z_{eff} must be replaced by $Z_{eff}(\varepsilon)$ (Eq.(5)) in order to take into account the non-Coulomb character of RE scattering $\eta \equiv E/E_{crit}$ and $E_{crit} = 4\pi e^3 \ln\Lambda n_e^*/mc^2$. Here , n_{e}^* is the electron density of bound and free electrons, and [3]:

$$F(\eta,\varepsilon) = \left\{1 - 1/\eta + 6(Z_{eff}(\varepsilon)-1)^2/\left(\eta^2+7.2\right)\left(Z_{eff}(\varepsilon)+5\right)\right\}^{-1/2}$$

The dependence of RE production rate (7) on ε for an electric field that is five times the critical one, $E=5E_{crit}$, is shown in Fig. 3. It demonstrates that the RE grows rate drops considerably because of non-Coulomb collision, particularly for high Z_{eff}.

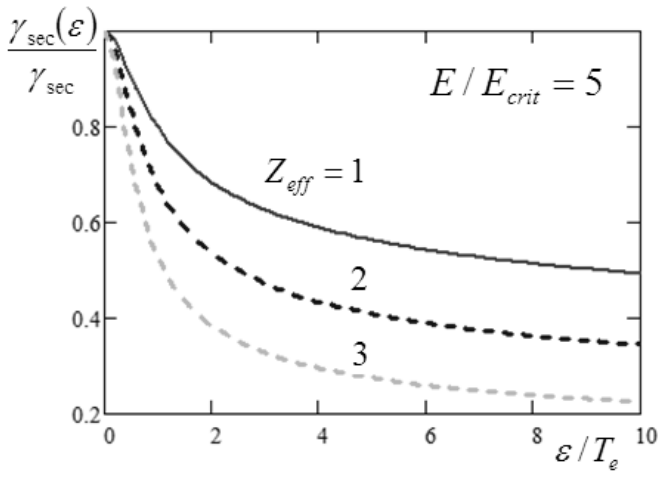

Fig. 3 The growth rate of secondary RE (normalized to $\gamma_{\text{sec}}=\gamma(\varepsilon=0)$) vs. RE electron energy (normalized to T_e) for various charge state values (Z_{eff}=1,2 and 3) for $E=5E_{crit}$.

The growth rate dependence on the electric field for a plasma with Ar impurities in different ionization charge states and corresponding to ITER size machine with aspect ratio R/a=3 was calculated (Fig. 4). We again confirm that there is a significant decrease of the growth rate as a result of non-Coulomb collisions of RE.

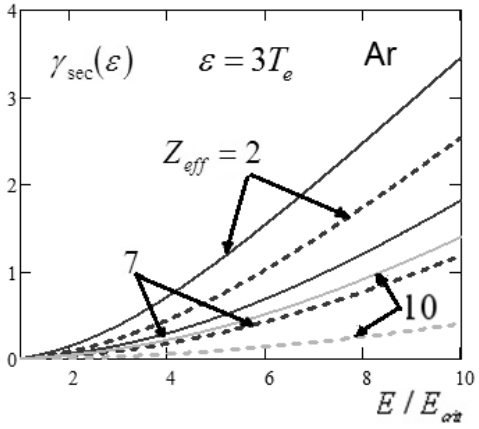

Fig. 4 The growth rate of secondary RE (in γ_0 units) vs. the electric field (normalized to E_{crit}) for different values of effective charge states (Z_{eff}=2,7 and 10).The calculation corresponds to ITER dimensions, R/a=3; dashed lines correspond to cases in which $\gamma_{\text{sec}}=\gamma_{\text{sec}}(\varepsilon=0)$.

One can also expect an exponential decrease of the primary production of RE with increasing electron kinetic energy. Specifically, the main contribution to the growth rate of primary RE depends exponentially on Z_{eff}. Again, by replacing Z_{eff} by $Z_{eff}(\varepsilon)$ one can write,

$$\gamma(\varepsilon)\equiv-\frac{\partial \ln n_e}{\partial t}\propto\left(\frac{E_D}{E}\right)^{3(1+Z_{eff}(\varepsilon))/16}\cdot\exp\left\{-\sqrt{(Z_{eff}(\varepsilon)-1)\frac{E_D}{E}}\right\} \quad (8)$$

Although the dependence of $Z_{eff}(\varepsilon)$ is weak (logarithmic) (see Eq.5), the growth rate (Eq.(8)) strongly decreases with increasing ε. Here E is the electric field and $E_D=4\pi e^3\lambda_i/T$. The dependence of the production rate (normalized to $\gamma(\varepsilon=0)$.) of primary RE on energy of incident electrons (normalized toT_e), is shown in Fig. 5.

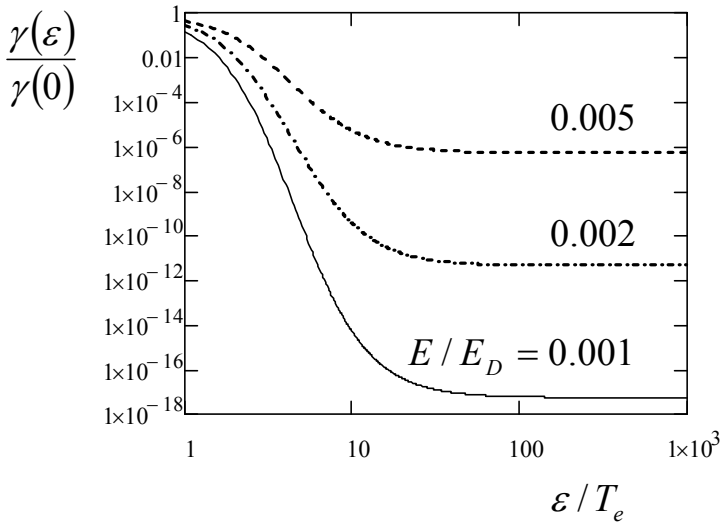

Fig. 5 The growth rate of primary RE (normalized to $\gamma(\varepsilon=0)$) versus the electron energy (normalized to T_e) for different values of the electric field E / E_D.

.

Conclusion

The penetration of relativistic and supra-thermal electrons through the electronic shells of partly ionized impurity atoms changes the character of their scattering in multi-component plasma from Coulomb to non-Coulomb. These conditions can occur during MGI of heavy atoms at the edge of ITER for the purpose of disruption mitigation. It is found that the deviation from Coulomb cross section reduces the growth rate of primary and secondary RE. Moreover, this reduction is enhanced for increasing RE energy. Non-Coulomb collisions are crucial for slightly ionized impurities when the difference between the nuclei charge and the ion charge state is large. These conditions one can expect during MGI. The growth rate of primary RE decays exponentially due to the dependence of Z_{eff} on the electron energy, whereas that of secondary RE decays according to a power law. Overall these effect could reduce the RE production during MGI in ITER and fusion reactor plasmas and thus must be taken into account in numerical simulations.

References

[1] M. Rosenbluth, S. Putvinski, Nuclear Fusion, Vol. 37, No. 10 (1997)
[2] S. Bozhenkov Analysis of disruptions and their mitigation using ultra-fast observation systems, Berichte des Forschungszentrums Jülich 4288;
[3] S. Putvinski, L. Zakharov, A. Kukushkin, Runaway electron suppression by repetitive gas injection,ITER_D_335UCW, May 2010
[4] V. Kirillov, et al, Sov.J.Plasma Physics.,vol.1(2), p.117,1975
[5] P. Yushmanov.,Sov. J. Plasma Physics.,vol. 6(2), p.259, 1980
[6] P.L. Andrews, R. Goldstone, Princeton University PPPL -1513, 1979
[7] D. Post, R. Jensen, C. Tarter., et al., Nuclear Fusion 17, 1187 (1977).
[8] V. Izzo., Nucl. Fusion 46 (2006) 541–547

III. CFC and W Monoblock Blanket Concepts for Fusion Reactor

Yu. Igitkhanov, B. Bazylev, I. Landman,
presented in the 15th International Conference on Fusion Reactor Materials (ICRFM-15), Charleston, South Carolina16-21 October 2011, published in Journal of Nuclear Materials 415 (2011) S845–S848

The thermal performance of the first wall blanket modules with carbon fiber composite (CFC) and tungsten W monoblocks, including a water cooling system with Cu pipes, was modeled for runaway electrons impact under reactor conditions. Calculations show that, in ITER, for an expected RE pulse duration ~ 0.01sec and deposition energy of ~30MJ/m^2, the heat generation in a W monoblock occurs within a thin surface (~10μm) which, however, does not melt. In CFC, heat generation occurs deep in the bulk (~1000μm) but CFC does not experience brittle destruction. The intensive X-ray radiation caused by runaways is strongly attenuated within a 10mm thick layer of W and does not pose any threat for the cooling system. For the CFC case, a small but significant heat generation can occur in the Cu pipe.

1. Introduction

The runaway electrons (RE) in the fusion reactor (ITER, DEMO etc.) will pose a serious problem for the first wall (FW) in regimes with dominant avalanche generation [1]. To optimize the first wall blanket design, it is necessary to assess the expected power deposition and the following consequences for the cooling system and material destruction [2, 3]. We analyze here the thermal performance of the FW blanket module under RE impact. As a model for our calculation, we have chosen a mono-block type blanket element made of CFC and W alloy (see **Fig.1**). It consists of a coolant tube, in which water acts as a coolant, embedded into the W or CHC matrix that is used as heat diffuser. The same material plays the role of armor, i.e., facing the plasma. Pure W is considered as well a suitable plasma-facing material because of its high melting point, high strength

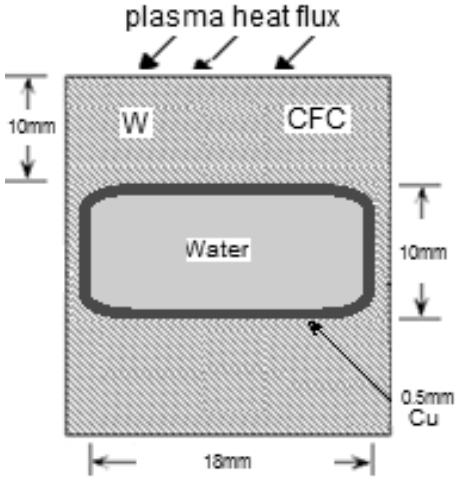

Fig. 1 Model of a mono-block W or CFC type blanket module with rectangular water pipe coolant channel used in the Monte Carlo MEMOS calculation.

at high temperatures, good thermal conductivity, low thermal expansion coefficient, high sputtering threshold energy and limited activation under neutron irradiation. Although W cannot be considered as a structural material because of its low ductility, its ductile brittle transition temperature (DBTT) can be reduced and its creep strength be improved by alloying it with, for example, rhenium, or by small quantities of oxides of cerium or lanthanum. CFC has a high heat capacity and, at a certain volume, it can absorb higher levels of energy primarily because CFC tolerates higher temperatures. This is an attractive property which serves as an effective heat-sink, i.e., converting the kinetic energy of RE to heat.

The Monte Carlo Energy Deposition code ENDEP together with the Fluid Melt Motion on Surface code MEMOS [4-6] were used to calculate the energy, particles and radiation deposition into W and CFC targets, caused by the RE under ITER and DEMO conditions. The code accounts for armor evaporation and melting and sub-cooled boiling at the coolant tubes. The main issue is to find the optimal distance from the plasma-facing surface to the cooling pipe, which will prevent the blanket from erosion and will avoid the degradation of the coolant-heat-removal capability. We also estimate how REs affect the cooling efficiency and the levels of erosion of the FW surface. The simulations were performed for RE in ITER with energy deposition of 30MJ/m^2 during 0.01-0.1sec assuming 1) an exponential distribution of RE in energy space with an average energy of ~ 12.5 MeV and 2) mono-energetic beams. The angle of RE incidence onto the FW surface was taken in the range of 5^o - 8^o. For the DEMO case, the deposition energy is estimated to be 50MJ/m^2 and the average RE energy is estimated to be ~18.5 MeV with exposition time between 0.05 and 0.5s. The RE parameters used in calculations are shown in **Table I**. The RE data for DEMO (PPCS model C) was found by extrapolating that from ITER based on scaling arguments [3,5].

Table I. Expected RE parameters for ITER & DEMO

RE impact	Av. Energy,MeV	W_{kin}, , MJ	Dep. area, m^2	Dep. time, msec
ITER	~12.5	20	0.6	10-100
DEMO*	~ 18.5	40	0.8	50-500

2. Numerical results and analysis

Calculations for the ITER case show that, the percentage of absorbed energy of incident RE reaches ~50% for W and 70% for CFC, while the percentage of energy emitted as photons is ~20% for W and ~3% for CFC. The RE beam generates a considerable amount of radiation upon impacting the W surface. The rest of the RE energy is reflected off by back-scattered electrons (~26-30%). The fraction of RE passing to the Cu pipe is negligible and therefore the heat transfer to the cooling system occurs though thermal conductivity. In the case of W, about 20% of the RE energy is converted into X-ray radiation and a half of it is reflected back into the plasma. Another half penetrates the bulk of W and is strongly attenuated within a 10-mm thick layer, so that only 0.5% turns into heat in the Cu pipe. For the CFC case a small amount of heat is generated but enough to rise the Cu pipe temperature.

Table II. Particles and radiation balance for RE impact (ITER)

material	ratio of electrons reflected back per one incident electron	ratio of electrons reached the Cu pipe per one incident	reflected back photons per one incident electron	ratio of photons reached the Cu pipe per one incident
W	0.74-0.67	$(1.3–1.8)\ 10^{-4}$	0.63-0.66	0.04-0.06
CFC	0.58-0.47	0.006-0.01	0.16-0.17	0.16-0.20

Table III. Energy balance for RE impact (ITER)

material	ratio of absorbed energy	ratio of reflected back electron energy	ratio of radiated energy	ratio of X-rays energy deposited in Cu
W	0.50 - 0.57	0.30 – 0.23	0.20	0.05-0.06
CFC	0.70 – 0.79	0.18	0.035	~ 0.02

Particle and energy balances for RE impacting W and CFC materials for ITER conditions are presented in **Tables II and III**. The first number corresponds to 5° and the second to 8° angles of RE incidence.

Heat generation (normalized to the RE input energy) in tungsten as a function of the penetration depth for mono-energetic and a Gaussian energy distributions of the RE for ITER and DEMO conditions are presented in **Fig. 2**. It is seen that the deposition is larger for smaller RE energies and shallow incidence angles. It is also shown that the heat generation in the W monoblock occurs within a thin surface of ~10μm. In the CFC case, the heat generation occurs rather in the bulk, ~1000μm. The evolution of the surface temperature is shown in **Fig. 3** for CFC and W during and after RE impact with an energy of 30MJ/m^2 and exposition times of 10-100ms. It is seen that for RE with exposition time of 10ms, the melting point for W is reached at~4ms, counting from the beginning of RE impact. At that moment the molten pool depth reaches 560μm and a W layer of ~3μm is evaporated. After the RE impact, the temperature decreases with the time scale of the material heat conductivity. For the RE with impact times longer or comparable with the heat conduction time, the W surface temperature remains below the melting point.

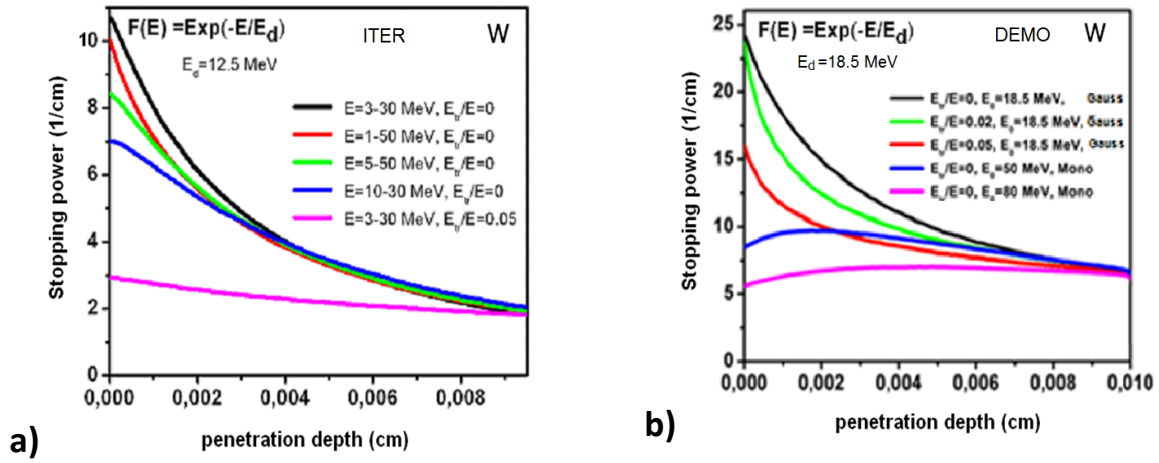

Fig. 2 Volumetric heat generation in W (normalized to the RE input energy) as a function of the radial distance from the FW surface for a RE energy deposition of (**a**) 20MJ (ITER) and (**b**) 40 MJ (DEMO). In both cases, a Gaussian and mono-energetic energy distribution of the incident runaways and an incident angle~5º has been used.

The volumetric heat generation in CFC and the heat sink in Cu pipe regions, for RE energy deposition of 30MJ/m^2 and duration 0.1sec and incident angles of 5º and 8º, are shown in **Fig. 4** as a function of the radial distance from the FW surface. For a flat surface, we find that a change of angle from 5º to 8º has a relatively small effect on the above results, although the penetration depth is deeper for the largest incidence angle. In our calculation, the temperature of CFC remains always below the triple point (~3900ºK at a pressure of ~100bar). The CFC material is thus far from brittle disruption. CFC has a high heat capacity and for a given volume can absorb higher levels of energy primarily because it tolerates higher temperatures. In our case the enthalpy is below the critical one, ~10 kJ/g, above which brittle disruption starts [7].

The main heat transfer channel towards the pipe is heat conductivity, which in the cases of W and CFC (along fibers) is equally large under normal conditions. The time evolution of the Cu pipe temperature for the CFC and W diffusers under impact of runaways of a power of 30MW/m^2 during 0.1 and 0.01sec (dashed lines) is shown in **Fig. 5.** It is seen that while the pipe temperature does not exceed 525°K for RE impact during 0.01-0.1 s in the case of W, for CFC it reaches 600°K for RE impacting during 0.01sec. Our analysis of the water cooling system is based on the model developed in [8]. This model shows that critical heat flux (CHF) can be

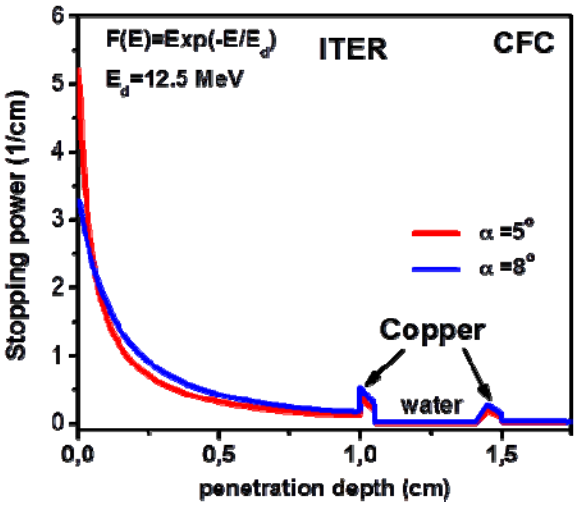

Fig. 3 Volumetric heat generation in CFC and heat sink (Cu) regions as a function of the radial distance from the FW surface, for a RE energy deposition of 30MJ/m2 during 0.1sec and an incident angle of 5º and 8º.

reached locally for the CFCcase. In that case, the effective heat transfer coefficient at the tube wall was set in our calculation to zero for Cu temperatures higher than ~300 °C, corresponding to a local CHF of ~9 MW/m^2 for a water temperature of 150°C, pressure of 3.6 MPa, and velocity of ~4 m/s in a rectangular tube size of 10 mm x 18mm. In the case of W, the coolant system remains under sub-cooled boiling regimes.

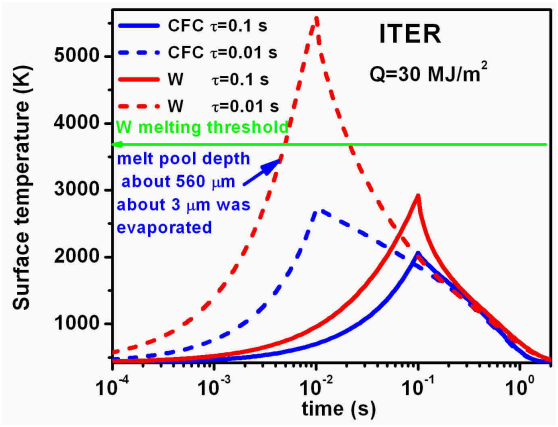

Fig. 4 Evolution of the surface temperature for CFC and W during and after RE exposition times in the range between 0.01 and 0.1 s and a RE energy of 30MJ/m^2.

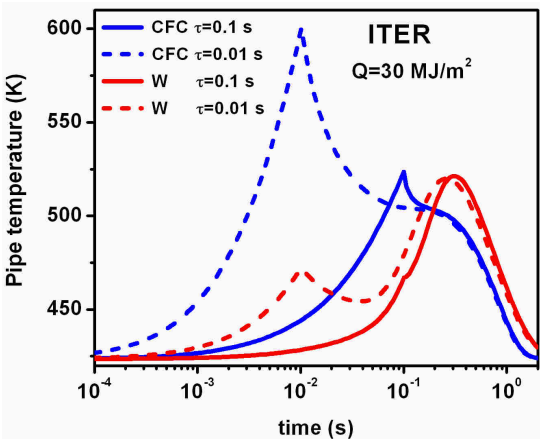

Fig. 5 Evolution of the Cu pipe temperature in the case of CFC and W impacted by runaways of a power of 30MW/m^2 during 0.1sec and 0.01sec (dashed lines).

Conclusions

The thermal performance of the FW blanket modules with CFC and W monoblocks, including a water cooling system with Cu pipes, was modeled for runaway electrons impact under reactor conditions. We have considered the optimal thickness of the layer between the plasma facing surface of the FW blanket module and the coolant tube, which, on the one hand, does not experience strong thermal stresses and, on the other hand, transfers heat into the coolant fast enough to avoid excessive surface erosion.

Calculations show that, although the W temperature during RE exposition exceeds the DBTT value (which is typically in the range from 300 to 600 °C), the averaged in time temperature is expected to be below DBTT. Therefore, the use of W alloy becomes mandatory.

Calculations of the RE stopping power onto the W material show that the RE heat deposition is rather a surface like phenomenon with considerable generation of X-ray photons and secondary electrons. Reflected back X-rays may pose a severe problem for diagnostic ports and antennas. Since the X-rays strongly attenuate in bulk W, they do not reach the Cu pipes for a 10-mm thick W armour and, therefore, pose no threat for the cooling system. For the expected RE-impact duration (~0.1s) and energy (~30MW/m^2) in ITER, the W surface does not melt or evaporate.

In the case of CFC, the heat deposition of RE is phenomenon occurring rather in the bulk, about hundred times deeper than in W for the same incident energies, in the range 1-50 MeV, and shallow incident angles 5-8º. Under these conditions, the maximum temperatures of CFC stay below sublimation and the CFC material does not experience brittle destruction. For the CFC module of 10-mm thickness, a small heat generation occurs in the Cu pipe, which could significantly increase the pipe temperature.

References

[1] ITER Physics Basis, Chapter 9: ITER contributions for Demo plasma development, *Nucl. Fusion* 47, (2007) S404; ITER DDD, WBS1.9, Physics Section 6.3, 1983;

[2] Yu Igitkhanov, B Bazylev, Effect of Off-Normal Events on Reactor First Wall, in *Physica Scripta* T, 2011 (in press)

[3] Yu Igitkhanov, B Bazylev, The PFC erosion in DEMO due to runaway electrons, *Fusion Science and Technology*, Vol.60, Jul.2011, p.349

[4] B Bazylev et al., *Physica Scripta*, T128**,** (2007) 229

[5] Yu. Igitkhanov, B. Bazylev, *Fusion Science and Technology*, Volume 60, Number 1, July 2011, Pages 349-353;

[6] Yu. Igitkhanov; B. Bazylev, I. Landman, *Journal of Nuclear Materials* 415 (2011) S845–S848

[7] H. Wuerz , B. Bazylev, I. Landman et al., *Journal of Nuclear Materials* 307–311 (2002) 60–68, V. Astrelin et al., *Nuclear Fusion* 37 (1997) 1541.

[8] ITER DDD, WBS 1.6, Blanket System, G 16 DDD 2 98-06-2 W 0.5, June 1998; A. Raffray et al., in: *Proceedings of the 12th Symposium on Fusion Technology*, Marseille,7-11 September, 1998; R. Raffray, G. Federici, *Journal of Nuclear Materials* 244 (1997) 85-100

IV. The PFC erosion in DEMO due to runaway electrons

Yu. Igitkhanov, B. Bazylev, TOFE-19, Las Vegas, has published in Fusion Science and Technology, vol.60,n.1,(2011) p.349-353

We have estimated the energy deposition of runaway electrons into the tungsten/EUROFER blanket structure for reactor DEMO conditions and calculated the consequent level of thermal erosion. Our simulations indicate that the heat generated by runaway electrons may pose a major lifetime limitation for the W armor. We find that the minimum thickness of W necessary to prevent EUROFER from stress destruction at high temperatures, Δ_{min} , could be already too large for an efficient cooling. Tungsten layers of thickness $\geq \Delta_{min}$ would erode by surface melting and vaporization since the thermal conductivity time is much larger than expected exposure time to runaways.

1. Introduction

During normal operation, the plasma facing components (PFC's), primarily the first wall (FW), of DEMO reactor will experience heat loads that exceed those in ITER since the fusion power in DEMO is expected about four times higher than that in ITER (Ref. 1). In addition, various types of off-normal high-power events, such as vertical displacement event and avalanche generation of runaway electrons (RE), are expected to occur and cause damage of the DEMO FW, owing to high local energy deposition. RE, in particular, can be generated not only during a disruption [2] but also during the injection of external impurities for conversion of thermal energy into radiation for disruption mitigation[3]. The main concern with regard to the behavior of plasma facing components (PFCs) is the intense heating of armor structure of the FW and coolant channels due to the volumetric energy deposition by RE. This issue has been intensively studied in many papers and characterized in detail for operating machines and for ITER relevant materials and conditions [4-14] A Monte Carlo approach is generally used to simulate the RE energy deposition into PFCs structure and erosion of the PF surface.

In this work we will use the same approach for simulation of DEMO specific FW/blanket materials and under DEMO specific conditions which was not considered yet. A possible option for DEMO's FW structure is to have a blanket design made of W (as armor to sustain high temperatures) and EUROFER (as the structural material). The reduced-activation ferritic martensitic steel EUROFER is considered in Europe as a reference structural material for DEMO reactor.[15] Although W/EUROFER bound is compatible with high neutron fluencies to minimize the necessary replacement of the in-vessel components and is "low-activation" type, the loss of creep strength at relatively low temperatures represents the main drawback of EUROFER as a structural material. Reinforcement by SiC fibers or oxide dispersion strengthened (ODS) steels may improve the high temperature creep resistance up to 1023°K,(Ref. 15) and we will take this value as a reference point in our study. The central problem is that impinging RE will affect mostly the FW and cause the excessive stresses in structural material. The level of W erosion under DEMO type RE impact is not known yet. Apart from protecting the W/EUROFER interface from heating above creep temperature, of particular interest is to avoid the formation of molten material at the surface of the W-armor since, e.g., it could be a source of plasma contamination [11,13].

The main issue that we address below is to find the thickness of the W armor such that, on the one hand, it will prevent EUROFER from creeping or thermal stress destruction and, on the other hand, it will transfer the RE energy into the coolant fast enough to avoid excessive W erosion (melting). Numerical simulations are performed with the Monte Carlo Energy Deposition code ENDEP together with the Fluid Melt Motion on Surface code MEMOS (Refs. 11,13) in order to calculate the energy deposition of the RE into W armours of various thickness and the level of erosion caused by the RE, respectively. ENDEP code calculates the armor melting, evaporation, and the heat transport in various material structures [13]

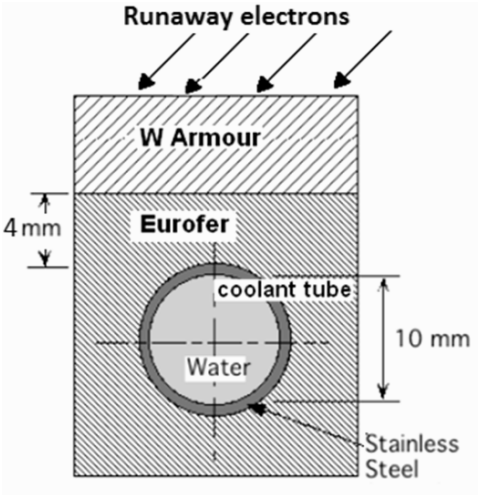

Fig. 1 Typical blanket first wall structure used for the Monte Carlo ENDEP computations of the runaway-electrons impact.

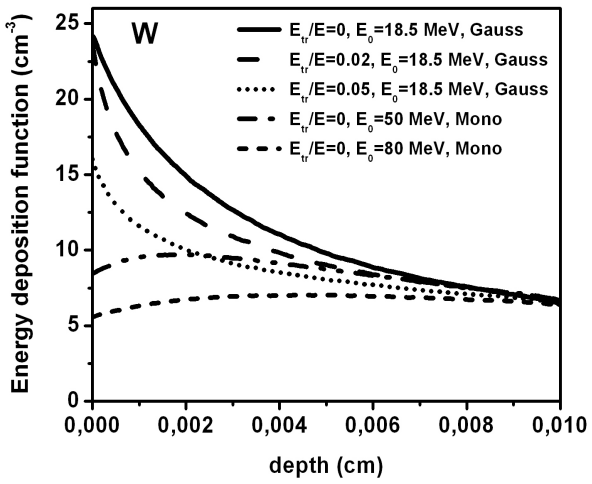

Fig. 2 Volumetric heat generation (normalized to the RE input energy) in W armour as a function of the penetration depth for mono-energetic and a Gaussian energy distribution of the RE beam; B=6T

The characteristics of RE in DEMO can be extrapolate from ITER data, using the scaling arguments [1]. For this purpose, we will choose the DEMO (PPCS model C) design parameters as a reference case [4]. A first step to assess the erosion is to estimate the energy deposition of RE per unit area. By considering that the thermal energy of the plasma in DEMO by at least two times higher than that in ITER, Ref(1) the beam energy of REs in DEMO can be estimated as W_{kin}~20MJ x 2≈40 MJ. Then, the wetted area can be estimated as ≤ 0.8 m^2, assuming a linear size scaling from ITER to DEMO. The RE wetted area in DEMO FW could be in R_{DEMO}/R_{ITER}~1.2-1.3 times larger, than that in ITER (≤0.6m^2) (Refs. 1,16,17). Therefore, the RE energy density of ~50MJ/m^2 is expected in DEMO FW. This value contains only the RE kinetic energy. We assume that the RE energy varies in the range of 30-100 MJ/m^2, keeping in mind that part of the poloidal magnetic energy will eventually also be converted into RE kinetic energy [2,3,16]. The RE current can be estimated as I_{re} ~10-15MA, which is about ≤70% of the total plasma current (similar to ITER). In our calculations we also assume that the energy deposition time of RE is in a range of 0.05-1s. This roughly corresponds to the loss time of high-energy REs due to the fact that their drift orbits intersect the wall in resistive time scale and this time depends on the thickness of the wall structure. We assume that in DEMO the RE deposition time about 5-10 times bigger than in ITER (Refs. 16,17).

2. Numerical results and analysis

As a model for our calculation, we have taken a sandwich-type blanket element that resembles ITER's FW structure (see Fig.1). It consists of a coolant tube embedded in the EUROFER heat sink, to which the W armor is attached. For our calculations, we have considered mono-energetic RE beams (50 and 80 MeV) and RE beams with a Gaussian energy distribution centred at some energy E_0. The energy E_0 can be estimated as $E_0 = W_{kin}/V\, n_{RE}$, where the RE density $n_{RE} = I_{RE}/ec\beta \cdot S \approx 6\cdot10^{15}$m^{-3}, $c\beta$ is the relativistic electron velocity (β ~1). For the plasma surface area in DEMO $S \sim \pi a^2 k \approx 48$m^2 ($k$ ~1.7 is the elongation) and the plasma volume $V \sim 2\pi R \cdot S \approx 2265$m^3, $E_0 \approx$ 18,5MeV. It is expected that RE current will flow along the magnetic field lines which can strike PFC surfaces in DEMO configuration (with B = 6T) under grazing angle~1° (Refs. 16,17). The RE strikes the plate with some incidence angle. For the given magnetic field and pitch angle the RE incidence angles depend on the energy ratio E_{tr}/E and spiral phase [10,12]. The incidence angles were evaluated by employing the randomly distributed phase following the procedure described in details in Refs.10,12. In the case when E_{tr}/E=0 incidence angle coincides with the magnetic pitch angle, which assumed to be ~1°; for E_{tr}/E=0.02 incidence angle varies randomly from 1° to 14°, and for

E_{tr}/E=0.05 it varies from 1° to 20°. Fig. 2 shows heat deposition profiles as a function of the penetration depth, normal to the FW surface, for Gaussian and mono-energetic energy distributions of the incident RE. We find that most of the RE energy is deposited within a thin armour layer of ~0.1mm. However, while for mono-energetic beams of 50-80 MeV the deposition in the first wall is constant over a thickness of at least ~0.1 mm, for Gaussian RE, the energy deposition is highly localized at the surface. Overall, mono-energetic beams deposit a smaller amount of energy because of the drop of the non-elastic cross-section for high energies. In agreement with previous our calculations[3], the heat generation is larger for smaller RE energies and shallower incidence angles. **Table 1** shows our results for the energy balance calculations. Note here that the RE beam also generates a considerable amount of radiation upon impacting the W surface. Our calculations show that the percentage of absorbed energy reaches ~ 60%, while the percentage of energy emitted as photons is ~ 11-15%. The rest of the RE energy is reflected off by back-scattered electrons (~16-34%). The fraction of RE passing to the structural material is negligible. That is, the direct RE energy deposition in EUROFER is zero.

Table I. RE energy balance in the W armor; E_{abs}, E_{ref}, and E_{rad}, represent the fraction of adsorbed energy, reflected energy, and energy of the radiation, respectively.

Scenario	$E_{abs.}$	E_{ref}	$E_{rad.}$
E_{tr}/E=0 Gaussian	0.54	0.34	0.11
E_{tr}/E=0.02 Gaussian	0.59	0.295	0.105
E_{tr}/E=0.05 Gaussian	0.68	0.215	0.088
E_{tr}/E=0, Mono 50 Mev	0.61	0.208	0.146
E_{tr}/E=0, Mono 80 Mev	0.633	0.16	0.152

The spectral distribution function of emitted photons, plotted in Fig.3 for different incident RE energy distributions. The sharp peaks are the characteristic spectral lines of W. The broad band corresponds to bremsstrahlung photons. Strong hard X-ray radiation from W surface caused by RE could be a matter of great concern and will require special protection, e.g., of diagnostic ports.

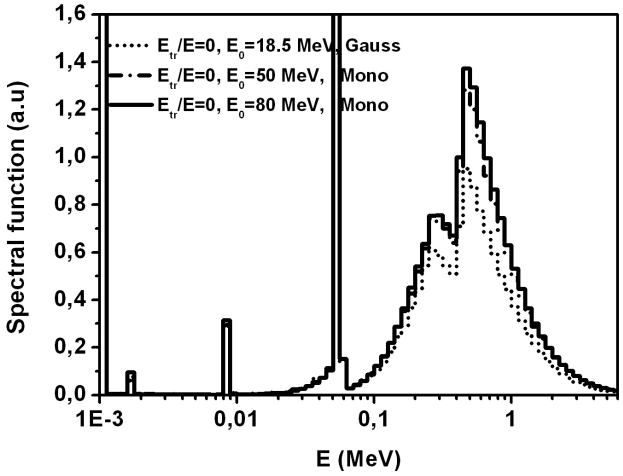

Fig. 3 The spectral distribution functions of emitted photons from the W surface under RE impact.

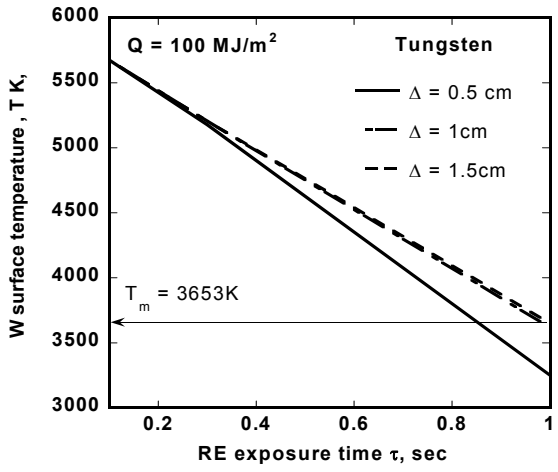

Fig. 4 Maximum W surface temperature as a function of exposure time for mono-energetic RE beams of 100MJ/m^2 and E_{tr}/E=0.

The heat deposition profiles of the mono-energetic beams in Fig. 2 were used as the input for the ENDEP code to determine the resulting thermal effect on the first wall armor. The maximum W surface temperature upon impact of mono-energetic RE beams and E_{tr}/E=0 is shown as a function of impact duration in Fig.4. It shows that (1) the larger the espouse time, the smaller the surface temperature and (2) the temperature at the surface becomes independent on the W thicknessprocess, Fig.4 also shows (for an energy deposition per unit area of 100MJ/m^2) that, only for relatively long exposure periods (~1s), melting could be avoided by using of sufficiently small thicknesses (≤ 1

cm). Fig.5 shows the thickness of the W molten layer as a function of armor thickness. One can see that the higher exposure time, the larger the molten layer thickness. This is consistent with the fact that the W heat conductivity drops with increasing temperature and that the conductivity time increases with armor thickness.

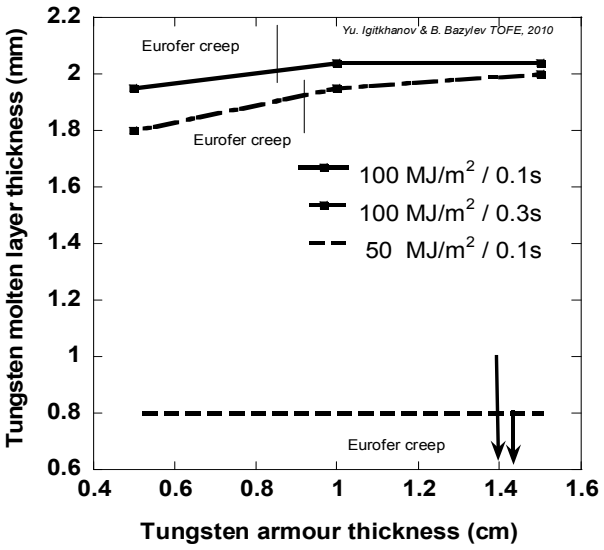

Fig. 5 W molten layer thickness as a function of armour thickness. The higher incident energy and the smaller the exposure time, the larger the molten layer thickness; the case of mono-energetic RE beams and E_{tr}/E=0.

It is also estimated, that the depth of W vaporization increases with increasing power and decreasing the exposure time. We have shown so far that the presence of a vaporized layer and a macroscopic molten layer is unavoidable for expected exposure times. This fact in itself points out

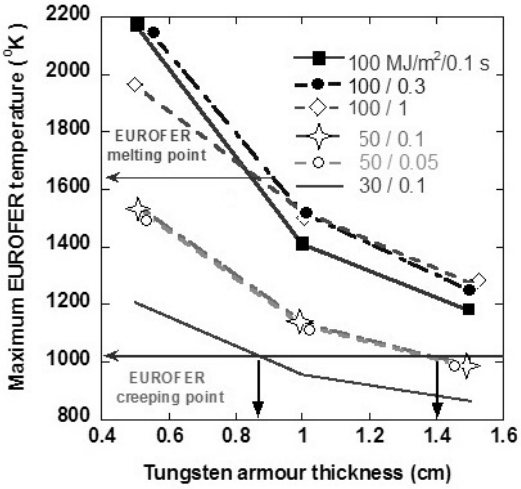

Fig. 6 Maximum EUROFER temperature in the W/EUROFER interlayer as a function of W armour thickness. EUROFER creep point defines the minimum W thickness (indicated by vertical arrows for 30 and 50MJ/m^2, τ=0.1s); the cases of mono-energetic RE beams with E_{tr}/E=0.

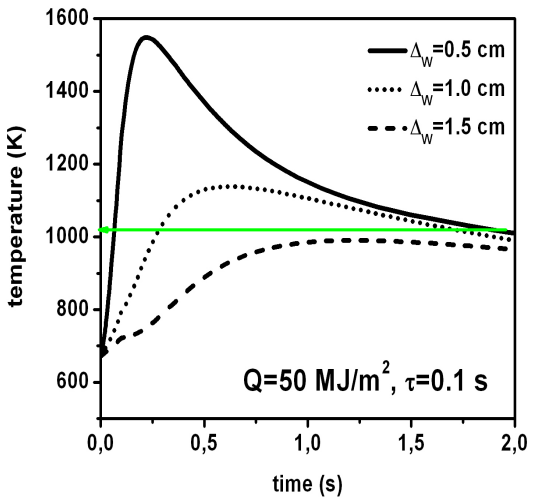

Fig. 7 Evolution of the temperature in the interlayer between W and EUROFER materials for different W armour thickness. The temperature varies according to W and EUROFER heat conductivities. The case of mono-energetic RE beam with E_{tr}/E=0.

that W is not suitable since it will contaminate the plasma by splashing metallic droplets within a time scale of μs, owing to the Rayleigh-Taylor instability.[11,13] Still, it remains to determine the role of the armor thickness in tuning the temperature of EUROFER. Fig.6 shows the maximum temperature at the W/EUROFER interface as a function of W-armor thickness. For instance, for

typical RE energy deposition per unit area and exposure time (50MJ/m^2 and 0.1s, respectively), the W armor thickness must exceed 1.4cm in order to reduce the interface's temperature below the creep point. The cases of 100MJ/m^2 shown in **Fig.6** are mainly to demonstrate the effect of changing energy time deposition, which can be explained by the W heat conduction variation It is also interesting to see the evolution in time of the maximum temperature at the W/EUROFER interface. For a RE energy deposition per unit area of 50MJ/m^2 and a deposition time of 0.1s, Fig. 7 confirms first of all that only a W-armor thicker than 1.5cm could shield the interface from its creep point at all times. It also shows that the residence time above the creep point becomes of the order of seconds at thicknesses between 1-1.4cm, though it slowly increases with decreasing thickness.

Conclusions

Our calculations show that for RE deposition energies $\geq$ 50MJ/m^2 and deposition times $\leq$ 0.1s, the minimum armor thickness required to prevent EUROFER from creeping or thermal destruction is Δ_{min}~1.4cm. However, such thick armor layers may melt and contaminate the plasma owing to the inefficient cooling that derives from the relatively small thermal conductivity of W and, moreover, of EUROFER. The time required for re-solidification is much larger than the characteristic RT instability time that can cause the ejection of W droplets into plasma. At higher RE energy deposition rates ($\geq$100MJ/m^2 in 0.1s), plausible in DEMO, the required armor thickness to prevent creeping destruction should become so large that the bulk of the armor layer is expected to melt and a macroscopic layer of W to evaporate.

It is worth noting, that we have considering here the creep temperature~1023°K, which is true for nanostructured ferritic 12-14% ODS steels. For EUROFER 98 the creep temperature is normally $\leq$ 923°K (Ref.15). Therefore, the limitations found above remain valid for this structural material. In any case, the temperature gradient in 0.4cm of EUROFER layer could also cause a stress, above the allowably one.

It seems thus that the use of W/EUROFER bound structure considered here should be limited to regions where energy deposition from RE is highly unlikely. Future effort is required to better understand the characteristics of RE and areas of energy deposition.

References

1. ITER Physics Basis, Chapter 9: ITER contributions for Demo plasma development, *Nucl. Fusion* **47**, (2007) S404
2. A.LOARTE, V.RICCARDO et al., "Magnetic energy flows during the current quench and termination of disruptions with runaway current plateau formation in JET and Implications for ITER", *Preprint EFDA–JET–PR(10)*, **23**, 2010
3. YU. IGITKHANOV, B. BAZYLEV and I. LANDMAN, *J. Nucl. Mat*. (2010) (in press)
4. D. MAISONNIER et al.,*Nucl. Fusion* **47**, (2007) 1524
5. T. KAWAMURA et al., *Fusion Engineering and Design* **9,** (1989) 39
6. H. BOLDT and H. CALEN, *Journal of Nuclear Materials*, **179-181,** (199l) 360
7. A. RUSSO et. al., *Nuclear Fusion* **31,** (1991) 117
8. T. KUNUGI, *Fusion Engineering and Design* **23,** (1994) 329
9. A. RAFFRAY et al., in: *Proceedings of the 12th Symposium on Fusion Technology*, Marseille,7-11 September, 1998
10. G. MILOSHEVSKI, H. WUERZ " 3-D Monte Carlo Calculations of Energy Deposition of Electron into Bulk Graphite and into Inhomogeneous Carbon Plasma Shield". Wissenschaftliche Berichte FZKA, **6482**, August 2000
11. B. BAZYLEV et al., *Physica Scripta*, **T128,** (2007) 229
12. V. SIZYUK and A. HASSANEIN, *Nucl. Fusion* **49,** 095003, 2009
13. B. BAZYLEV, YU. IGITKHANOV, I. LANDMAN, and A. LOARTE, 14th ICFRM, Sapporo Japan, will be published in *J. Nucl. Mat*. (2011)
14. A. HASSANEIN, T. SIZYUK, V. SIZYUK, G. MILOSHEVSKI, *Fusion Engineering and Design* **85,** (2010) 1331
15. R.LINDAU, A. MOSLANG, *Fusion Engineering and Design* **75-79**, (2005) 989

16. V. Lukash et al., Proc. 6th IAEA TCM on Energetic Particles in Magnetic Confinement Systems (Naka, Japan, 2000) JAERI-Conf. 2000-04, 13.
17. M. SUGIHARA et al., in 36th EPS Conference on Plasma Phys. Sofia, June 29 - July 3, 2009 ECA Vol.**33E**, P-4.165, (2009)

V. Effect of Off-Normal Events on Reactor First Wall

Yu. Igitkhanov, B. Bazylev, presented in
PFMC-13, (Rosenheim), published in
Physica Scripta T 145 (2011), 014056

In the paper we analyse the energy deposition and erosion of W/EUROFER blanket module for the first wall (FW) of DEMO due to the runaway electrons (RE) and vertical displacements events (VDE). The DEMO data for transients where extrapolate from ITER data by using the scaling arguments. The simulations were performed for the RE deposition energy in the range of 30-100MJm^{-2} over 0.05-0.3s. In the case of a hot VDE all stored in plasma energy is deposited to the FW band over~1sec. For a VDE following the thermal quench phase the remaining magnetic energy is deposited to the FW over~0.3sec. It is shown that the minimum W thickness needed to prevent failure of the W/ EUROFER bond (assumed to be the EUROFER creep point) is so large that causing the armour melting. Both RE and VDE in DEMO will pose a major life-time issue depending on their frequency.

1. Introduction

A stored energy in DEMO will largely exceed the ablation and melt limits of any wall materials during normal operation. To stay below the maximum acceptable power limit for the plasma facing components a DEMO reactor theoretically require radiated power fraction more than 90%[1-3]. However, the realistic concept of a DEMO reactor should also consider a possible failure of the control of transients. The various types of off-normal conditions can occur during the reactor operation, which represent a potential threat to the integrity and availability for fusion reactor. In this paper we consider a consequence of two types of transient events: a VDE caused by loss of plasma vertical stability and RE generation that can occur during the current quench following a disruption or as a consequence of disruption mitigation by means of massive gas injection. In the case of a VDE, one can distinguish between a VDE following a thermal quench phase of disruption, when most of the plasma thermal energy is lost before the onset of vertical motion, but the kinetic and magnetic energy stored in the RE beam can be deposited to the wall. Another type of vertical displacement, so-called "hot" VDE can occur due to accidental loss of control and the plasma column drifts towards the wall with appreciable plasma thermal energy and with a slow drift speed. Conversion of the initial plasma current to RE current through knock-on avalanche processes may occur following disruption, loss-of-control VDE or fast plasma shutdown. Both VDE and RE energy deposition would affect mostly the first wall. The exact energy density on the first wall depends on the plasma parameters and assumed deposition area.

In the case of "hot" VDE in DEMO, we assume that ≤ 2GJ (~0.7GJ of plasma thermal energy and ~1.2 GJ of magnetic energy) will eventually be deposited on the FW structure. The resulting energy density can be estimated in the range of ~30-100 MJ/m^2, which includes toroidal and poloidal peaking factors similar to ITER and assumption that the deposited area~$2\pi Rd$ is about 20-24m^2 corresponding to toroidally continuous band d = 0.5m and the DEMO major radius R=7.5m. In this case of accidental control loss the plasma column drifts toward the wall with the resistive growth time of vessel structure, which we assume in DEMO of the order of~1sec.

In general, vertical instability can arise after thermal quench, so that current channel (with or without the RE, depending how fast it happens) moves towards the wall during current decay and the most of the remaining plasma energy (mainly magnetic) can be deposited to the FW. We assume in our calculations that in this case about half of magnetic energy is deposited to the FW surface band of 24m^2 over~0.3sec. It also could partly be converted to runaway kinetic energy and the exact energy density can be much higher, because the deposition area in the case of RE is generally smaller.

The characteristics of RE in DEMO can be extrapolate from ITER data, using the scaling arguments [4]. For our purpose, we will choose the DEMO (PPCS model C) design parameters as a

reference case **[**2**].** Since the stored plasma energy in DEMO is by at least a factor of two higher than that in ITER [3], the beam energy of REs in DEMO can be estimated as W_{kin}~20MJ x 2≈40 MJ. The RE wetted area on the FW is envisage for ITER as ~0.6m^2 [5]. It is reasonable to assume that the wetted area scales at first linear with machine size, so that it can be estimated for DEMO FW as ≤ 0.8 m^2, that is in R_{DEMO}/R_{ITER}~1.2-1.3 times larger, than that in ITER. Therefore, the RE kinetic energy density of ~50MJ/m^2 is expected in DEMO FW. We assume that the total RE energy varies in the range of 30-100 MJ/m^2, keeping in mind that part of the poloidal magnetic energy could eventually also be converted into RE kinetic energy [4,6]. The RE current can be estimated as I_{re} ~10-15MA, which is about ≤70% of the total plasma current (similar to ITER). In our calculations we also assume that the energy deposition time of RE is in a range of 0.05-1s. This roughly corresponds to the loss time of high-energy REs due to the fact that their drift orbits intersect the wall in resistive time scale and this time depends on the thickness of the wall structure. We assume that in DEMO the RE deposition time about 5-10 times higher than that in ITER **[**4**].**

The off-normal events will affect mostly the FW structure causing both the excessive erosion of armour and stresses in structural material. A possible option for DEMO's FW design is a sandwich type block structure which consists of a water coolant tube embedded in the EUROFER heat sink, to which the W armor is attached [4,7]. The reduced-activation ferritic martensitic steel EUROFER is considered in Europe as a reference structural material for DEMO reactor. Although W/EUROFER bound is compatible with high neutron fluencies to minimize the necessary replacement of the in-vessel components and is "low-activation" type, it has relatively low creep temperature which could be the main drawback of EUROFER as a structural material. Reinforcement by SiC fibers or oxide dispersion strengthened (ODS) steels may improve the high temperature creep resistance up to 1023°K [7], and we will take this rather optimistic value as a reference point in our study.

For calculation of RW impact, we have considered mono-energetic RE beams (50 and 80 MeV) and RE beams with a Gaussian energy distribution centred at some energy E_0. This energy was estimated in [4] as $E_0 \approx$ 18,5MeV.

2. Numerical results and analysis

The calculations of the VDE/RE energy deposition and consequent erosion were performed by means of the Monte Carlo Energy Deposition code ENDEP and the Fluid Melt Motion on Surface code MEMOS [4,9]. It was found that in the case of a VDE (without RE) the power deposition of about several keV of electrons and ions occurs in very small (~ several *n*m) W armor surface layer. Whereas in the VDE case the deposition is a surface phenomenon, in the RE case, it occurs over a finite thickness of the armour. The most of the RE energy is deposited within ~0.1mm of armour layer. However, while for mono-energetic beams of 50-80 MeV the deposition in the first wall is constant over a thickness of at least ~0.1 mm, for Gaussian RE with the average energy of 18.5MeV, the energy is mainly deposited at the surface. In general, the mono-energetic beams deposit a smaller amount of energy because of the drop of the non-elastic cross-section for high energies. It explains why heat generation in armour is larger for smaller RE energies and shallow incidence angles.

Table 1. Summary of results for RE and VDEs for W armour of 10 mm thickness.

Event	Energy density (MJm^{-2})/deposition time (s)	Deposited area area (m^2)	Max. EUROFER temperature, (°K)	W molten layer thickness (mm)	W evaporated thickness (mm)
Hot VDE	~50–100/1	24	~1610	~0.85	0.011[a]
Cold VDE	~30–50/0.3–1	24	~1260	~0.740	0.009[a]
RE	~100/0.05–0.3	0.8	~1500	~1.8	~0.035

[a]Vapour shielding effect is taken into account.

The energy balance calculations show that in the case of VDE almost all plasma energy is converted into heat causing melting, evaporation and radiation from the W surface. In the case of RE the percentage of absorbed energy in W armour reaches ~60%, while the percentage of energy emitted as photons is ~11-15%. The RE beam generates a considerable amount of radiation upon impacting the W surface. The rest of the RE energy is reflected off by back-scattered electrons (~16-34%). The fraction of RE passing to the structural material is negligible and therefore the heat transfer from armor to EUROFER occurs though the thermal conductivity.

From the results of calculation summarized in **Table I**, the following observations can be made. There is no major difference between the RE and hot VDE cases in terms of EUROFER temperature, melt layer thickness and heat flux to the coolant since for W armour the heat deposition occurs very close to the surface. For the RE case, a somewhat larger part of the heat generation occurs deeper in the material in particular for the mono-energetic RE beams. Consequently, the RE energy deposition results in thicker melt layer, higher maximum EUROFER temperature and higher evaporated thicknesses than VDE energy deposition. The later occurs because of because the vapor screening effect is less pronounced for the RE case. The total molten and evaporated thickness is ~2 mm for W, which, depending on the VDE and RE frequencies, would seriously restrict the lifetime.

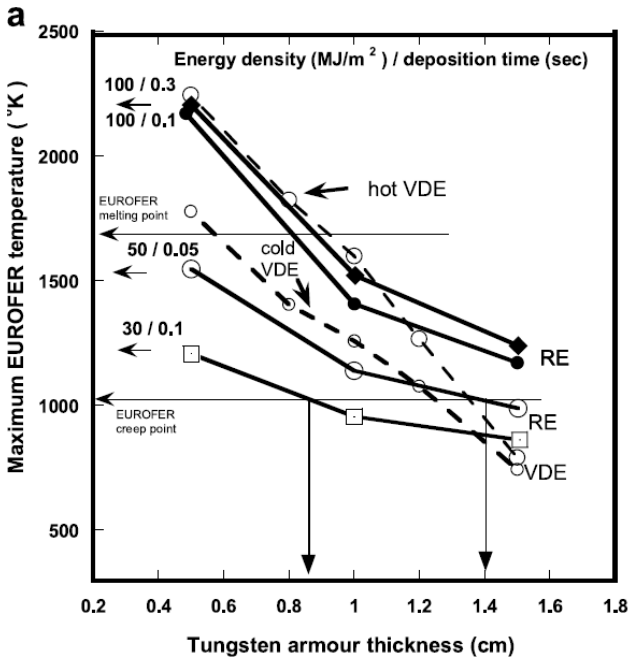

Fig. 1 Maximum EUROFER temperature as a function of W armour thickness. The EUROFER creep point limits the minimum W thickness (indicated by vertical arrows for 30 and 50MJ/m^2, τ=0.1s); the case of mono-energetic RE beams and ~1° of the incidence angle and hot VDE.

It is shown, that in the case of a VDE and ≥10mm of armour thickness the surface temperature will exceeds the W melting temperature, for deposition times ≥1s. The RE beams with 100MJ/m^2 /0.3s will melt the W surface at any thicknesses. For an energy deposition of 100MJ/m^2 and

relatively long exposition periods ~1s, melting could be avoided for smaller armour thicknesses <1cm.For the RE with 30MW/m^2 and t=0.1s the temperature remains below the melting point and is independent on armour thickness. In general, the larger the incident energy, the higher the surface temperature and it becomes independent on the W thickness for deposition periods shorter than the tungsten thermal conductivity time. deposition per unit area and exposure time (50MJ/m^2 and 0.1s,

The maximum of EUROFER temperature as a function of W armour thickness is show in **Fig.1**. The EUROFER creep point limits the minimum W thickness (indicated by vertical arrows for 30 and 50MJ/m^2, τ=0.1s). For instance, for typical RE energy the W armor thickness must be ≥ 1.4cm in order to reduce the interlayer temperaturebelow the creep point. However, at that thickness the W armour will melt.

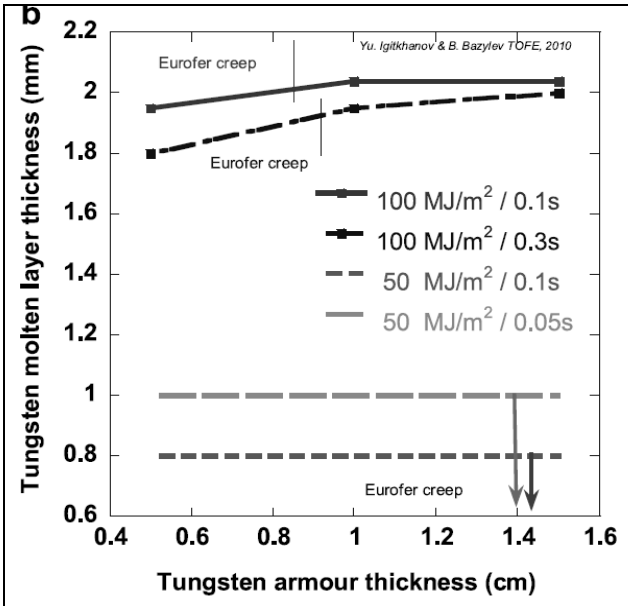

Fig. 2 Maximum molten layer as a function of W armour thickness. The EUROFER creep point limits the minimum W thickness (indicated by vertical arrows for 30 and 50MJ/m^2, τ=0.1s); the case of mono-energetic RE beams and ~1° of the incidence angle and hot VDE.

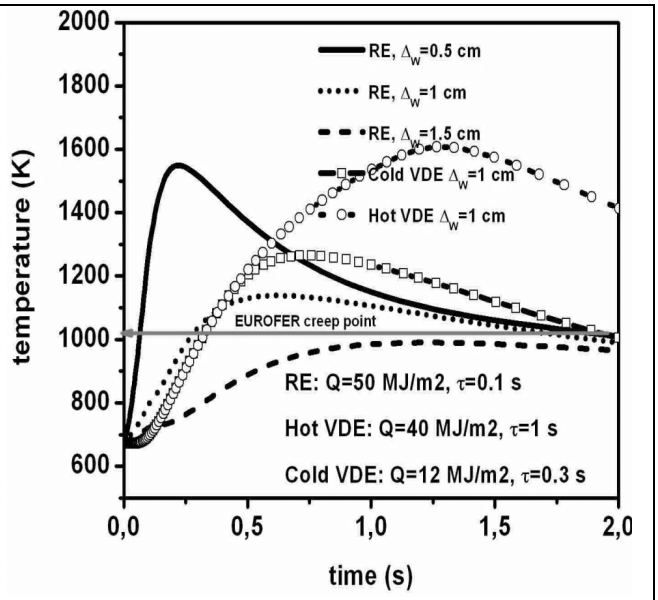

Fig. 3 Evolution of the maximum EUROFER temperature for three armour thickness values Δ_w. The temperature varies according to W and EUROFER heat conductivities. The case of mono-energetic RE beam with ~1° of the incidence angle and the hot VDE and the VDE after thermal quench cases for Δ_w = 10 mm.

Only in the case of 30MJ/m^2/0.1s for thickness ≤ 0.8cm the W surface doesn't melt and it is possible to avoid the creep thermal stresses. In the cases of 100MJ/m^2 the creep point is always exceeded and, moreover, EUROFER will melt for armour thickness ≤ 0.8cm. **Fig.2** also shows the depth of the W molten layer as a function of armor thickness. It is shown that the higher incident energy and the smaller the exposure time, the larger the molten layer thickness. This is consistent with the fact that the W heat conductivity drops with increasing temperature and that the conductivity time increases with armor thickness. The calculation of W vaporization depth shows that it reaches 100 μm for 100MJ/m^2 over 0.1sec deposition. The depth of vaporization increases with increasing power and decreasing the deposition time.

The evolution of the maximum temperature at the W/EUROFER interlayer in time shows (see **Fig. 3)** that for a RE energy deposition per unit area of 50MJ/m^2 and a deposition time of 0.1s only a W-armor thicker than 1.5cm could keep the interface below its creep point at all times. In the case of a VDE the maximum EUROFER temperature remains all time above the creep point f0or armor thickness~10mm.

Conclusions

Our calculations show that in the VDE case the energy deposition of plasma particles into the W armour is surface phenomenon, whereas for the high energetic RE, it take place over a finite thickness because of the drop of the non-elastic cross-sections at higher energies, carried by RE

For RE deposition energies $\geq 50 MJ/m^2$ and deposition times $\leq 0.1s$, the minimum armor thickness required to prevent EUROFER from creep or thermal stresses is $\geq 1.4cm$. However, such thick armor layers doesn't provide quick heat transfer to the coolant (even for relatively high thermal conductivity of W) to prevent the W surface from melting. At higher RE energy deposition rates ($\geq 100 MJ/m^2$ in 0.1s), the required armor thickness to prevent creeping destruction is even larger so that the bulk of the armor layer will melt and evaporate.

The accommodation of slow VDE power requires thicker W armour to transfer the energy to the coolant over time and to maintain the maximum heat flux and temperature in the material structure to acceptable level. It is shown so far that the presence of a vaporized layer and a macroscopic molten layer is unavoidable for expected exposition times and power loads.

Although W/EUROFER bound is compatible with high neutron fluencies, the loss of creep strength at relatively low temperature represents the main drawback of EUROFER as a structural material. Therefore RE and VDE transients will pose in DEMO a major lifetime issue depending on their frequencies. Future effort is required to better understand the characteristics of transients and areas of energy deposition.

References

[1] Word D and Han W., DEMO. Results of Systems Studies for DEMO, TW6-TRP-002, DEMO/UKAEA/PROCESS5 July 2007

[2] Maisonnier D. et al., *Nucl. Fusion* **47**, (2007) 1524

[3] ITER Physics Basis, Chapter 9: ITER contributions for Demo plasma development, *Nucl. Fusion* **47** (2007) S404–S413; ITER DDD, WBS1.9, Physics Section 6.3, 1983;ITER DDD, WBS 1.6, Blanket System, G 16 DDD 2 98-06-2 W 0.5, June 1998

[4] Igitkhanov Yu., Bazylev B. and Landman I., *J. Nucl. Mat*. (2010) (in press)

[5] Sugihara M. et al., in 36th EPS Conference on Plasma Phys. Sofia, June 29 - July 3, 2009 ECA Vol.**33E**, P-4.165, (2009)

[6] Loarte A., RiccardoV.et al., "Magnetic energy flows during the current quench and termination of disruptions with runaway current plateau formation in JET and Implications for ITER", *Preprint EFDA–JET–PR(10)*, **23**, 2010

[7] Lindau R., Moslang A., *Fusion Engineering and Design* **75-79**, (2005) 989

[8] Miloshevski G., H. Wuerz " 3-D Monte Carlo Calculations of Energy Deposition of Electron into Bulk Graphite and into Inhomogeneous Carbon Plasma Shield". Wissenschaftliche Berichte FZKA, **6482**, August 2000

[9] Bazylev B. et al., *Physica Scripta*, **T128,** (2007

VI. Plasma facing material lifetime in DEMO reactor

Yu. Igitkhanov and B. Bazylev, presented on the 10th International Symposium on Fusion Nuclear Technology (ISFNT-10), 11-16 September 2011, Portland, submitted to Fusion Engineering and Design

We analyze the first wall blanket W/EUROFER configuration for DEMO under steady-state normal operation and off-normal conditions, like vertical displacements events (VDE) and runaway electrons (RE). The main issue is to find the optimal thickness of the W armor which will prevent tungsten surface from evaporation and melting and, on the other hand, will keep EUROFER below the critical thermal stresses. Under steady state operation heat transfer into the coolant must remain below the critical heat flux (CHF) to avoid the possible severe degradation of the coolant heat removal capability. From the plasma side it is particularly demanding to keep the bulk plasma contamination during the reactor long operational discharges below the fatal level. The possible damage of the FW materials due to the plasma sputtering erosion is estimated. The minimum thickness of the tungsten amour about 3mm for W/EUROFER sandwich structure will keep the maximum EUROFER temperature below the critical limit for EUROFER steel under steady-state operation and ITER like cooling conditions.

1. Introduction

The plasma material interface in DEMO will be more challenging than that in ITER, due to requirements for approximately four times higher heat flux from the plasma and approximately five times higher average duty factor [1]. The key questions to be resolved for DEMO are a limitation on the lifetime of the plasma facing functional and structural materials. For DEMO reactor under normal operation the power and particle loads on PFC is expected as: in the blanket amour (FW) power flux is about~0.5MW/m^2, the particle fluence~2 10^{21} m^{-2} and the temperature ~100-500 eV. On divertor plates the power flux is about~10-20MW/m^2, particles fluence~5 10^{21} m^{-2} and the plasma temperature~500-1000eV [2]. To operate within an acceptable power loading level on material structure a considerable amount of energy (>90%) have to be radiated [2,3]. In the case of detach or semi-detached operation, charge-exchange flux of neutral atoms on the material structure will pose the main erosion lifetime constrain for buffles. For operation with off-normal events like VDE and the RE the consequent erosion due to excessive power and particle loads on plasma facing

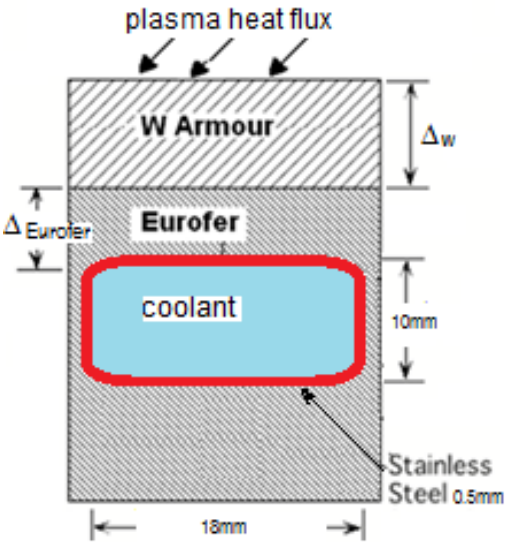

Fig. 1 Sandwich type blanket first wall module used for the Monte Carlo MEMOS computation of the plasma impact.

components (PFC) have to be expected in DEMO. The DEMO data for off-normal events can be extrapolated from ITER data based on scaling argument [1,4]. The main issue that we address below is to find the optimal thickness of the W armor which, on the one hand, will prevent EUROFER as a structural material from thermal stress destruction and, on the other hand, will transfer heat into the coolant fast enough to avoid excessive W erosion. Numerical simulations are performed with the Monte Carlo Energy Deposition code ENDEP together with the Fluid Melt Motion on Surface 3-D code MEMOS [5] in order to calculate the energy deposition into W armours of various thickness and the level of erosion caused by the RE and VDE impact. The ENDEP code calculates the armor melting, evaporation, and the heat transport in various material structures. As a model for our calculation, we have chosen a sandwich-type blanket element that resembles ITER's FW structure (see Fig.1). It consists of a coolant tube with water as a coolant embedded into the EUROFER heat sink, to which the W armor is attached**.** The reduced-activation ferritic martensitic steel EUROFER is considered in Europe as a reference structural material for a DEMO reactor. Although W/EUROFER bound is compatible with high neutron fluencies to minimize the necessary replacement of the in-vessel components and is of "low-activation" type, it has relatively low creep temperature which could be the main drawback of EUROFER as a structural material. Reinforcement by SiC fibers or oxide dispersion strengthened (ODS) steels may improve the high temperature creep resistance from 550°C up to 750°C [6]. We will take 550°C as a reference critical temperature for EUROFER in our study. The thermal analysis were performed with the code MEMOS which solves 3D thermal diffusion equation in sandwich type various materials structures. The code has also the capability to account for armour evaporation and melting and sub-cooled boiling at the coolant tubes [5].

2. Steady-state operation

Here we consider steady state DEMO operation under normal conditions. We analyze the cases, when heat fluxes into coolant (water) remains under critical heat flux (CHF) value. We assume the heat transfer into rectangular tube of 10mm x 18mm cross-section with a water temperature of 150°C. The rest parameters and limitations are similar to ITER blanket cooling system described in [7].

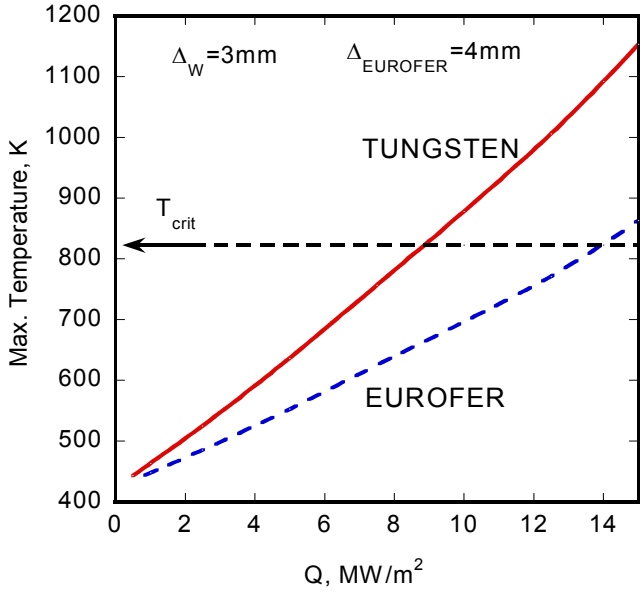

Fig. 2 W surface temperature and maximum EUROFER temperature vs net incoming heat flux Q under steady-state operation.

During normal operation the erosion of the FW and baffle surface could mainly occur due to collisions with hot neutral atoms and actions of transients. Undergoing charge–exchange collisions with ions at the separatrix or in pedestal region, energetic neutrals will deliver the plasma energy to the armour surface. Much considerable heat loads can occur due to transients. We vary Q in the range of 0.5-15MW/m^2. Fig. 2 shows the armour surface temperature and the maximum EUROFER temperature (interlayer temperature) for different incoming heat flux values Q. When Q reaches ~14 MW/m^2 the interlayer temperature exceeds the critical value $T_{crit.}$~ 550ºC and EUROFER can experience intolerable thermal distraction [6]. Such values of Q one can expect in DEMO due to transient events like ELMs or convective radial plasma losses, associated with unstable convective cells in the SOL region during steady-state operation. Calculations show that for expected incoming fluxes the W surface temperature remains below the melting point and evaporation is negligible. Calculation where performed for armour thickness Δ_W=3mm and for EUROFER thickness $\Delta_{EUROFER}$ = 4mm. Fig. 3 shows the maximum W temperature under design heat load (13.5 MW/m^2 for the limiter, and 0.5 MW/m^2 for the FW) as a function of the W armour thickness. It is shown that under steady-state operation for heat flux value ~ 13.5 MW/m^2 the surface armour temperature increases with increasing the armour thickness, whereas the W/EUROFER interlayer temperature remains almost unchanged.

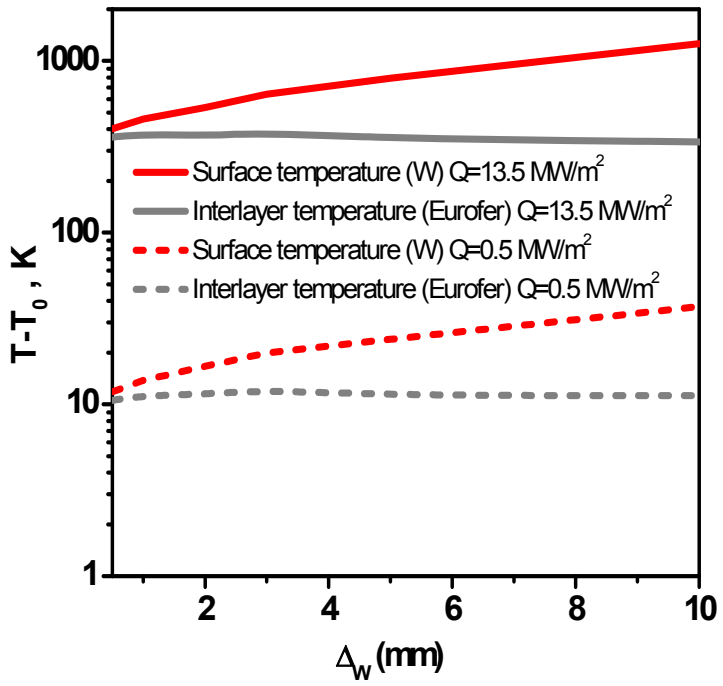

Fig.3 Maximum armour surface temperature and maximum EUROFER temperature vs armour thickness Δ_W for two cases of incoming heat fluxes Q=13.5MW/m^2 and 0.5MW/m^2; SS water cooled rectangular channel; Δ_{EROFER}= 4mm, Δ_{SS} =0.4mm, $T_{coolant}$=150 ºC. The temperature is calculated from the initial value $T_0 = T_{coolant}$.

For low power load of ~ 0.5MW/m^2 a weak dependence of the armour surface temperature and the interlayer temperature on armour thickness is shown.

Under expected steady-state operation heat loads and the thickness of W armour, surface temperature remains well below the vaporization and melting points and, as calculations also show, coolant heat flux remains below CHF thus avoiding severe degradation of the heat removal capability.

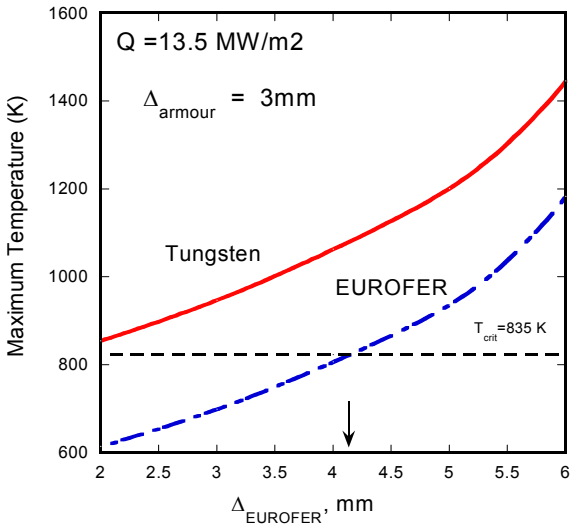

Fig. 4. Maximum temperature of W and EUROFER vs EUROFER thickness. For $\Delta_{EUROFER} < 4.3$ mm max EUROFER temperature remains below the critical value.

For incoming heat flux $\geq$ 10 MW/m^2 W temperature approaches a soft limit of ~ 900-1050K based on degradation of the structural properties and on possible crack growth through the W could also affect the EUROFER eventually. To keep the W surface temperature below 1keV, the armour thickness should be taken $\leq$ 3-4 mm. As it will be show further this thickness could be sacrificed during three years of continuous operation by taking into account only the sputtering erosion.

Variation of the surface armour temperature and interlayer temperature with EUROFER thickness is shown in Fig. 4. for given Δ_W =3mm and Q=13.5MW/m^2. Under these conditions and $\Delta_{EUROFER} \leq$ 4.5mm there will be no thermal degradation of the structural material properties. Fig. 5 shows heat loads and corresponding thickness of EUROFER when operation causes no thermal degradations (region below the curve). Arrow indicates the thickness value for the same case as in **Fig.4.**

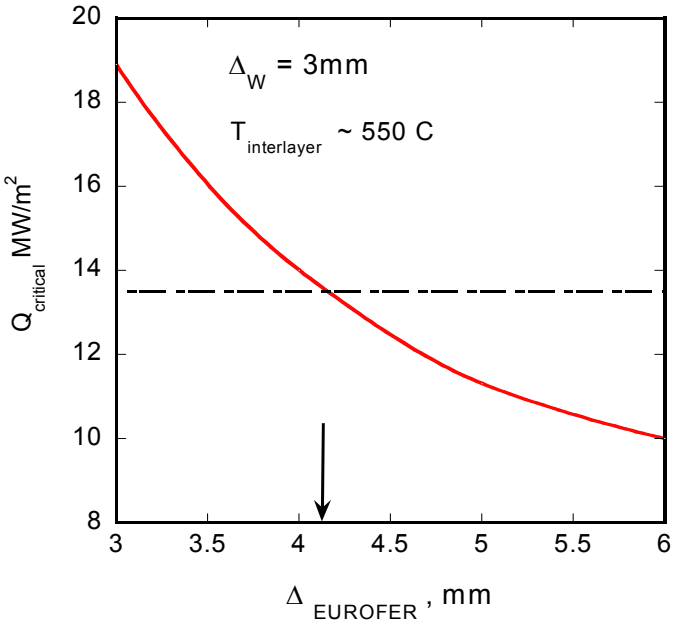

Fig. 5 Critical incident heat flux Q_{crit} vs EUROFER thickness when interlayer EUROFER temperature exceeds the critical value ~550 ºC that poses a thermal stress problem; W armour thickness Δ_w=3mm.

Calculations show that the volumetric heating associated with the neutrons is not particularly demanding for the first walls blanket design, whereas the surface heating is important in term of allowable temperatures and stresses.

3. Effect of off-normal events on the FW

The various types of off-normal conditions can occur during the DEMO operation, which represent a potential threat to the integrity and availability for a fusion reactor. Here we consider a consequence of two types of off-normal events: a loss-of control "hot" and following a disruption "cold" VDEs and RE generation that can occur during the current quench following a disruption or as a consequence of disruption mitigation by means of massive gas injection. Both VDE and RE energy deposition would affect mostly the first wall [8]. Although VDE and RE events are taken place within a short time and limited number of events in DEMO life time, the thermal stresses can accumulate and pose a potential danger of enhanced creeping in structural materials. The exact energy density on the first wall depends on the plasma parameters and assumed deposition area. The characteristics of VDE in DEMO can be assessed by extrapolate data from ITER based on the scaling arguments [8,9]. The input parameters for calculation are given in Table I [8].

events	Energy density, MJm^{-2}/deposition time, sec	Deposited area, m^2	Max. EUROFER temperature, ^oK
hot VDE	~50-100/1	24	~1610
cold VDE	~30-50/0.3-1	24	~1260
RE	100/0.05-0.3	0.8	~1500

The off-normal events will affect mostly the FW structure causing both the excessive erosion of armour and stresses in structural material. For calculation of RW impact, we have considered mono-energetic RE beams (50 and 80 MeV) and RE beams with a Gaussian energy distribution centred at some energy E_0. This energy was estimated in [8] as $E_0 \approx$ 18,5MeV.

Calculations show that in the case of VDE almost all plasma energy is converted into heat causing melting, evaporation and radiation from the W surface. In the case of RE the percentage of absorbed energy in W armour reaches ~60%, while the percentage of energy emitted as photons is ~11-15%. The RE beam generates a considerable amount of radiation upon impacting the W surface. The rest of the RE energy is reflected off by back-scattered electrons (~16-34%). The fraction of RE passing to the structural material is negligible and therefore the heat transfer from armor to EUROFER occurs though the tungsten thermal conductivity. There is no major difference between the RE and hot VDE cases in terms of EUROFER temperature, melt layer thickness and heat flux to the coolant since for W armour the heat deposition occurs very close to the surface. For the RE case, a somewhat larger part of the heat generation occurs deeper in the material in particular for the mono-energetic RE beams. Consequently, the RE energy deposition results in thicker melt layer, higher maximum EUROFER temperature and higher evaporated thicknesses than VDE energy deposition. The later occurs because of the vapor screening effect, which is less pronounced for the RE case. The total molten and evaporated thickness is ~2 mm for W, which, depending on the VDE and RE frequencies, would seriously restrict the armour lifetime.

It is shown, that in the case of a VDE and ≥10mm of armour thickness the surface temperature will exceeds the W melting temperature, for deposition times ≥1s. The RE beams with $100MJ/m^2$ /0.3s will melt the W surface at any thicknesses. For an energy deposition of $100MJ/m^2$ and relatively long exposition periods ~1s, melting could be avoided for smaller armour thicknesses <1cm.For the RE with $30MW/m^2$ and t=0.1s the temperature remains below the melting point and is independent on armour thickness. In general, the larger the incident energy, the higher the surface

temperature and it becomes independent on the W thickness for deposition periods shorter than the thermal conductivity time in tungsten.

The maximum of EUROFER temperature and maximum W melt layer as a function of W armour thickness is show in Fig.6. The EUROFER creep point limits the minimum W thickness (indicated by vertical arrows for 30MJ/m^2/0.1s and 50MJ/m^2/0.05s cases). For instance, for the RE case with moderate energy deposition density and exposure time (50MJ/m^2 and 0.05s, respectively), the W armor thickness must be ≥ 1.4cm in order to reduce the EUROFER temperature below the creep point. However, at that thickness the W armour will melt. Only in the case of 30MJ/m^2/0.1s for thickness ≤ 0.8cm the W surface doesn't melt and it is possible to avoid the potential thermal stresses. In the cases of 100MJ/m^2 the critical point is always exceeded and, moreover, EUROFER will melt for armour thickness ≤ 0.8cm. It is also shown on the right ordinate the depth of the W molten layer as a function of armor thickness.

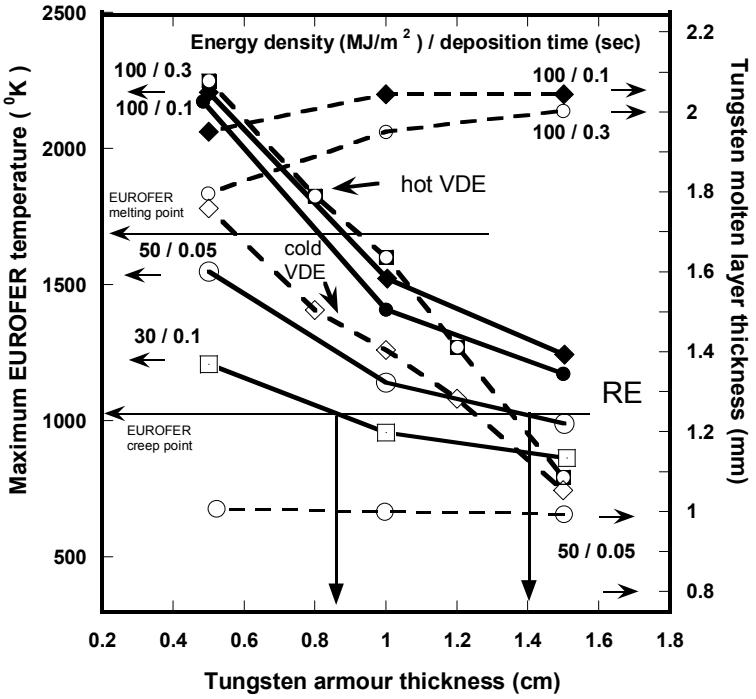

Fig. 6 The maximum EUROFER temperature and the maximum W melt layer as a function of W armour thickness in the cases of mono-energetic RE beams and VDEs. The EUROFER critical temperature (1023 Kº) limits the minimum W thickness (indicated by vertical arrows for 30 and 50MJ/m^2, τ=0.1s); the higher incident energy and the smaller the exposure time, the larger the molten layer thickness.

It is shown that the higher incident energy and the smaller the exposure time, the larger the molten layer thickness. This is consistent with the fact that the W heat conductivity drops with increasing temperature and that the conductivity time increases with armor thickness. heat generation in W armour occurs very close to the surface and there is no major difference between the RE and VDE cases in terms of EUROFER temperature melt layer thickness and heat flux to the coolant. The evaporated thickness is smaller owing to the vapor screening effect. The total melted and evaporated thickness is ~2 mm for W, which, depending on the VDE and RE frequencies, would seriously affect the armour life-time.

4. Sputter erosion in a long-range operation

The important erosion process for the FW and baffles under steady-state DEMO operation is expected to be physical sputtering, since the W surface temperature remains below the melting point and ignition of arcing is insufficient for life-time limitation under normal operation [10]. The

thickness, d of plasma facing elements (e.g. the FW blanket armour, limiter, etc.) sputtered during Δt operation time by incident particle fluxes Γ_j of different species j, can be expressed as [11]

$$d(t) = \Delta t \cdot \frac{A_t \cdot m_p}{\rho_t} \cdot \sum_j \langle Y_j \Gamma_j \rangle \qquad (1)$$

where A_t is the target atomic mass (in amu), ρ_t is the target material density, $Y_j(E,\theta)$ is the sputtering yield of particle j with energy E and angle of incidence θ and Γ_j, is the flux of particles j. The brackets in (1) represent an average over the angular and energy distribution of incident particles. Thus, the precise determination of the erosion rate needs the correct form of the energy distribution function of the incident particles and the sputtering yield $Y_j(E,\theta)$. Here we present the results of erosion rate calculation taking into account deviation the distribution function at the divertor plates from Maxwellian due to the sheath acceleration and the angular dependence of the sputtering yield.

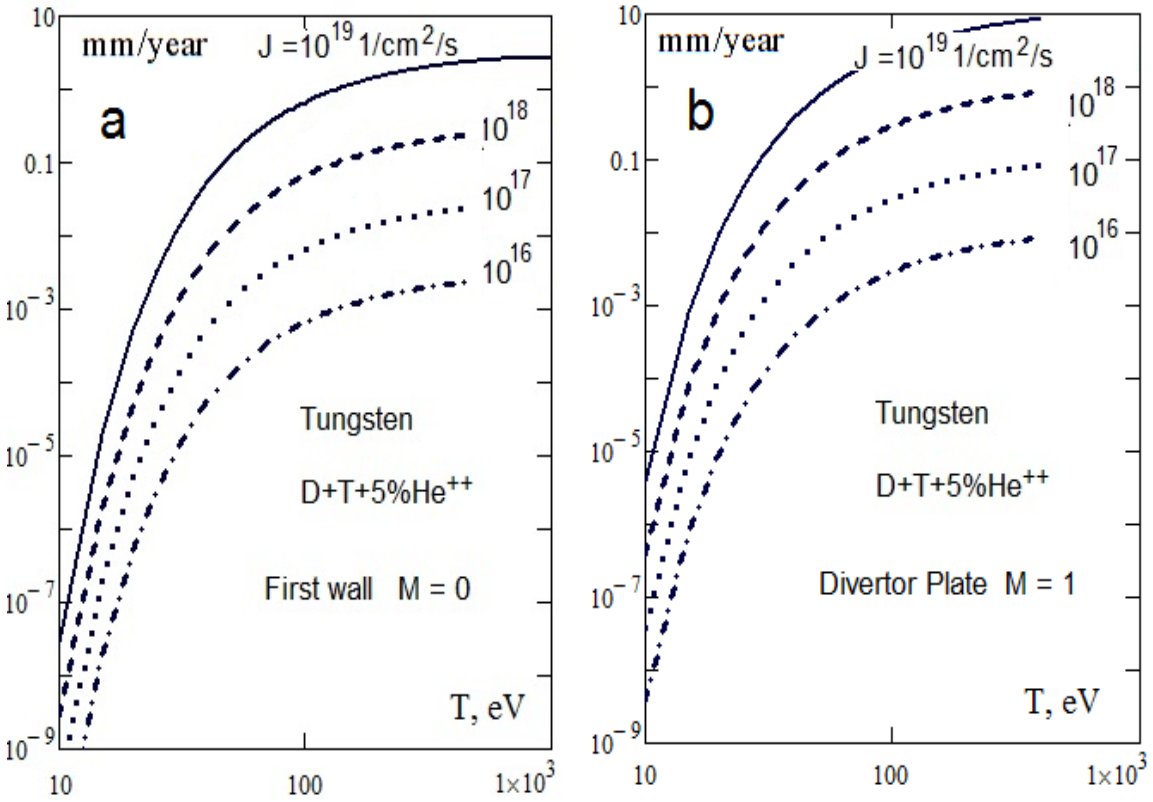

Fig. 7. The thickness of W armour (a) and divertor plate (b) sputtered during one year of continues operation by various particle fluxes of D+T+5%He of incident ions J ($cm^{-1}sec^{-1}$).

Following [11] the twice averaged sputtering yield, defined as the yield averaged over the distribution of energy and angle of incidence of the projectiles, is given by

$$\overline{Y_j}\left(\frac{atom}{ion}\right) = S_0 \int_0^1 \int_{\varepsilon^*}^{\infty} \exp\left(-\frac{\varepsilon}{\beta}(1-t^2)\right) \times \exp\left[-\left(\sqrt{\frac{\varepsilon}{\beta}t^2 - \delta} - M_0\right)^2\right] \cdot tS(\varepsilon,t) \cdot \varepsilon d\varepsilon \qquad (2)$$

where

$$S_0 = \frac{2E_{Th}^2}{T_i^2 F(M_0)}, \quad t \equiv \cos\theta, \quad \varepsilon = E/E_{Th} \quad \varepsilon^* = \max(1,\delta);$$

$$\beta = T_i / E_{Th}, \quad \delta = Z_j e\varphi_0 / T_i$$

M_0 is the Mach number of incoming particle flux (which must be taken to one at the divertor plate according to Bohm condition and to zero at the FW), $S(\varepsilon, t)$ represents, the sputtering yield for a certain energy and angle of incidence of the particles. This dependence can be described by the

revised Bohdansky formula [12] for the energy dependence and the Yamamura formula [13] for the angular dependence. Using these formulas, the erosion rate of W armour sputtered during one year of continues operation by various particle fluxes of D+T+5%He^{++} incident ions is shown in Fig.7a for the FW and in Fig. 7b for divertor all-W plate. Stronger erosion of divertor plates compare with the FW erosion is due to the acceleration of incoming ions in the sheath potential and strong deviation of energy distribution function from Maxwellian [11]. It is seen that at temperatures ≤ 100eV sputtering of W material is negligible. However, for neutrals, undergoing the charge-exchange collisions in the pedestal region, strong erosion can be expected for particle fluxes several orders of magnitude exceeding the expected for DEMO values: 10^{14}-10^{15}/cm^2/s. The most intensive W ions release due to charge-exchange collisions is expected from baffles. However, due to rather low level of W sputtering rates even for higher pedestal temperatures and expected particle fluxes of hydrogen isotopes and 5% of helium the impurity concentrations will remain below the fatal values for W impurities ~0.005% under steady-state operation and normal conditions. However, the sputtering with external impurity ions (not included here) could result in much stronger erosion and consequent plasma contamination. This issue requires numerical simulation by transport code.

Conclusions

Our calculations show that under steady state operation and ITER like coolant conditions the interlayer temperature is weakly dependent on the W armour thickness in the wide range of incoming heat fluxes.

The maximum W armour thickness is limited by the maximum allowable temperature of EUROFER under maximum steady-state design loads. The armour surface temperature increases with an increase of the armour thickness and for reference case of ~3mm remains well below the tungsten melting point.

Both temperatures of the W surface and the EUROFER interlayer are increasing with an increase of incoming heat flux. For reference conditions (Δ_W~3mm, $\Delta_{EUROFER}$ ~ 4mm) the maximum heat flux which does not causes intolerable thermal stresses in structural material is about ~13.5MW/m^2.

Calculations show that for envisaged in DEMO conditions [2] (particle fluxes and boundary temperatures) the total sputtering erosion of W armour by the charge-exchange DT neutrals could reach ~1mm during one year of steady-state operation.

Our estimations of erosion by incoming ions show that it is important to take into account the acceleration of ions in the sheath potential at the divertor plates.

In the case of off-normal operation calculations show that in the ‘hot’ VDE case the energy deposition into the W armour is very shallow (~nm) and causes surface melting and evaporation. The accommodation of slow VDE power requires thicker W armour to maintain the maximum heat flux and temperature in the material structure to acceptable level. It is shown that the presence of a vaporized layer and a macroscopic molten layer is unavoidable for expected exposition times and power loads. The RE deposit their energy deeper into armour and for energies ≥ 50MJ/m^2 and deposition times ≤ 0.1s, the minimum armor thickness required to prevent EUROFER from thermal distraction is ≥1.4cm.However, this size of layers doesn’t prevent the W surface from melting. At higher RE energy deposition rates (≥100MJ/m^2 in 0.1s), the required armor thickness to prevent creeping destruction is even larger so that the bulk of the armor layer will melt and evaporate.

Although W/EUROFER bound is compatible with high neutron fluencies, the loss of creep strength at relatively low temperature represents the main drawback of EUROFER as a structural material. Therefore RE and VDE transients will pose a major lifetime issue in DEMO depending on their frequencies.

References

[1] ITER Physics Basis, Chapter 9: ITER contributions for Demo plasma development, *Nucl. Fusion* 47, (2007) S404; ITER DDD, WBS1.9, Physics Section 6.3, 1983;

[2] D Word and W Han., DEMO. Results of Systems Studies for DEMO, TW6-TRP-002, DEMO/UKAEA/PROCESS5 July 2007

[3] D Maisonnier et al., *Nucl. Fusion* 47, (2007) 1524

[4] Yu Igitkhanov, B Bazylev, Effect of Off-Normal Events on Reactor First Wall, in Physica Scripta T, 2011 (in press)

[5] B Bazylev et al., *Physica Scripta*, T128**,** (2007) 229 ; B. Bazylev, Yu. Igitkhanov, I. Landman, et.al., 14th ICFRM, Sapporo Japan, will be published in *J. Nucl. Mat*. (2011)

[6] R Linday, A Moslang, *Fusion Engineering and Design* 75-79, (2005) 989

[7] ITER DDD, WBS 1.6, Blanket System, G 16 DDD 2 98-06-2 W 0.5, June 1998; A. Raffray et al., in: *Proceedings of the 12th Symposium on Fusion Technology*, Marseille,7-11 September, 1998

[8] Yu. Igitkhanov, B. Bazylev *Fusion Science and Technology*, Volume 60, Number 1, July 2011, Pages 349-353;

[9] Yu Igitkhanov, B Bazylev and Landman I., *J. Nucl. Mat*. (2010) (in press)

[10] Yu. Igitkhanov, B. Bazylev, *Journal of Modern Physics*, 2011, 2, 131-135; R. Raffray, G. Federici, Journal of Nuclear Materials 244 (1997) 85-100

[11] V. Abramov, Yu. Igitkhanov, V. Pistunovich and V. Pozharov, *J. Nucl. Mater*. 162-164 (1989) 462.

[12] W. Eckstein, C. Garcia-Rosales, J. Roth and W. Ottenberger, Max-Planck-Institut ftir Plasmaphysik Report, IPP 9/82 (1993).

[13] Y. Yamamura, Y. Itikawa and N. ltoh, Nagoya University Report, 1PPJ-AM-26 (1983)

VII. Sputtering yield for the PF components under reactor plasma edge conditions.

Yu. Igitkhanov, updated version of the work published erlier in Journal of Nuclear Materials 162-164 (1989) 462-466 (by V. Abramov, Yu. Igitkhanov, et al., Wall and Divertor Plate sputtering in tokamak reactor)

It is now recognized that the lifetime of a tokamak reactor is determined by damage of structural elements facing the plasma (e.g. the first wall and divertor plates). For this reason, it is important to obtain the most accurate estimates of erosion rates for these elements. Available experimental data applied to steady state or long pulse operation indicate that the first wall erosion rate is due mainly to charge exchange neutral sputtering, and that the erosion rate of divertor plates is determined by fuel and impurity ion sputtering (particularly self-sputtering).

1. Introduction

Here the calculations are presented for the sputtering yields averaged over energy and angular distributions of incident deuterium and tritium ions on various materials proposed for the divertor plates and first wall of a tokamak reactor (C, Al, Ti, Fe, MO, W). Modifications to the particle distribution function due to acceleration in the sheath electric field are included and the calculations are performed over the energy range characteristic of the particles in the plasma boundary. The results are restricted to the case of magnetic field lines normal to the divertor plate surface.

Calculations of the sputtering yield for first wall materials have been performed in several papers (see, e.g. ref. [30]), Assuming normal incidence, the different expressions are extrapolated to the low energy range characteristic of the plasma edge and used to calculate the divertor plate erosion rate. In general, the sputtering yields so obtained correspond to those which would be produced by particles whose are consistent with acceleration through the Debye sheath. It is easy to show that the thickness, A of structural elements sputtered during one year of continuous operation, by particle fluxes of different species j, can be expressed as

$$\Delta = \frac{5.27 \cdot 10^{-16}}{\rho} A \sum_j \left\langle S_j q_j \right\rangle \qquad (1)$$

Here Δ is in mm/year, A is the target atom mass (in amu), ρ is the target material density (g/cm3), $S_j(E,\theta)$ is the sputtering yield of particle j with energy E and angle of incidence θ and q_j, is the flux of particles j (particles cm^{-2} s^{-1}). The brackets $\langle\ \rangle$ represent an average over the angular and energy distribution of incident particles. Thus, the precise determination of the erosion rate needs the correct form of the energy distribution function of the incident particles and the sputtering yield $S_j(E,\theta)$. Although a Maxwellian distribution is commonly chosen, the distribution function of charged particles near the divertor plates may be strongly distorted. This paper presents the results of erosion rate calculations taking into account modifications of the distribution function and the angular dependence of the sputtering yield.

2.Distribution functions

Let us consider the distribution function for particles arriving at a material surface. It is clear that many effects can influence the energy distribution function near the divertor plates. In practise, it is impossible to take into account all of these effects by an exact method. For this reason we consider only the main effects which determine the difference between the near and far distribution functions in the edge plasma flow.

Far from the divertor plates, the ion distribution function can be considered a Maxwellian shifted by some velocity V_0. The longitudinal gradients in the boundary plasma, particle sources and acceleration in the presheath field determine the value of V_0, [31]. For typical boundary plasma parameters the inequality $\rho_e \le \lambda_D < \rho_i < \lambda_p$ is satisfied ($\rho_{e,i}$ is the electron (ion) Larmor radius, λ_D is the Debye length and λ_p - the mean free path of a charged particle). If λ_p, exceeds the characteristic length of the neutral atom distribution near the plate, then this neutral gas will not influence the charged particle distribution function. This condition is satisfied if the plasma density, which determines the width of the neutral atom spatial distribution exceeds or is comparable with the atom density. The effect on the distribution function of a magnetic field and of ionization of atoms may be neglected for the conditions considered here.

The ion velocity distribution at the plasma sheath interface (i.e. at a distance λ_D, from the plate) can be expressed as

$$f_0(M_0) = \frac{2j_0}{V_T^2}\frac{1}{\pi V_T^2}\exp\left[-u_{\perp 0}^2 - (u_{//0} - M_0)^2\right] \qquad (2)$$

where $j_0 = n\sqrt{T/2\pi m_i}$ is the ion flux to the plate, $u_{\perp 0} = V_\perp / V_T$, $u_{//0} = V_{//} / V_T$ are the transverse and longitudinal components of the velocity along the magnetic field normalized to the thermal velocity $V_T = \sqrt{2T_i / m_i}$ and $M_0 = V_{//} / V_{T0}$. Expression (2) represents the distribution function for collisionless ions accelerated by the presheath field so that at the entrance to the sheath their mean velocity satisfies the Bohm sheath criterion. According to this condition, the value of M_0 at the plasma-sheath interface is given by $M_0 = \sqrt{Z_j e\varphi_0 / T_i} \approx \sqrt{Z_j / 2}$ where Z_j is the charge of an ion accelerated in the presheath field, $e\varphi_0 \sim T_e / 2$.

In so far as that in this regime the distribution function is determined only by the constants of motion, near the plate the distribution function is

$$f = \iint f_0(u_{//0}, u_{\perp 0})\delta\left(u_\perp^2 - u_{\perp 0}^2\right)\delta\left(u_{//}^2 + \frac{Z_j e(\varphi - \varphi_0)}{T_i} - u_{//0}^2\right) du_{//0}^2 du_{\perp 0}^2 \qquad (3)$$

Here φ is the plasma potential far from the plate, and δ is the Dirac delta function. Taking the plate potential to be zero, the distribution function for the ions at the plate may be written as:

$$f_d = \begin{cases} \dfrac{2j_0}{V_T^4 F(M_0)}\exp\left(-u_\perp^2 - \left(\sqrt{u_{//}^2} - \dfrac{Z_j e\varphi_0}{T_i} - M_0\right)^2\right) & u_{//} > \sqrt{\dfrac{Z_j e\varphi_0}{T_i}} \\ f_d = 0 & u_{//} < \sqrt{\dfrac{Z_j e\varphi_0}{T_i}} \end{cases}, \qquad (4)$$

and $F(M_0) \equiv 2\pi\int_0^\infty f(V)dV_\perp \int_0^\infty V_{//}dV_{//} = e^{-M_0^2} + \sqrt{\pi}M_0 Erf(-M_0)$ (5)

It should be noted that in obtaining eq. (4) the ions are assumed to completely recombine on the plate and the lines of force are assumed to be oriented normally to the divertor plates. Clearly, if the angle, θ, between the normal to the plate and the line of force increases, then the value of M_0, which is proportional to $\cos\theta$ tends to zero. In the limiting case of grazing incidence ($\theta \to \pi/2$) the distribution function (4) transforms into an unshifted Maxwellian. The effect of the magnetic

field can be neglected in this case since $\rho_i > \lambda_D$. The dependence of the shift in the distribution function on the inclination angle of the line of force is connected with the fact the sheath electric field is oriented normal to the surface. The value of the component of this field along the direction of the lines of force decreases when the inclination angle increases. In reality, they are normal and tangential intersections of the lines of force with the surface because of surface roughness. The most unfavourable case, corresponding to normal incidence (θ = 0), has been taken into account in the calculations of sputtering yields which follow. The usual expression for the potential drop in the sheath is used: $e\varphi_0 \approx T_e \ln\sqrt{m_i / 2\pi m_e}$ .This expression is valid in the absence of secondary electron emission and if the inequality $\sum_k n_{Z_k} Z_k << n_i$ is satisfied, (n_i is the plasma ion density and n_z, is the density of impurity ions in ionization state Z_k ,). From eq. (4) we note that in general there is a large difference between the distribution of ions arriving at the plate and a simple Maxwellian. For the distribution function of neutrals near the plate, we assume the ion distribution function of eq. (2). This assumption is based on the fast relaxation (over a time of order the collision time) of the distribution function of cold atoms leaving the plate surface to the ion distribution function near the plate. We assume further that the distribution function of the atoms arriving at the first wall is also Maxwellian.

3.Energy dependence of the sputtering yield

We now turn to the energy dependence of the sputtering yield for the case of normal incidence. The exact solution of the sputtering yield problem for the low energy range $E < 1keV$ has not obtained yet. For this reason, we must use empirical relations that agree well with the available (scarce) experimental data. The following expression for the sputtering yield is proposed in [32-34]:

$$S_1(E,0) = \frac{C}{U_0} Z_1^{3/4}(Z_2 - 1.8)^2 \left(\frac{M_1 - 0.8}{M_2}\right)^{3/2} \cdot \frac{(E - E_{TH})}{\left(E - E_{TH} + 50 Z_1^{3/4} Z_2^{3/4}\right)^2} \qquad (6)$$

where $C = 2 \cdot 10^3$ for hydrogen atoms (ions) and $C = 400$ for other projectiles. U , is the binding energy of the surface atoms (sublimation energy) in eV , Z_1, Z_2, M_1, M_2 are the atomic numbers and masses (in amu) of the target and projectile respectively, $\boldsymbol{E}$ is the projectile energy (eV) and E_{TH} **,** is the threshold energy given by the expression (7):

$$E_{TH} = \frac{(4M_1 + M_2)^2}{4M_1 M_2} \qquad (7)$$

From equation (6) we see that $S_1 \sim 1/E_1$ for large E but the experimental data agree fairly well with the law $S \sim \ln E / E$ [33]. The expression proposed in [34], based on the results of both theoretical and experimental investigations, and predicts just such energy dependence.
According to [34] the sputtering yield is

$$S_2(E,0) = Q\left\{3.441\sqrt{\frac{E}{E_{TF}}} \ln\left(\frac{E}{E_{TF}} + 2.718\right) \cdot \left[1 - \left(\frac{E}{E_{TF}}\right)^{-2/3}\right] \cdot \left(1 - \frac{E_{TH}}{E}\right)^2\right\} \cdot F(E, E_{TH}) \qquad (8)$$

where

$$F(E, E_{TH}) = \left\{1 + 6.355\sqrt{\frac{E}{E_{TF}}} + \frac{E}{E_{TF}}\left(6.882\sqrt{\frac{E}{E_{TF}}} - 1.708\right)\right\}^{-1} \qquad (9)$$

Here, E_{TF} **,** is the energy in the centre-of-mass system for a head-on collision with the screening radius for a Thomas-Fermi potential as the closest approach and E_{TH} **,** is the threshold energy. The

parameters Q, E_{TF}, E_{TH} are given in [34] for some representative cases. Calculations show that the predictions of equation (8) are somewhat closer to the experimental data than those from equation (6). We therefore choose the former for use in our estimation of the sputtering yields at low energy.

4.Angular dependence of the sputtering yield

Several authors (see, e.g. [32]) have considered the sputtering yield dependence on the projectile angle of incidence.

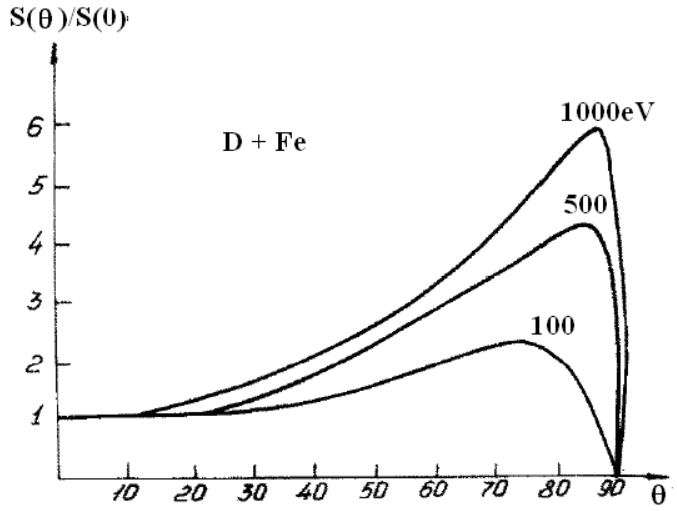

Fig. 1. The angular dependence of the sputtering yield $S(\theta)$ for varying projectile energy.

The most complete treatment is given in [34], according to which the following approximation may be used:

$$S(\theta) = \frac{1}{\cos^{f}\theta} \exp\left\{ - f \cos\theta_{opt} \cdot \left(\frac{1}{\cos\theta} - 1 \right) \right\} \qquad (9)$$

The parameters f and θ_{opt}, have been determined both from available experimental data and numerical calculations. f is independent of projectile energy for the case of sputtering by light ions, and θ_{opt} (in degrees) is given by the expression

$$\theta_{opt} = 90^{\circ} - 57.3 \frac{\eta}{E^{1/4}} \qquad (10)$$

f and η (for $E = 1$ keV) are given in ref. [35] for H, D, T, He and various target materials. **Fig. 1** shows the function $S(\theta)$ for the combination (D +Fe). It should be noted that equation (9) and (10) predict the angular dependence of the sputtering yield well only for light ion sputtering. Their validity to the case of heavy ion sputtering is doubtful, especially if calculations of the sputtering yield averaged over an energy spectrum are required. In addition, it can be shown that the sputtering yield averaged over the energy and angular distributions of the incident particles is very sensitive to the behaviour of its components in the near threshold energy range and near $\theta = 90^{\circ}$. There is evidence that equations (9) and (10) are not valid in this case.

5.The average sputtering yield

The twice-averaged sputtering yield, which we define as the yield averaged over the distributions of energy and angle of incidence of the projectiles, is given by

$$\overline{S_j} = \frac{\int f_d S(E,\theta) V_{//} dV}{\int f_d V_{//} dV} =$$

$$= \frac{\int f_d(E,\theta) S(E,\theta)\sqrt{E}\,dE\cos\theta\cdot d(\cos\theta)}{\int f_d(E,\theta)\sqrt{E}\,dE\cos\theta\cdot d(\cos\theta)} \qquad (11)$$

This expression may be transformed to the following

$$\overline{S_j}\left(\frac{atom}{ion}\right) = S_{T_0}\int_0^1 tS(t)\int_{\varepsilon^*}^{\infty}\exp\left(-\frac{\varepsilon}{\beta}(1-t^2)\right)S(\varepsilon)\exp\left[-\left(\sqrt{\frac{\varepsilon}{\beta}t^2-\delta}-M_0\right)^2\right]\varepsilon d\varepsilon \qquad (12)$$

where

$$S_{T_0} = \frac{2E_T^2}{T_i^2 F(M_0)}, \qquad t=\cos\theta, \qquad \varepsilon^* = \max(1,\delta); \qquad \varepsilon = E/E_{TH}$$

$$\beta = T_i/E_{TH} \qquad \delta = Z_j e\varphi_0/T_i$$

In equation (12) $S(t)$ represents, the angular dependence of the sputtering yield [see eq. (9)] and $S(\varepsilon)$ the energy dependence [see eq. (9)]. We note that the dependence of $\overline{S}$ on δ (i.e. on Z_j and φ_0) is rather complex. On the one hand $\overline{S}$ evidently increases when δ increases due to an increase in the population of fast particles, but on the other hand, $\overline{S}$ must decrease if the minimum energy gained in the sheath exceeds the threshold energy so long as the integration region over ε decreases when δ increases.

6.Results and conclusions

In accordance with the above, we have calculated the twice-averaged sputtering yields for a number of target/projectile combinations. Table 1 shows the results for deuterium ion sputtering. Table 2 shows the results for the same target materials but for the case of incident tritium ions. It is interesting to note that in both cases the sputtering yield decreases as the target mass increases in this low energy range; this is valid even for mono-energetic ions.

Table I

Variation of the twice averaged sputtering yield, $\overline{S}$ for various target materials as a function of the temperature of incident deuterium ions

T (eV)	Target					
	C	Al	Ti	Fe	Mo	W
5	3.23(−3) [a]	2.2(−4)	1.75(−5)	6.8(−5)	2.8(−12)	2.63(−14)
10	1.97(−2)	5.8(−3)	1.08(−3)	2.94(−3)	3.9(−7)	3.62(−8)
50	5.85(−2)	5.1(−2)	1.8(−2)	3.95(−2)	2.6(−3)	1.53(−3)
100	5.63(−2)	6.06(−2)	2.44(−2)	5.36(−2)	6.3(−3)	4.57(−3)
500	2.9(−2)	4.45(−2)	2.32(−2)	5.4(−2)	1.1(−2)	1.07(−2)
1000	1.9(−2)	3.18(−2)	1.8(−2)	4.29(−2)	1.01(−2)	1.11(−2)

[a] Note: 3.23(−3) means 3.23×10^{-3}.

Table 2

Variation of the twice averaged sputtering yield $\overline{S}$, for various target materials as a function of the temperature of incident tritium ions T (ev)

T (eV)	Target					
	C	Al	Ti	Fe	Mo	W
5	1.82(−3) [a]	7.99(−4)	1.6(−4)	3.12(−4)	4.15(−7)	1.62(−12)
10	2.94(−2)	1.24(−2)	3.97(−3)	7.81(−3)	1.6(−4)	3.59(−7)
50	1.94(−1)	7.72(−2)	3.63(−2)	7.37(−2)	1.08(−2)	3.57(−3)
100	2.12(−2)	8.99(−2)	4.68(−2)	9.7(−2)	1.75(−2)	9.29(−3)
500	1.3(−1)	6.52(−2)	4.31(−2)	9.57(−2)	2.36(−2)	2.00(−2)
1000	8.9(−2)	4.66(−2)	3.32(−2)	7.60(−2)	2.08(−2)	2.05(−2)

[a] Note: 1.82(−3) means 1.82×10^{-3}.

These calculations enable us to estimate the relative importance of the effects of acceleration in the sheath potential, modifications of the distribution function and the angular dependence of the sputtering yield. Analysis of the results shows that variations in the sputtering yield are mainly due to the accelerating potential. So, if for example, we take into account only the angular dependence for deuterium atoms at $T = 100eV$ incident on tungsten, then the sputtering yield is increased by about a factor 3 over that for the case of normal incidence. Taking into account the sheath acceleration the yield is enhanced by a factor 35. Fig. 2 show the effect of the angular dependence on the sputtering yield. One can see that the ratio of the twice averaged yield to the energy averaged yield (for the case $\delta = 0,\ M_0 = 0$) increases as the temperature increases. This result is expected so long as the fast particle population increases as the temperature increases since, from equation (9) the yield is enhanced as grazing incidence is approached. The above leads us to the following conclusion: despite the weak dependence of the sputtering yield on the angle of incidence

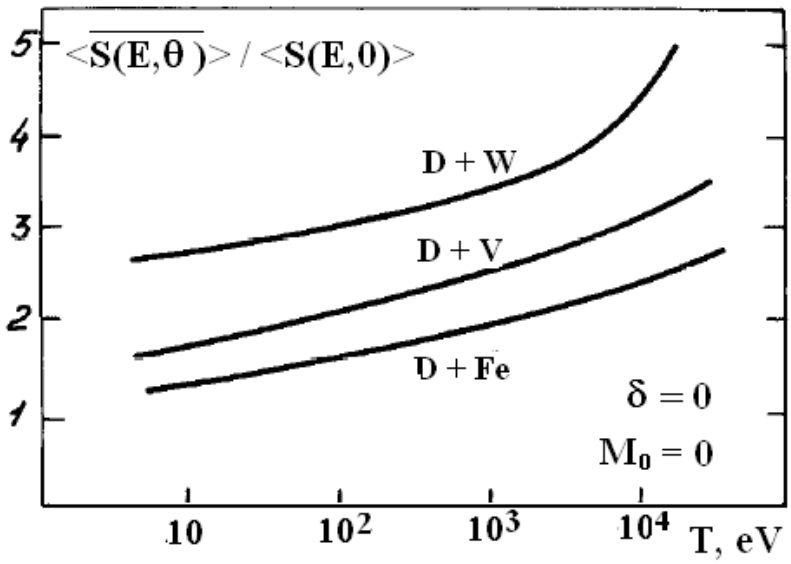

Fig. 2. Ratio of the sputtering yield averaged over energy and angle of incidence to the yield averaged over energy only (i.e. for $\theta = 0$).

in the energy range below 200 eV, it is essential to account for the angular dependence in this range if the energy averaged sputtering yield is to be accurately predicted. For example, even at $T = 10eV$, the enhancement factor is 2.5 for D-W sputtering. The calculated data also show that the distribution function distortion introduced by the sheath acceleration effect leads to sputtering yield increases of 1.5-2. This enhancement is comparable with that due to the angular effect. As an illustration, it is interesting to compare the calculated values of the yield with those obtained from equation (8) for $E = 5.5Z_jT_e$ the energy gain because of acceleration in the sheath and pre-sheath electric fields. It is easy to show that for all projectile/target combinations the values of s given in tables 1 and 2 exceed those of $S_2(3.5ZT)$ the actual enhancement factor depends on the type of projectiles' result also valid if we use expression (8) to estimate the sputtering yield for

$E = 5.5.Z_j T_e$ .The sputtering yields averaged over the distribution function and over the projectile incident angle have been obtained for some candidate target materials (C, Al, Ti, Fe, MO, W) and incident deuterium and tritium ions.

We have shown that the sputtering yield increases if the sheath potential is taken into account and that the usual estimation of the sputtering yield at energy $E = 3.5Z_j T_e$ is too low

It is found that it is essential to account for the angular distribution of incident light ions at low and high temperatures in order to calculate correctly the sputtering yield averaged over the distribution function of the incident particles [36]. Duble averaged sputtering yield of W by various elements is shown in **Fig. 3.**

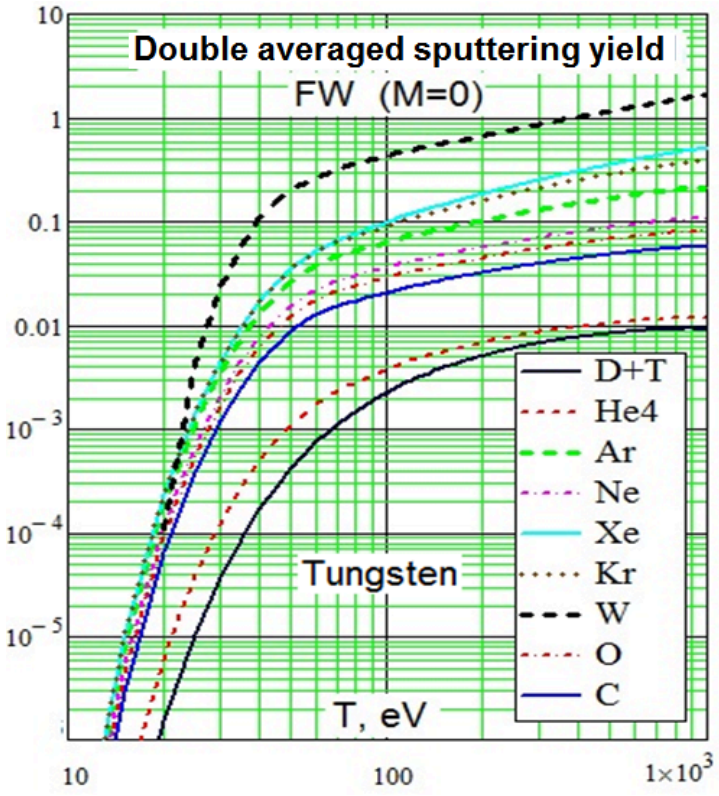

Fig. 3. The sputtering yields of W averaged over energy and angle of incidence taken for various incedent ions are shown; the ions are at the most representative ionization charge state at given temperature [8]

References

[1] Guseva M.,. Ionova E and Martynenko Yu., IAE preprint IAE- 3225 (1979).
[2] Igitkhanov Yu., Pistunovich V.and Pozharov V., IAE preprint IAE-4217/8 (1985).
[3] Smith D.et al. Proc. 9th Symp. on Engineering Problems in Fusion Research, Chicago, IL, USA, 1981.
[4] Martynenko Yu., Itogi nauki i tekniki [Science and Tech. Results] 3 (1982) 119.
[5] Bohdansky J. et al. Nucl. Fusion Special issue (1984) 61.
[6] Yamamura Y., Itikawa Y. and Itoh N., Institute of Plasma Physics, Nagoya University, Report IPPJ-AM-26 (1983).
[7] Igitkhanov J., Journal of Nuclear Materials 162-164 (1989) 462-466
[8] Post D. E., Jensen R. V., Tarter C. B., Grasberger W. H., Lokke W. A., *Atomic Data and Nuclear Data Tables* 20, 397-439 (1977).

VIII. Numerical Simulation of Tungsten Melt Layer Erosion caused by JxB force at TEXTOR

B. Bazylev, Yu. Igitkhanov, J.W. Coenen, V.Philipps, Y. Ueda

*Tungsten in form of macrobrush is foreseen as one of candidate materials for the ITER divertor. Melting of tungsten, the melt motion and melt splashing are expected to be the main mechanisms of damage determining the lifetime of plasma facing components. Experiments with long time plasma action at the target surface in the strong magnetic field demonstrated that the **JxB** force generated by thermo-emission electrons dominates in the acceleration of the melt layer and leads to a high target erosion. In the paper numerical simulations for the TEXTOR experiments on tungsten targets damage under the long time plasma heat loads are performed. Numerical simulations demonstrated a reasonable agreement with the TEXTOR experimental data on tungsten target erosion allowed the projections upon the surface damage at ITER and DEMO conditions.*

1.Introduction

Tungsten is foreseen as one of the armour materials for plasma facing components (PFCs) in the ITER divertor and dome and as the main material of DEMO. During the transients expected in tokamaks (disruptions, ELMs, and VDE) the armour will be exposed to hot plasma streams and localized impacts of runaway electrons (RE). The heat fluxes are expected to be so high that they can cause severe erosion of PFCs thereby limiting their lifetime. During the intense transients the melting, melt motion, melt splashing and surface evaporation are seen as the main mechanisms of metallic armour erosion [1-5]. In case of RE impact and long time transients (VDE) a melt layer can exist up to several seconds [6]. Experiments at the TEXTOR [7,8] with long time plasma action at the target surface in the strong magnetic field demonstrated that the **JxB** force generated by thermo-emission electrons dominates in the acceleration of the melt layer and leads to a high target erosion (up to 1 mm per event).

The expected erosion of ITER PFCs under short time transients has been properly estimated using the code MEMOS validated against plasma gun target erosion experiments in cases of short time transients, in which the **JxB** force is practically negligible [1-5]. The erosion of W target caused by JxB force in short time transients has been properly estimated using the code MEMOS validated against plasma gun target erosion experiments at QSPA Kh-50 [9]. Simulations of the long time plasma-tungsten interaction in the TEXTOR experiments [10], in which the **JxB** force generated by thermo-emission electrons produced large scale melt motion damages, showed that Richardson-Dushman expression used in the code MEMOS significantly overestimates thermo-emission and the code MEMOS has to be significantly upgraded to simulate large scale melt layer displacement observed in the TEXTOR experiments.

To simulate the TEXTOR experiments with the large time scale and large scale melt layer displacements the code MEMOS was significantly updated, in particular acquiring some additional 3D features of the experimental. New models of space-charge limited thermo-emission were also implemented. In the paper new MEMOS simulations for the TEXTOR experiments on tungsten targets damage under long time plasma heat loads with heat fluxes in the range 15 – 30 MW/m^2 on the timescale of 5-6 s in a strong magnetic field are performed, with taking into account 3D geometrical peculiarities of the experiments. The melt layer damage is calculated for single shot using 2D version of the code MEMOS. Main attention is focused on investigations of influence of evaporated material on surface heat load and melts layer erosion caused by the JxB force generated by thermo-emission electrons.

2.Erosion of tungsten target in TEXTOR experiment. Simulations vs. Experiment.

a) Main experimental results being important in the numerical simulations. Experiments have been performed by introducing a limiter into plasma at TEXTOR. Experimental conditions in more detail are described in [7,8]. After limiter introduction into the plasma the average temperature of tungsten rises up to 3500 K with an average heat flux of 10 MW/m^2. The upper part of the tungsten sample can receive up to 45 MW/m^2 for leading edges. The typical heat flux is 20 MW/m^2 for plasma load duration of 5-6 s. The peak temperatures are 4000 – 6000 K. Constant temperature level after 2 s is observed in experiments (plasma shielding caused by the evaporated tungsten?) The answer on this question found by means of numerical simulations. Typical melt layer thickness observed in experiments is about 1-1.5 mm. Typical erosion of the tungsten brushes caused by the **JxB** force generated by thermo-emission electrons in the strong magnetic field (B=2.25 T) after single shot can reach 1 mm. The thermo-emission current estimated in experiments is about several tens A/cm^2

b) Numerical simulations. The significantly upgraded code MEMOS [1] have been applied for numerical simulations of melt motion damage experiments [7,8] at the TEXTOR. The melt motion in the code MEMOS is described in the 'shallow water' approximation of the Navier-Stokes equations, with the surface tension, viscosity of molten metal, and the radiative losses from the hot surface taken into account. The plasma pressure gradients along the divertor plate, as well as the gradient of surface tension and the **JxB** force of the currents crossing the melt layer immersed in strong magnetic field, produce the melt acceleration. In case of TEXTOR experiments the current is thermo-emission current which is estimated by model model of space-charge limited thermo-emission current with modified Child-Langmuir expressions instead of Richardson-Dushman formula [11]. The model implemented into the code is fitted to be in correlation with the experimental values. A two-dimensional heat transport equation with two boundary conditions at the moving vapor-liquid- and liquid-solid interfaces describes the temperature inside the target. Temperature dependent thermo-physical data are used [12]. The model of the plasma shielding well developed, validated against experiments at plasma gun facilities, and described in details in ref. [13] have been implemented into the code MEMOS to take into account influence of the evaporated material on the surface heat loads.

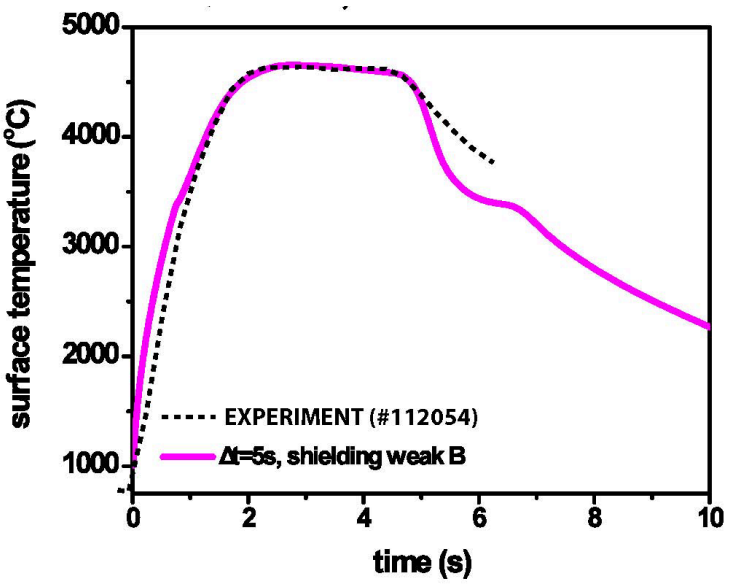

The numerical simulations of TEXTOR experiments were carried out for the tungsten castellated targets preheated up to 200°C using 2D version of the code MEMOS. The heat loads with the reference incoming energy fluxes Q = 18, 20, 22 and 30 MW/m^2, τ =5 and 6 s having rectangular space profile and time shape were applied.

Fig. 1. Dependence of tungsten surface temperature at a typical target position on time . MEMOS Simulations vs. TEXTOR Experiment. Scenario Q=22 MW/m2, τ=5 s

The plasma pressure at the target were p=200 Pa (as at TEXTOR experiments), magnetic field B=2.25 T. The brush size is taken D=1 cm with distance between brushes 0.05 cm and radius of the

brush edge rounding R_e=0.2 cm, thickness of the tungsten target is taken of 3 mm. It is also assumed that the back side of the tungsten target is cooled radiatively.

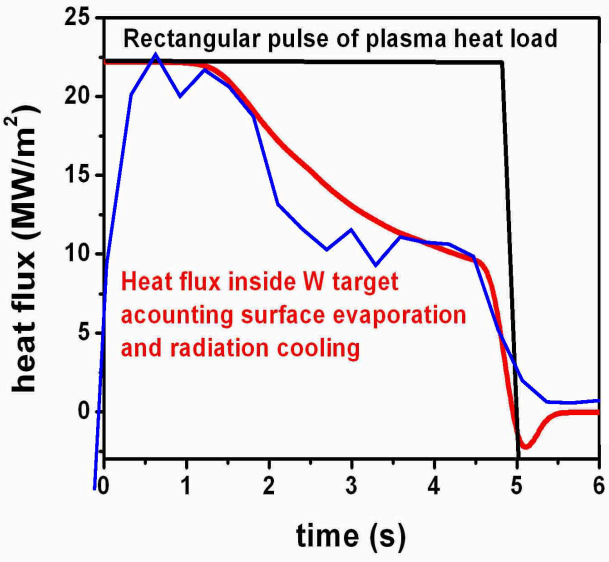

Fig. 2. Dependence of absorbed heat fluxes at a typical target position on time. MEMOS Simulations vs. TEXTOR Experiment. Incoming heat flux in MEMOS simulation has rectangular shape. Scenario Q=22 MW/m^2, τ=5 s

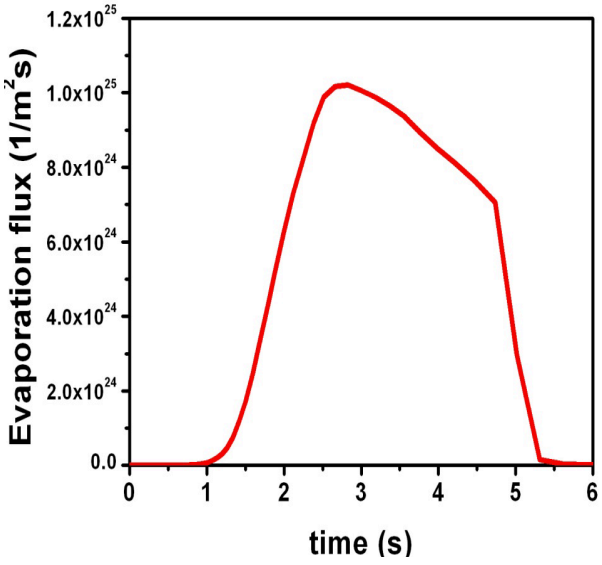

Fig. 3. Dependence of tungsten evaporation flux $F = \rho_{vap} V_{vap}$ at a typical target position on time . MEMOS Simulations. Scenario Q=22 MW/m^2, τ=5 s

Let us use scenario Q = 22 MW/m^2, τ=5 to illustrate physical processes of plasma tungsten interaction in the TEXTOR experiments. Impacting plasma with the rectangular shape in time heats the tungsten target (See Fig. 1,2): after 1 s surface temperature exceeds the melting temperature and then after approximately 2 s surface temperature becomes high enough (>4000) for starting significant evaporation. Measured and calculated absorbed energy flux during first 2 seconds are practically constant (**Fig. 2**). Tungsten evaporated from the target produces plasma shielding above

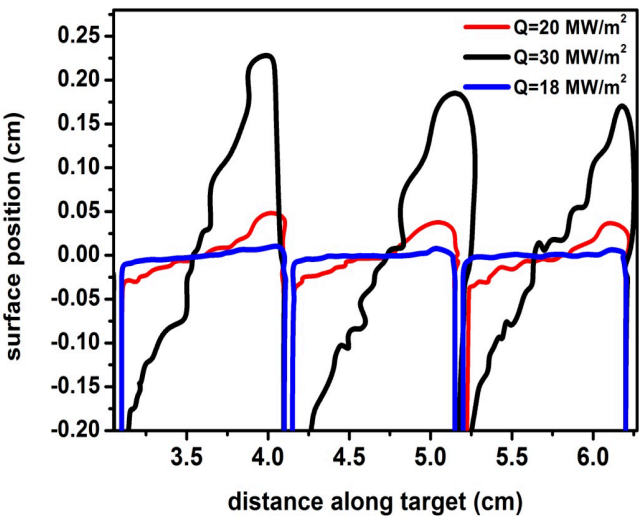

Fig. 4. Final erosion profile of macrobrush tungsten targets for different heat load scenarios. MEMOS Simulations. Scenarios: Q=18 MW/m^2, τ=6 s; Q=20 MW/m^2, τ=6 s, Q=30 MW/m^2, τ=6 s.

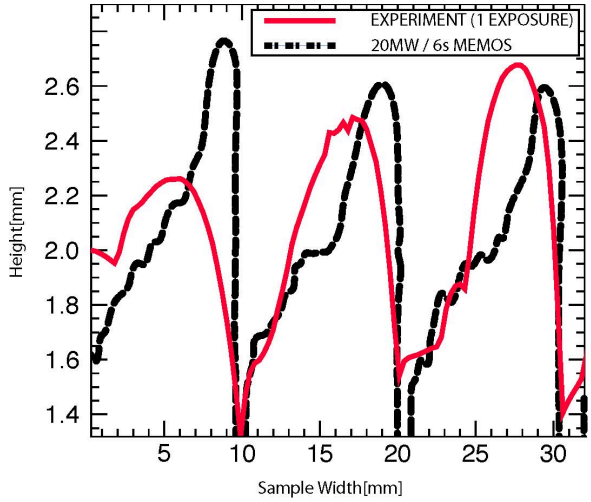

Fig. 5. Comparison of final erosion profile of macrobrush tungsten target. MEMOS Simulations vs. TEXTOR Experiment. Scenario Q=20 MW/m^2, τ=6 s

the surface leading to the noticeable surface screening from the impacting plasma: calculated and measured absorbed flux significantly drop down, and surface temperature stabilizes at T ~ 4500K (see **Fig. 1-3**). Typical calculated thickness of a melt layer is about 1.3-1.5 mm that is in a rather good agreement with the measured data. Enhance evaporation from the tungsten surface leads to significant mass loses: final thickness of evaporation is about - 200 – 400 μm in dependence of heat load.

Simulation of brush erosion caused by **JxB** force for the 3 heat load scenarios Q = 18, 20, and 30 MW/m^2, 6 s demonstrated large scale displacement of the melt layer and significant brush damage (see **Fig. 4**). Typical maximal amplitudes of the thermo-emission current calculated by new model are about 30 A/cm^2 for Q=20 MW/m^2 , 60 A/cm^2 for Q=30 MW/m^2. **JxB** force generates melt layer motion with velocities of about several tens cm/s. The final damages of the tungsten brushes (see Fig. 4) are of 0.1 mm for scenario Q = 18 MW/m^2, of 0.5 mm for scenario Q = 20MW/m^2, of 2 mm for scenario Q = 30 MW/m^2. Comparison of the final calculated brush damages with the measured ones (see **Fig. 5**) demonstrated reasonable agreement results of numerical simulations with the TEXTOR experiments.

Conclusions

To simulate large time scale and large space scale melt motion in TEXTOR experiments the code MEMOS was significantly updated, in particular accounting for some additional 3D features.
The thermo-emission current model was improved accounting for space charge limitation.
Numerical simulations carried out for the heat loads in the range 18 – 30 MW/m^2 on the timescale of 5-6 s have demonstrated a reasonable agreement with TEXTOR experimental data on time dependents of absorbed energy, surface temperatures and on tungsten target erosion.
Further numerical simulations of TEXTOR single pulse and multi-pulse experiments using 2D and 3D version of the code MEMOS will be further performed.
The code MEMOS validated against long time heat load experiments at TEXTOR allow to use the code for the projections upon the surface damage at ITER and DEMO conditions.

References

[1] B. Bazylev, H.Wuerz, J. Nucl. Mater. 307-311 (2002) 69-73.
[2] B. Bazylev et al J. Nucl. Mater. 337-339 (2005) 766-770.
[3] Bazylev B. et al, 2009, Fusion Eng. Des. **84** Iss 2 441.
[4] B. Bazylev et al. J. Nucl. Mater. 363-365 (2007) 1011-1015.
[5] B. Bazylev et al. J. Nucl. Mater. 386-388 (2009) 919-921.
[6] B. Bazylev et al. Erosion simulation of first wall beryllium armour after ITER transient heat loads and runaway electrons action, Journal of Nuclear Materials, ICFRM-14
[7] J.W. Coenen et al. Tungsten Melt Layer Motion and Splashing on Castellated Surface at the Tokamak TEXTOR. Journal of Nuclear Materials, PSI2010
[8] J.W. Coenen et al. Analysis of Tungsten Melt Layer Motion and Splashing under Tokamak Conditions at TEXTOR. Nuclear Fusion , IAEA I2010
[9] I.E. Garkusha et al. Journal of Nuclear Materials . (2007), **363-365**, , 1021
[10] G. Sergienko et al. n Journal of Nuclear Materials . (2007), **363-365**, , 96
[11] S. Takamura et al. Contrib. Plasma Phys. (2004) **44.** Nb. 1-3, 126
[12] Y.S. Touloukian (ed). Thermophysical Properties of Materials, New York, 1970.
[13] H. Wuerz et al. 2007Fusion Sceince and Technology **40,** 191

IX. Erosion simulation of first wall beryllium armour after ITER transient heat loads and runaway electrons action

B. Bazylev, Yu. Igitkhanov, I. Landman, S. Pestchanyi, A. Loarte , Journal of Nuclear Materials 417 (2011) 655–658

Beryllium is foreseen as plasma facing armour for the first wall (FW) in ITER in form of Be-clad blanket modules in macrobrush design with brush size about 8–10 cm. In ITER significant heat loads during transient events (TE) and runaway electrons impact are expected at the main chamber wall that may leads to the essential damage of the Be armour. The main mechanisms of metallic target damage remain surface melting, evaporation, and melt motion, which determine the life-time of the plasma facing components. The melt motion damages of Be macrobrush armour caused by the tangential friction force and the J x B forces are analyzed for bulk Be and different sizes of Be-brushes. The damage of the FW due to heat loads caused by runaway electrons is numerically simulated.

1.Introduction

So far, the modeling effort on damage to plasma facing components (PFCs) under transient heat loads expected in ITER (disruptions and Type I ELM loads) was concentrated upon the divertor target [1–6]. Namely, a significant effort has been recently dedicated to model the damage to the divertor W and CFC armour and only recently an estimation of Be armour damage under transients, accounting melt motion damage, was done in [7]. The transient release of energy (TE) from the confined plasma onto divertor and the first wall (FW) by multiple ELMs and disruptions can play a determining role in the life-time of these components. It is expected [8] that about 50–70% of the ELM energy releases onto divertor armour and the rest is dumped onto the FW armour. The expected transient thermal fluxes Q at PFCs of the ITER FW are: (1) Type I ELM: Q = 0.5–2 MJ/m2, s = 0.3–0.6 ms; (2) thermal quench: Q = 0.5–5 MJ/m2, s = 1–3 ms; (3) mitigated disruptions stimulated by massive noble gas injection into ITER vessel generate radiative loads at the FW Q = 0.1–2 MJ/m2 and s = 0.2–1.0 ms. In the case of the ITER transients, the material evaporated from the divertor expands into the SOL and generates radiation heating of the FW armour up to several GW/m2 during a few milliseconds that can also lead to a noticeable damage. During the current quench of the disruptions runaway electrons (RAEs) are generated in the plasma, which cause additional damage to the first wall armour. Numerical simulations were carried out using tokamak geometry and runaway impact parameters [9], which demonstrated huge melting of the metallic PFCs of up to several millimeters in depth. Simulations of energy deposition of RAEs on carbon and molybdenum PFCs were carried out in [10] for electron energy of 100 MeV in wide range of incident angles. Unfortunately, such important process as material vaporization from the armour surface was not taken into account in [9,10]. Neglecting vaporization can lead to essential overestimation of the melting depth because rather large amount of absorbed energy is consumed for the vaporization rather than f the absorbed energy propagates inside the material and is spent for melting. A beryllium macrobrush armour design (size of about 8–10 cm) is foreseen as FW plasma facing component (PFC) in ITER. During the intense TE (plasma impact and radiation loads) in ITER the surface melting, melt motion (caused by the plasma pressure gradient, the tangential friction force, and the J x B forces), melt splashing and evaporation are seen as the main mechanisms of Be-erosion. The expected erosion of the FW Be armour under TE have been numerically simulated using the melt motion code MEMOS in [7]. The aim of this work is to provide further reliable estimations of the damage to the Be armour under the mentioned Type I ELM and the runaway electron impact (using the code MEMOS [1–6]) taking into account the most important erosion processes (melting, evaporation, melt motion and melt splashing). Volumetric heat loads of runaway electrons inside the Be armour were calculated using the Monte Carlo numerical code ENDEP.

2.Numerical simulations of Be armour erosion under plasma loads

Numerical simulations of Be armour damage caused by the plasma heat loads were carried out for the bulk beryllium and beryllium macrobrush armour [7]. Influences of the tangential friction force and the J x B force (interaction of the hallo current with toroidal magnetic field) on the Be-brush target damage was investigated for the reference Type I ELM scenarios with the energy loads of 1 MJ/m2 and ELM duration of 0.5 ms. It was demonstrated that the tangential friction force generates violent melt motion with the velocities (V_{max}) exceeding 7 m/s at the bulk target, of 1.2 m/s at the Be-brush target with brush size D = 1 cm, of 5.5 m/s for D = 4 cm, and of 7 m/s for D = 8 cm. Such violent melt motion leads to formation of the final roughness of 6 lmin case of the bulkBe target and of 1 lm at the brush edges for macrobrush target with D = 1 cm, and of 6 cm for D = 4 cm. Thus the final brush roughness the Be-brush target with D > 4 cm the final brush roughness becomes comparable with that of bulk Be armour. Numerical simulations for the Type I ELM scenario with the energy loads of 1.25 MJ/m^2, ELM duration of 0.5 ms and toroidal magnetic field of 5T demonstrated that the J x B force generates violent melt motion with the velocities linearly dependent on current density, reaching about 1.5 m/s for I = 0.5 kA/c m^2, about 3.5 m/s for I = 1 kA/c m^2, and about 7.5 m/s for I = 2.0 kA/c m^2 (see **Fig. 1**) Such melt motion causes formation of the roughness of about 10 lm per one ELM (see **Fig. 2**). As for ITER disruption scenarios, estimated magnitude of the halo current crossing Be surface does not exceed 0.05 kA/cm2 with duration of several ms. Simulations demonstrated that melt motion damage caused by J x B force linearly depends on current density and current duration. Thus for the disruptions decreasing the current density in comparison with above mentioned ELMs scenarios is compensated by increasing the current duration. Thus for disruptions final erosion caused by J x B force is expected to be up to ten micrometers per 1 shot. In case of disruptions additional mechanism of surface damage appears. J x B forces caused by the interaction of eddy currents induced by the flattening of the current profile during the thermal quench and the poloidal magnetic field is directed out of target and perpendicular to the surface. They cause significant splashing due to Rayleigh–Taylor (RT) instability. For the typical poloida field for ITER scenario 2 (15 MA) of 0.5 T, droplet splashing will occur for currents above the critical eddy current value of 0.004 MA/ m^2. For the variations of the poloidal field expected during the thermal quench (~10 T/s), the induced current on the surface is~0.1 MA/m^2, i.e. more than an order of magnitude larger than that needed to exceed the RT instability threshold. As a consequence, droplet splashing is also expected by this mechanism during disruptions.

3. Numerical simulations of runaway electrons energy deposition function.

The volumetric energy depositions by RAEs in the Be armour is calculated by the Monte Carlo code ENDEP. The Monte Carlo model describing propagation of relativistic particles inside materials is based mainly on the pair collisions approximation. Long distance electron–electron interactions are taken into account statistically by a multiple-scattering model. The following processes are included in the Monte Carlo model: (1) electron–electron scattering, (2) electron–electron collisions (long distance), (3) electron-nuclear scattering, (4) Bremsstrahlung, (5) Compton scattering, (6) Auger processes, (7) photo ionization and recombination, (8) electron–positron interactions, (9) electron and photon avalanche simulations. Most features of the Monte Carlo model are described in detail in [11]. Numerical simulations are carried out for the sandwich target design: 1 cm Be layer – at the top of target and 1 cm Cu layer–at the target bottom. It is assumed that incident electrons move along the toroidal magnetic field line rotating with the Larmor frequency. Thus an incident angle of the impacting electrons strongly depends on the Larmor parameters and magnetic field direction (α angle between target surface and magnetic field lines). The Larmor radius is determined by the ratio of electron kinetic energy across magnetic field and total electron kinetic energy, Etr/Ee. Simulations are carried out for $\alpha = 1.5°$ and setting Etr/Ee = 0, 0.02, 0.05, 0.1, 0.2 for the reference relativistic electron energy Ee = 15 MeV (the range of RAEs energies expected in ITER – 10–50 MeV?). For the parallel electron impact Etr/Ee = 0 impacting energy is mostly deposited near the surface (see **Fig. 3**) and more than half of impacting electrons are reflected, and only the half of impacting energy is absorbed in target (see Fig. 4). With an increase

of the ratio Etr/Ee electrons penetrate deeper and deeper and electron reflection drops down. The energy deposition functions become slopping (see **Fig. 3**), and more than 70% of the incoming energy is absorbed in the target (see **Fig. 4**) even for small ratio Etr/Ee > 0.02. Calculated energy deposition functions are used as input parameters in the code MEMOS for simulations of the Be armour damage under RAEs impact.

4. Numerical simulations of Be armour damage under RE impact.

Numerical simulations of Be armour damage caused by the RAEs action are carried out for the Be bulk armour because it was demonstrated [7] that macrobrush of large sizes behaves as bulk target. The Be target is heated by RE beam having of the Gaussian spatial profile of the energy deposition with a half-width H_w = 10 cm and an e-beam width of 5 cm. For the reference e-beam heat load Q=20 MJ/m2 with s = 0.1 s rectangular t-shape are assumed. For e-beam with ratio Etr/Ee = 0.02 the dependences of the surface damage on pulse duration τ (0.05, 0.1, and 0.2 s) and heat loads Q (10, 20, 30 MJ/m2) are investigated.

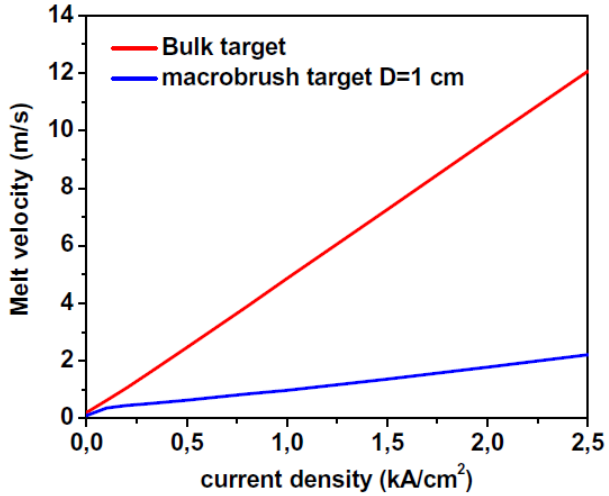

Fig. 1. The maximum of melt motion velocity vs. current for bulk and macrobrash targets. Reference Type I ELM scenario Q=1.25MJ/m^2, τ=0.5ms.

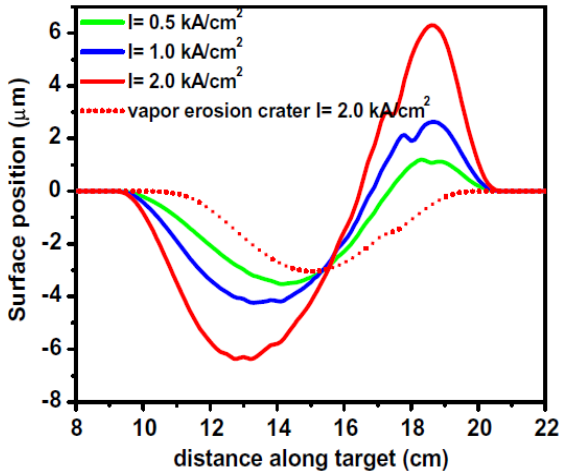

Fig. 2. Final erosion profile of bulk Be target for reference Type I ELM scenario Q=1.25MJ/m^2, τ=0.5ms. and different current densities.

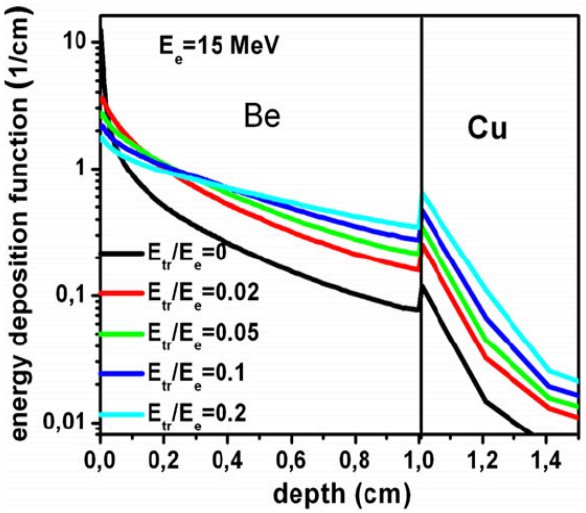

Fig. 3. RE energy deposition function inside Be/Cu armor for different scenarious of energy ratio. Reference scenario E=15 MW, field inclination angle, α=1.5°.

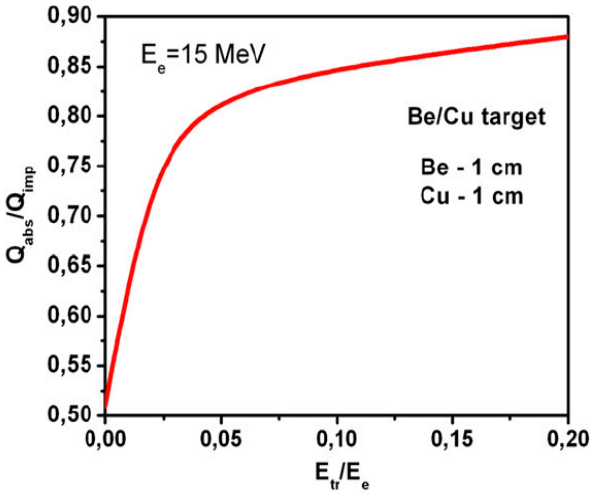

Fig. 4. Dependence of absorbed energy of RE as function of energy ratio. Reference scenario E=15 MW, field inclination angle, α=1.5°.

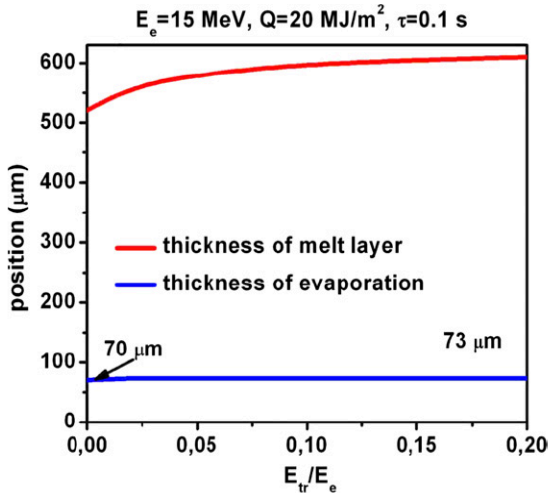

Fig. 5. Damage of Be and bulk target caused by RE beam: melt pool and evaporation depths as function of energy load. Reference scenario E=15 MeV, field inclination angle, α=1.5°, Q=20MJ/m^2, τ=0.1ms.

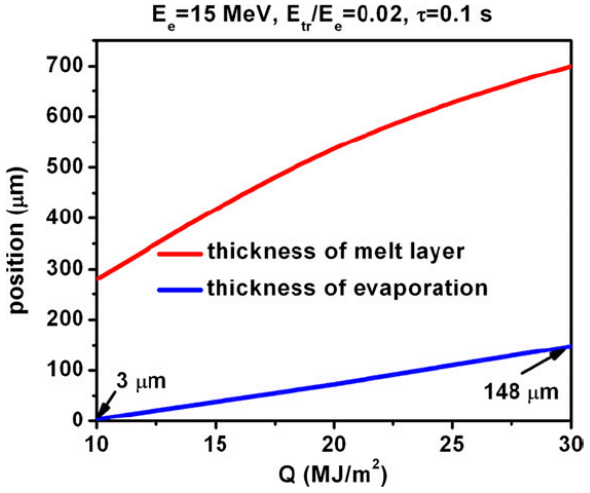

Fig. 6. Damage of Be and bulk target caused by RE beam: melt pool and evaporation depths as function of energy load. Reference scenario E=15 MeV, field inclination angle, α=1.5°, E_{tr}/E=0.02MJ/m^2, τ=0.1ms.

Numerical simulations demonstrate that impacting RE heat the targets and for the most investigated scenarios here temperature significantly exceeds the melting temperature: the maximum surface temperature reaches 2350 K at the armour surface. Due to so high temperature of the melted material huge evaporation of the Be occurs. A lot of the absorbed energy is used for evaporation. Due to this fact much less energy is spent for the melting and therefore the final depth of melt pool does not exceed 0.75 mm for all calculated scenarios (see **Figs. 5–7**). The evaporation depth practically does not depend on the ratio Etr/Ee and reaches about 73 lm for the reference scenario. However the depth of melt pool increases with increasing the ratio Etr/Ee from 520 up to 610 lm (**Fig. 5**). Magnitude of the evaporated material linearly depends on incident energy (**Fig. 6**) and rises up to 148 lm for scenario Q = 30 MJ/ m^2 with s = 0.1 s, the depth of melt pool increases also up to 720 lm. For the given incident energy Q, depth of the evaporated material as well as the melt pool depth decrease with increasing the pulse duration (**Fig.** 7). The maximum surface temperature is

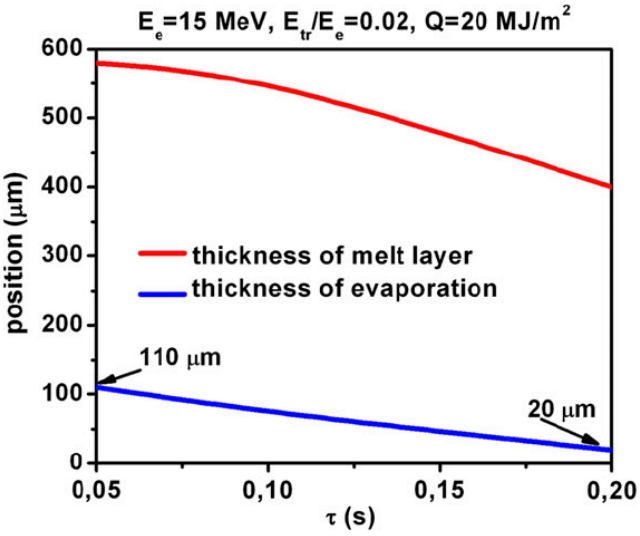

Fig. 6. Damage of Be and bulk target caused by RE beam: melt pool and evaporation depths as function of pulse duration. Reference scenario E=15 MeV, field inclination angle, α=1.5°, Q=20MJ/m^2, E_{tr}/E=0.02MJ/m^2.

linearly depends on power density. At the same energy density at increasing pulse durations the maximum temperature then decreases, that leads to decreasing melt pool dept. As it is mentioned above the melt layer is unstable. J x B forces caused by the interaction of eddy currents and the poloidal magnetic field can generate significant splashing due to RT instability. Thus all the melted material can be splashed away from the surface, because of RE impact the melting layer exists during long time (about 0.2–0.4 s) that exceeds by several orders the characteristic time of RT growth, which is about 1–10 ms. Results obtained in this paper are in contradiction with results obtained in [9] in which the depth of the melted material exceeds 2 mm for similar scenarios. So all the melted material (2 mm) will be splashed away. So large difference is caused by neglecting of vaporization in [9]. Thus evaporation of the Be armour significantlydecreases melting depth and decreases total damage caused by the RE impact.

Conclusions

Numerical simulations of Be armour damage under the runaway electrons heat loads and transient heat loads are carried out using the Monte Carlo code ENDEP and the code MEMOS. Numerical simulation demonstrated that mechanism of the surface evaporation significantly decreases melting by at least two times that is more favorable for ITER FW armour. Numerical simulations demonstrate that expected life-time of the FW armour increases significantly in comparison with previous estimations

References

[1] B. Bazylev, H. Wuerz, J. Nucl. Mater. 307–311 (2002) 69–73.
[2] B. Bazylev et al., J. Nucl. Mater. 337–339 (2005) 766–770.
[3] B. Bazylev et al., Fusion Eng. Des. 75–79 (2005) 407–411.
[4] B. Bazylev et al., Phys. Scr. T128 (2007) 229–233.
[5] B. Bazylev et al., J. Nucl. Mater. 363–365 (2007) 1011–1015.
[6] B. Bazylev et al., J. Nucl. Mater. 390–391 (2007) 810–813.
[7] B. Bazylev et al., J. Nucl. Mater. 386–388 (2009) 919–921.
[8] A. Loarte et al., in: Proceedings of the 21st IAEA Conference Chengdu, 2006, ISNB:92-0100907-0/ISSN 0074-1884 (16–21 October).
[9] G. Maddaluno et al., J. Nucl. Mater. 313–316 (2003) 651–656.
[10] T. Kanugi, Fusion Eng. Des. 23 (1994) 329–339.
[11] G. Myloshevsky, H. Würz, 3-D Monte Carlo Calculations of Energy Deposition of Electrons into Bulk Graphite and into an Inhomogeneous Carbon.

X. Modeling of Runaway Electron Beams for JET and ITER

B. Bazylev, G. Arnoux, W. Fundamenski, Yu. Igitkhanov, M. Lehnen and JET EFDA contributors, Journal of. Nucl. Mat. v.415, 1 (2011) S841-S844; presented on 19th PSI Conference. San Diego, California USA

A major concern for ITER operation in H-mode with high fusion gain is the occurrence of disruptions which can damage Plasma Facing Components (PFCs) and therefore limit their lifetime. Moreover, Runaway Electrons (RE) can be generated and further damage the first wall. Numerical simulations of consequence of RE impact at the PFCs are carried out for JET and ITER conditions. This work is focus on the benchmark of the codes (ENDEP and MEMOS) used for predictive modeling for ITER with experimental observations of RE beams in JET. Reasonable qualitative and quantitative agreements between numerical simulations and experiments at JET are demonstrated. Numerical simulation carried out for Be first wall demonstrated that mechanism of the surface evaporation significantly influence on melt layer thickness for metallic PFCs under RE impact.

1. Introduction

A major concern for ITER operation in H-mode with high fusion gain is the occurrence of disruptions which can damage plasma facing components (PFCs) and therefore limit their lifetime. It is expected [1] that during several milliseconds of the disruption more than 50 % of plasma energy is dumped onto the first wall during the so-called thermal quench (TQ). Moreover, runaway electrons (RE) can be generated and further damage the first wall. To mitigate the transient heat loads to the first wall massive gas injection (MGI) of noble gas is proposed to be used prior to disruptions. However, MGI can in the specific cases also cause the generation of runaway electrons (RE) during the MGI TQ, with following localized heat loads by RE impact. For instance, at JET, the generation of a RE beam has been observed in MGI with Ar, but not with other noble gases or gas mixtures with deuterium [2]. In case of MGI with Ar and generation of RE beam an increase the temperature of upper CFC plates up to 1500^{o}C was detected. The last experimental results on RE–FW interactions observed in MGI at JET are presented in [3]. Sparse numerical simulations of PFCs damage performed by runaway impact [4-6] demonstrated huge melting of the metallic PFCs of up to several millimeters depth. Unfortunately, such an important process as material vaporization from the armour surface was not taken into account. The neglecting of vaporization can lead to essential overestimation of the melting depth. Recent numerical simulations of beryllium armour damage by mono-energetic RE beam (with electron energy E=15 MeV) for ITER using the Monte-Carlo code ENDEP and the melt motion code MEMOS [7] have demonstrated significant PFC damages due to surface melting and evaporation. These simulations were carried out for the mono-energetic RE beams of different relativistic electron energies. However, simulations of the PFCs damage using monoenergetic RE beams inadequately describe this phenomena because the exponential distribution of RE on energy ($f(E)\sim\exp(-E/E_0)$) was observed in experiments.

In this work we focus on the benchmarking of codes, used for predictive modeling for ITER, with experimental observations of RE beams in JET. For clarification of consequences of RE impact on the JET first wall and parameters of RE beams during MGI the numerical simulations are performed, including most important peculiarities of the JET first wall, by using the codes ENDEP [7] and MEMOS [8-9]. The JET dedicated simulations were done for different RE distribution functions on energy E focusing on exponentially decaying distribution ($f(E)\sim\sim\exp(-E/E_0)$, E_0=5, 8, 10 MeV). The RE beam energy density and the ratio of transversal electron energy (E_{tr}) to longitudinal energy (E) in the magnetic field were varied in wide ranges. Detailed temperature evolution and spatial distributions over CFC tiles installed in JET during the RE impact were simulated.

The calculated temperature and cooling rate of the areas heated by RE as functions of heat load density are compared with the experimental data. The results show a good qualitative and quantitative agreement. This allowed one adequate predictive simulations of consequences of RE impact on the Be first wall and the clarification of tolerable RE beams parameters during MGI in ITER. Those simulations are done for exponentially decaying RE distribution (f(E)~~exp(-E/E_0), E_0=12,5 MeV) and the expected energy loads.

2. Numerical simulations of runaway electrons impact for JET experiments.

Simulations of impact of the runaway electrons generated during MGI experiments at JET at the CFC first wall are divided by two steps. At the first step volumetric energy deposition functions are calculated using the Monte Carlo code ENDEP. At the second step the code MEMOS are applied for the calculations of temperature distributions inside the CFC target with taking into account temperature-dependent thermo-physical properties of the CFC.

The Monte Carlo model describing propagation of relativistic particles inside materials is based mainly on the pair collisions approximation. Long distance electron-electron interactions are taken into account statistically in frame of multiple-scattering model. The following processes are included in the Monte Carlo model: 1) electron-electron scattering, 2) electron-electron collisions (long distance), 3) electron-nuclear scattering, 4) Bremsstrahlung, 5) Compton scattering, 6) Auge processes, 7) photo ionization&recombination, 8) electron-positron interactions, 9) electron&photon avalanche simulations. Most features of the Monte Carlo model are described in detail in [10]. The density effect correction; which reduces the effectiveness of the long distant collisions due to polarization of the material [11] is also taken into account.

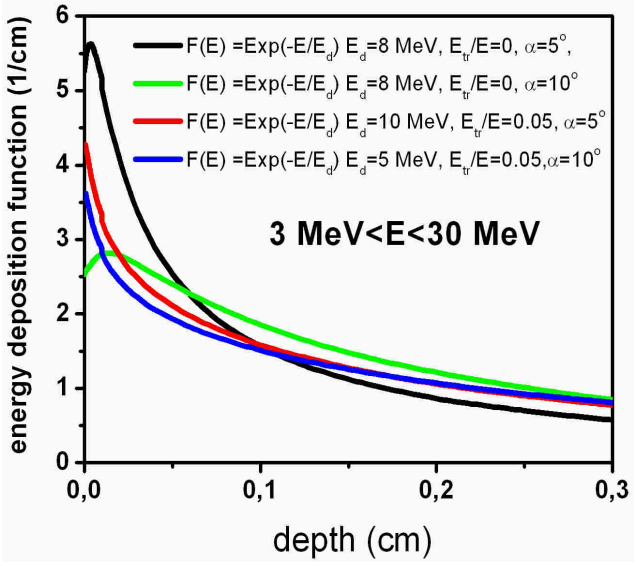

Fig. 1. Runaway electron energy deposition function inside CFC/Cu JET armor for different scenarios of energy ratio E_{tr}/E, field inclination angle, and exponential distributions of RE on energy (f(E)~exp (-E/E_0))

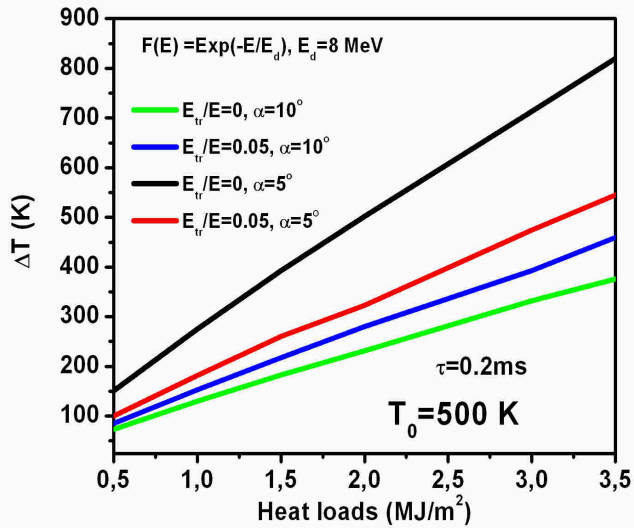

Fig. 2. Dependence of surface temperature rise at the center of RE impact spot as a function of heat loads for different scenarios of RE impact.

Numerical simulations are carried out for the sandwich target design: 2 cm CFC layer at the top of target and 1 cm Cu layer at the target bottom. It is assumed that incident electrons move along the toroidal magnetic field line rotating with the Larmor frequency. Thus an incident angle of the impacting electrons strongly depends on the Larmor parameters and magnetic field direction (α angle between target surface and magnetic field lines, B=3.5 T). The Larmor radius is determined by the ratio of electron kinetic energy across magnetic field and total electron kinetic energy. E_{tr}/E_e. Simulations are carried out for α=5 and 10 degree, set of the E_{tr}/E_e=0, 0.05, and for the exponentially decaying RE distribution with E_0=5, 8, 10 MeV (the range of RAEs energies expected in JET – 3-30 MeV).

For the parallel electron impact E_{tr}/E_e=0 with α=5° impacting energy is mostly deposited near the surface (see **Fig. 1**) and less than 20% of impacting energy are reflected with escaping primary and secondary electrons. With increasing of the ratio E_{tr}/E_e electrons penetrate deeper and deeper, electron reflection drops down, and energy deposition function becomes more slopping. The energy deposition functions is very smooth for parallel impact and rather large inclination angle α=10. More than 80% of the incoming energy is absorbed in the target for all calculated scenarios. Calculated energy deposition functions are used as input parameters in the code MEMOS for further simulations.

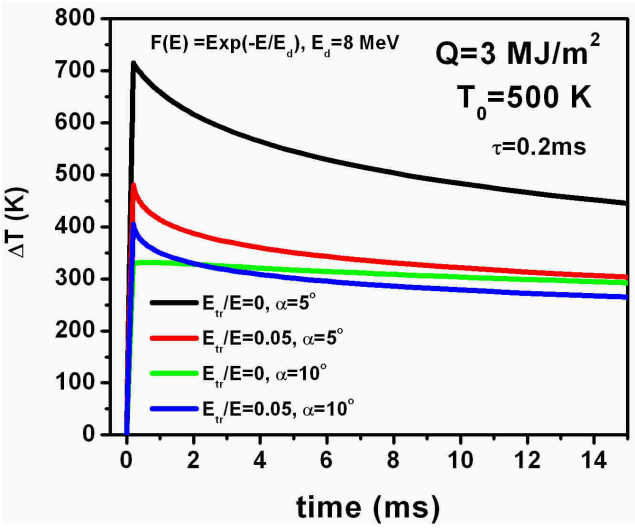

Fig. 3. Dependence of surface temperature at the center of RE impact spot as function of time for different scenarios of RE impact.

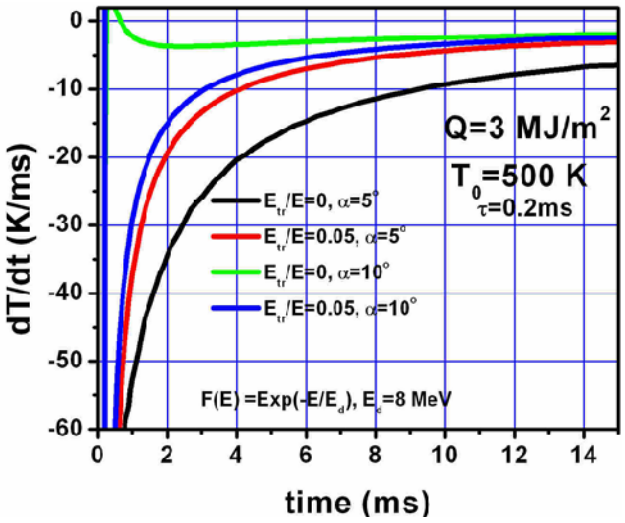

Fig. 4. Dependence of the cooling rate (dT/dt) at the center of RE impact spot as function of time for different scenarios of RE impact.

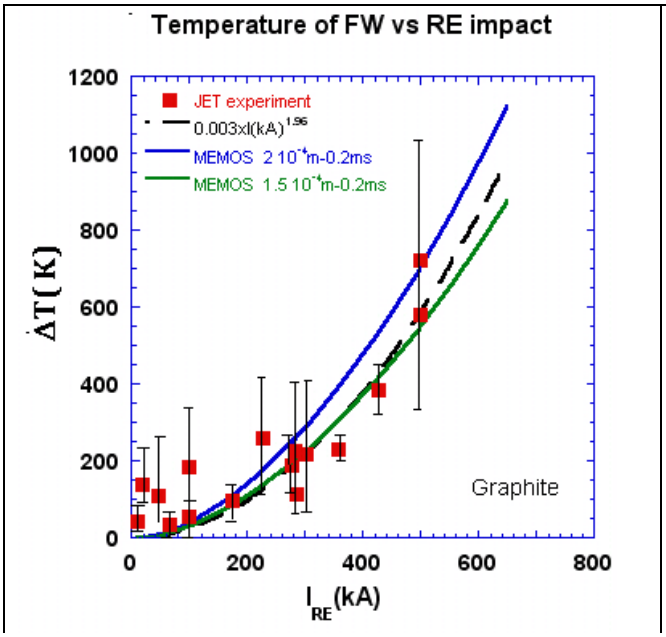

Fig. 5. Average energy increase measured on the JET FW due to RE impact as a function of the RE current - read squares; dashed curve is a fit; the blue and green curves correspond the MEMOS results, shown on **Fig. 3**, and for two values of penetration depth of 0.2.and 0.15 mm.

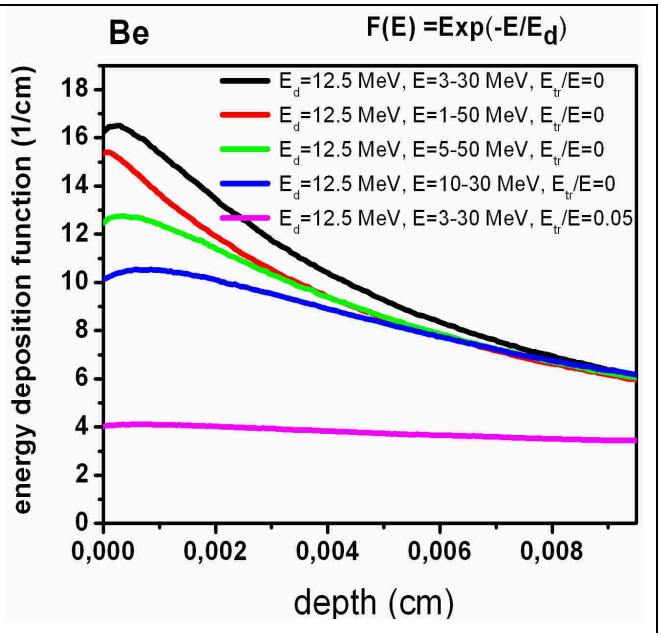

Fig. 6. Runaway electron energy deposition function inside Be/Cu ITER-like armor for different scenarios of energy ratio E_{tr}/E, field inclination angle, and exponential distributions of RE on energy ($f(E)\sim\exp(-E/E_0)$)

In the MEMOS simulations the CFC target is heated by RE beam having the Gaussian spatial profile of the energy deposition with the half-width H_w=10 cm and the e-beam width of 10 cm. The heat load ranged between Q= 0.5 MJ/m^2 and Q= 3.5 MJ/m^2 with τ = 0.2 ms, rectangular t-shape, and

initial target temperature of 500° K are assumed. Heat conductivity coefficient is approximated by the expression: $\kappa = 4.8 + 136.4/(1 + T/300)$, which gives $\kappa = 73$ Wm/K at 0°C, and $\kappa = 42$ Wm/K at 500°C.

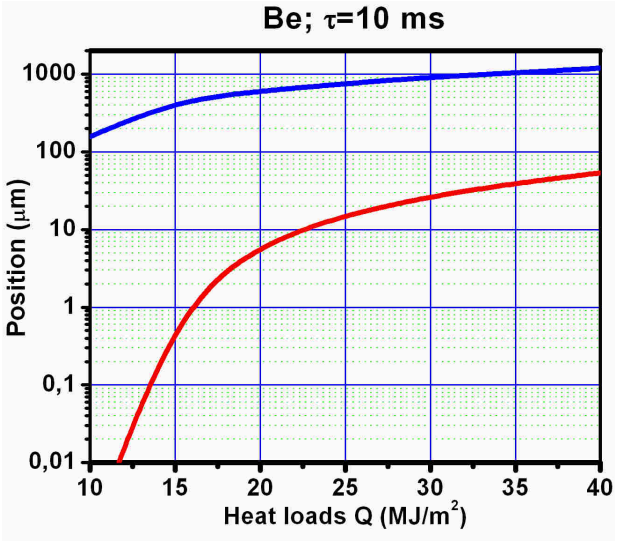

Fig. 7. Damage of Be and bulk target caused by runaway electrons beam: melt pool and evaporation depths as a function of heat loads. Reference scenario for E_0=12.5 MeV, α=1.5 degree, parallel impact.

Dependences of the maximum surface temperature versus heat load density are shown in **Fig. 2** for different scenarios of the RE impact. Parallel impact of RE with α=5 gives maximal increase of the surface temperature. Dependences of the surface temperature and the cooling rate (dT/dt) on time for the scenario with parallel impact of RE under α=5 (**Figs 3,4**) most closely correspond to the experimental results obtained at JET (**Fig. 2** [3]). The cooling rate during first 10 ms estimated from the experimental data is about 10 - 20 K/ms, which is in good agreement with simulated one for this scenario. To compare in more detail results of the simulations with the data obtained at the JET experiments the dependence of surface temperature on heat loads has to be transformed to the dependence of surface temperature on RE current. To do this transformation it is assumed, that RE electrons produce ohmic heating of CFC target of surface area about $S \sim 0.03 m^2$. Dependence obtained in experiments $\Delta T \propto AI^{1.96}$ (**Fig. 3** [3]) confirms this assumption. Assuming that the electric conductivity of CFC is obtained from Wiedemann-Franz-Law and is about $R \sim 1.8 \cdot 10^{-9}$ ohm for the RE penetration length into graphite target $\Delta \sim 0.2$ mm and $R \sim 1.3 \cdot 10^{-9}$ ohm for $\Delta \sim 0.15$ mm, one can estimate the value of ohmic current, $I(Q)$ in the target which corresponds to the heat load due to RE impact, Q MJ/m^2:

$$I(\Delta T) \approx \sqrt{\frac{Q(\Delta T) \cdot S}{\tau \cdot R}} \qquad (1)$$

Dependence of $I(\Delta T)$ is plotted in the **Fig 5** for two cases of different resistivity corresponding to different penetration lengths mentioned above. Comparison shows a reasonable qualitative and reasonable quantitative agreement with experiment (**Fig.3.** [3]).

3. Numerical simulations of Be armour damage under RAEs impact.

To estimate consequence of RE impact on Be FW under expected ITER conditions the following numerical simulations are carried out for the sandwich target design: 1 cm Be layer at the top of target and 1 cm Cu layer at the target bottom. It is assumed that incident electrons move along the toroidal magnetic field line (B=5 T) rotating with the Larmor frequency. Simulations are carried out for α=1.5 degree, set of the $E_{tr.}/E_e$=0, 0.05, and for the exponentially decaying RE distribution with E_0=12.5MeV (the range of RE energies expected in ITER – 1-50 MeV).

In the case of the parallel electron impact E_{tr}/E_e=0 impacting energy is mostly deposited near the surface (see **Fig. 6**) and less than 45% of impacting energy are reflected with escaping primary and secondary electrons. Increasing of the ratio E_{tr}/E_e electrons leads to larger penetrate depth, electron reflection drops down, and energy deposition function becomes more slopping.

Numerical simulations of the Be armour damage caused by the RE action are carried out for the Be bulk armour. The Be target is heated with by RAEs beam having the Gaussian spatial profile of the energy deposition with the half-width H_w=10 cm and the e-beam width of 5 cm. The heat load ranged between Q= 5 MJ/m^2 and Q= 40 MJ/m^2 with τ = 10 ms, rectangular t-shape and initial target temperature of 500^o K are assumed.

Numerical simulations demonstrate that impacting RE heat the targets and for the most investigated here scenarios temperature significantly exceeds the melting temperature, the maximum surface temperature exceeds 2000 K at the armour surface. Due to so high temperature of the melted material huge evaporation of the Be occurs. A lot of the absorbed energy is lost due to evaporation. Due to this fact much less energy is needed for the melting and therefore the final depth of melting pool slightly exceeds 1 mm for Q>35 MJ/m^2 scenarios (see **Fig. 7**). Melting threshold corresponds to Q> 5 MJ/m^2. Significant evaporations starts for heat loads Q>12 MJ/m^2 and evaporation depth reaches about 47 μm for heat load Q=40 MJ/m^2. Melt layer exist rather long time up to 0.2 s, that is very dangerous because of melt layer instability could cause a splashing.

4. Conclusions

Numerical simulations of consequences of RE impact at the PFCs where carried out for JET and ITER conditions using the Monte Carlo code ENDEP and the code MEMOS. This work is focused on the benchmarking of the codes, used for the predictive modeling of ITER with experimental observations of RE beams in JET. Reasonable qualitative and quantitative agreements between numerical simulations and experiments at JET are demonstrated.

Numerical simulations of Be armour damage under the runaway electron heat loads where carried out. Numerical simulation has demonstrated that mechanism of the surface evaporation significantly (by several times) decreases the melting that is more favorable for ITER FW armour.

References

[1] A. Loarte et al. Physica Scripta T128, p 222, (2007)
[2] M. Lehnen et al. J. Nucl. Mater. 390-91 (2009) 740-746.
[3] G. Arnoux et al. This conference O31.
[4] T. Kunugi Fusion Eng. Design. 23 (1993) 329-339.
[5] G. Maddaluno et al. J. Nucl. Mater. 313-316 (2003) 651-656
[6] V. Sizyuk and A. Hassanein, Nucl. Fusion **49** (2009) 095003 (9pp)
[7]B. Bazylev. Erosion Simulation of First Wall Beryllium Armour after ITER Transient Heat Loads and Runaway Electron Action, 14th ICFRM, September 6-11 2009, Sapporo Japan, 1BO3
[8] B. Bazylev et al Physica Scripta. T128 (2007) 229-233.
[9] B. Bazylev et al. J. Nucl. Mater. 390-391 (2007) 810-813.
[10] G. Myloshevsky, H Würz. 3-D Monte Carlo Calculations of Energy Deposition of Electrons into Bulk Graphite and into an Inhomogeneos Carbon Plasma Shield. Report FZKA 6482, Forschungszentrum Karlsruhe 2000.
[11] Yu. Igitkhanov; B. Bazylev, I. Landman. This conference, paper P1-99.

Resume

Our activity was mainly devoted to a) benchmarking of MEMOS and ENDEP codes with experiments from JET and TEXTOR b) to predictive simulation of PFC lifetime under reactor conditions. Since the design of the rector FW blanket for DEMO is still under disccusion, we have in our calculations considered above two models, namely 1) a sandwich type model and 2) mono-block model, made from W alloy with water cooling system.

- It was indicated an importance of the RE magnetic energy contribution in the observed increase of the temperature in a spot on the JET dump plate upon increasing the RE current. This contribution is important for DEMO and will be included in future calculations.
- The comparison with experimental results indicates the importance of the polarization effect. The density effect correction in the SP is significant for the higher RE energies and low Z materials like Be, amounting to as much as 15% of the mass collisional SP at energies of 10 MeV. In the case of high Z materials like W the density effect is smaller, because the electrons are more strongly bound and hence are less effective in polarizing the medium.
- Predictive calculation for ITER FW Be armour erosion under RE impact indicate a strong erosion. The threshold energy for Be melting is about 5MJ/m^2, whereas the RE heat deposition is expected to be almost twice as large. Under ITER conditions, however, W will not melt, since the threshold energy for W melting is about 65MJ/m^2. The W surface temperature Tmax ~ 2100 K remains much below the melting temperature (~3600K).
- Numerical simulations of Be armour damage under the runaway electrons heat loads and transient heat demonstrate that the surface evaporation significantly decreases melting by at least two times that is rather favorable for ITER FW armour. The expected life-time of the FW armour increases significantly due to vapour screening effect.
- The code MEMOS validated against long time heat load experiments at TEXTOR allow to use the code for the projections upon the surface damage at ITER and DEMO conditions. It was updated to account for some additional 3D features in order to simulate large time scale and large space scale melt motion in TEXTOR experiments.. Additionally, the thermo-emission current model was improved accounting for space charge limitation. Numerical simulations carried out for the heat loads in the range 18 – 30 MW/m^2 on the timescale of 5-6 s have demonstrated a reasonable agreement with TEXTOR experimental data on time dependents of absorbed energy, surface temperatures and on tungsten target erosion.
- The penetration of relativistic and supra-thermal electrons through the electronic shells of partly ionized impurity atoms changes the character of their scattering in multi-component plasma from Coulomb to non-Coulomb. It is found that the deviation from Coulomb cross section reduces the growth rate of primary and secondary RE. Moreover, this reduction is enhanced for increasing RE energy. Non-Coulomb collisions are crucial for slightly ionized impurities when the difference between the nuclei charge and the ion charge state is large. The growth rate of primary RE decays exponentially due to the dependence of Z_{eff} on the electron energy, whereas that of secondary RE decays according to a power law. Overall these effect could reduce the RE production during MGI in ITER and fusion reactor plasmas and thus must be taken into account in numerical simulations.
- The thermal performance of the FW blanket modules with CFC and W mono-blocks, including a water cooling system with Cu pipes, was modeled for RE impact under reactor conditions. The optimal thickness of the layer between the plasma facing surface of the FW blanket module and the coolant tube was found, which, on the one hand, does not experience strong thermal stresses and, on the other hand, transfers heat into the coolant fast enough to avoid excessive surface erosion.
- Calculations show that, although the W temperature during RE exposition exceeds the DBTT value (which is typically in the range from 300 to 600 °C), the averaged in time temperature is expected to be below DBTT. Therefore, the use of W alloy becomes mandatory.

- Calculations of the RE stopping power onto the W material show that the RE heat deposition is rather a surface like phenomenon with considerable generation of X-ray photons and secondary electrons. Reflected back X-rays may pose a severe problem for diagnostic ports and antennas. Since the X-rays strongly attenuate in bulk W, they do not reach the Cu pipes for a 10-mm thick W armour and, therefore, pose no threat for the cooling system. For the expected RE-impact duration (~0.1s) and energy (~30MW/m^2) in ITER, the W surface does not melt or evaporate.
- In the case of CFC, the heat deposition of RE is phenomenon occurring rather in the bulk, about hundred times deeper than in W for the same incident energies, in the range 1-50 MeV, and shallow incident angles 5-8º. Under these conditions, the maximum temperatures of CFC stay below sublimation and the CFC material does not experience brittle destruction. For the CFC module of 10-mm thickness, a small heat generation occurs in the Cu pipe, which could significantly increase the pipe temperature.
- Our calculations show that for RE deposition energies ≥ 50MJ/m^2 and deposition times ≤ 0.1s, the minimum armor thickness required to prevent EUROFER from creeping or thermal destruction is Δ_{min}~1.4cm. However, such thick armor layers may melt and contaminate the plasma owing to the inefficient cooling that derives from the relatively small thermal conductivity of W and, moreover, of EUROFER. The time required for re-solidification is much larger than the characteristic RT instability time that can cause the ejection of W droplets into plasma. At higher RE energy deposition rates (≥100MJ/m^2 in 0.1s), plausible in DEMO, the required armor thickness to prevent creeping destruction should become so large that the bulk of the armor layer is expected to melt and a macroscopic layer of W to evaporate. It is worth noting, that we have considering here the creep temperature~1023°K, which is true for nanostructured ferritic 12-14% ODS steels. For EUROFER 98 the creep temperature is normally ≤ 923°K (Ref.15). Therefore, the limitations found above remain valid for this structural material. In any case, the temperature gradient in 0.4cm of EUROFER layer could also cause a stress, above the allowably one.
- It is concluded that the use of W/EUROFER bound structure must be limited to regions where energy deposition from RE is very unlikely. Future effort is required to better understand the characteristics of RE and areas of energy deposition.
- Calculations show that in the VDE case the energy deposition of plasma particles into the W armour is surface phenomenon, whereas for the high energetic RE, it take place over a finite thickness because of the drop of the non-elastic cross-sections at higher energies, carried by RE
- For RE deposition energies ≥ 50MJ/m^2 and deposition times ≤ 0.1s, the minimum armor thickness required to prevent EUROFER from creep or thermal stresses is ≥1.4cm. However, such thick armor layers does not provide quick heat transfer to the coolant (even for relatively high thermal conductivity of W) to prevent the W surface from melting. At higher RE energy deposition rates (≥100MJ/m^2 in 0.1s), the required armor thickness to prevent creeping destruction is even larger so that the bulk of the armor layer will melt and evaporate.
- The accommodation of slow VDE power requires thicker W armour to transfer the energy to the coolant over time and to maintain the maximum heat flux and temperature in the material structure to acceptable level. It is has shown, so far that the presence of a vaporized layer and a macroscopic molten layer is unavoidable for expected exposition times and power loads.
- Although W/EUROFER bound is compatible with high neutron fluencies, the loss of creep strength at relatively low temperature represents the main drawback of EUROFER as a structural material. Therefore RE and VDE transients will pose in DEMO a major lifetime issue depending on their frequencies. Future effort is required for better understanding the characteristics of transients and areas of energy deposition.
- Under steady state operation and ITER like coolant conditions the interlayer temperature is weakly dependent on the W armour thickness in the wide range of incoming heat fluxes.

- The maximum W armour thickness is limited by the maximum allowable temperature of EUROFER under maximum steady-state design loads. The armour surface temperature increases with an increase of the armour thickness and for reference case of ~3mm remains well below the tungsten melting point. Both temperatures of the W surface and the EUROFER interlayer are increasing with an increase of incoming heat flux. For reference conditions (Δ_W~3mm, $\Delta_{EUROFER}$ ~ 4mm) the maximum heat flux which does not causes intolerable thermal stresses in structural material is about ~13.5MW/m^2.
- Calculations show that for envisaged in DEMO conditions [2] (particle fluxes and boundary temperatures) the total sputtering erosion of W armour by the charge-exchange DT neutrals could reach ~1mm during one year of steady-state operation.
- Our estimations of erosion by incoming ions show that it is important to take into account the acceleration of ions in the sheath potential at the divertor plates. Sputtering cross-sections and erosion of W was calculated for verity of impurity species. We have shown that the sputtering yield increases if the sheath potential is taken into account and that the usual estimation of the sputtering yield at energy $E = 3.5Z_jT_e$ is too low. It is found that it is essential to account for the angular distribution of incident light ions at low and high temperatures in order to calculate correctly the sputtering yield averaged over the distribution function of the incident particles
- In the case of off-normal operation calculations show that in the 'hot' VDE case the energy deposition into the W armour is very shallow (~nm) and causes surface melting and evaporation. The accommodation of slow VDE power requires thicker W armour to maintain the maximum heat flux and temperature in the material structure to acceptable level. It is shown that the presence of a vaporized layer and a macroscopic molten layer is unavoidable for expected exposition times and power loads. The RE deposit their energy deeper into armour and for energies $\geq$ 50MJ/m^2 and deposition times $\leq$ 0.1s, the minimum armor thickness required to prevent EUROFER from thermal distraction is $\geq$1.4cm.However, this size of layers doesn't prevent the W surface from melting. At higher RE energy deposition rates ($\geq$100MJ/m^2 in 0.1s), the required armor thickness to prevent creeping destruction is even larger so that the bulk of the armor layer will melt and evaporate.

Acknowlegement
This work supported by the European Communities under the contract EFDA/05-1305 between EURATOM and Forschungzentrum Karlsruhe, was carried out within the framework of the European Fusion Development Agreement. The views and opüinions expressed herein not necessarly reflect those of the European Commission.

Appendix I Calculation of sputtering yield and erosion rate

1) The thickness, Δ of W armour eroded due to the sputtered during one year of continuous operation, by incident particle fluxes Γ_j of different species, eg. j = d+t+He4 etc., can be expressed as

$$\Delta = \frac{5.27\cdot 10^{-16}}{\rho}\cdot A\cdot \sum_j \left\langle S_j\cdot \Gamma_j \right\rangle \approx \frac{5.27\cdot 10^{-16}}{\rho}\cdot A\cdot \sum_j \Gamma_j \cdot \overline{S_j}$$

Here
Δ is in mm/year,
A is the W atom mass (in amu), A=183.84
ρ is the target material density (g/cm^3), 19.25 at r.t and 17.6 g·cm^{-3}at m.p.(3695 K)
$S_j(E,\theta)$ is the sputtering yield of particle j with energy E and angle of incidence θ and
Γ_j, is the flux of particles j (particles cm^{-2} s^{-1}).

2) After averaging the sputtering yield over velocities and angles of incident particles:

$$\overline{S_j}\left(\frac{atom}{inc.ion}\right) = S_{T_0}\int_0^1 tS(t)\int_{\varepsilon^*}^{\infty}\exp\left(-\frac{\varepsilon}{\beta}\left(1-t^2\right)\right)\cdot S(\varepsilon)\exp\left[-\left(\sqrt{\frac{\varepsilon}{\beta}t^2-\delta}-M_0\right)^2\right]\varepsilon d\varepsilon .$$

Here

$$S_{T_0} = \frac{2E_{TH}^2}{T_i^2 F(M_0)}, \qquad t=\cos\theta$$

$$\varepsilon^* = \max(1,\delta); \qquad \varepsilon = E/E_{TH}; \quad \mu = E_{TH}/E_{TF}$$

$$\beta = T_i/E_{TH} \qquad \delta = Z_j e\varphi_0/T_i;$$

$$M_0 = \sqrt{Z_j e\varphi_0/T_i} \approx \sqrt{Z_j/2}$$

Z_j is the charge of an ion accelerated in the pre-sheath field,
$e\varphi_0 \sim T_e/2$.

3) The angular dependence we choose as [5

$$S(\theta) = \frac{1}{\cos^f\theta}\exp\left\{-f\cos\theta_{opt}\cdot\left(\frac{1}{\cos\theta}-1\right)\right\}$$

$$\theta_{opt} = 90^\circ - 57.3\frac{\eta}{E^{1/4}}$$

The parameters f and η are given in ref. [6] for H, D, T, He and various target materials, including W.

4) The energy dependence we choos as:

$$S(\varepsilon) = Q\left\{3.441\sqrt{\varepsilon\mu}\ln(\varepsilon\mu+2.718)\cdot\left[1-(\varepsilon)^{-2/3}\right]\cdot\left(1-\frac{1}{\varepsilon}\right)^2\right\}\cdot F(\varepsilon)\text{, and}$$

$$F(\varepsilon) = \left\{1+6.355\sqrt{\varepsilon\mu}+\varepsilon\mu\left(6.882\sqrt{\varepsilon\mu}-1.708\right)\right\}^{-1}, \qquad \mu \equiv E_{TH}/E_{TF}$$

5) An alternative fitting formula for $S(\varepsilon)$ is given by Eckstein and Preuss, which gives generally a better description of the available yield values :

$$Y(E_0) = q\ s_{\mathrm{n}}^{\mathrm{KrC}}(\varepsilon)\frac{\left(\frac{E_0}{E_{\mathrm{th}}}-1\right)^{\mu}}{\lambda+\left(\frac{E_0}{E_{\mathrm{th}}}-1\right)^{\mu}}$$

with the nuclear stopping power for the KrC (WHB) potential

$$s_{\mathrm{n}}^{\mathrm{KrC}} = \frac{0.5\ln(1+1.2288\varepsilon)}{\varepsilon+0.1728\sqrt{\varepsilon}+0.008\varepsilon^{0.1504}},$$

the reduced energy

$$\varepsilon = E_0\frac{M_2}{M_1+M_2}\frac{a_{\mathrm{L}}}{Z_1 Z_2 \mathrm{e}^2}$$

and the *Lindhard* screening length

$$a_{\mathrm{L}} = \left(\frac{9\pi^2}{128}\right)^{1/3} a_{\mathrm{B}}\left(Z_1^{2/3}+Z_2^{2/3}\right)^{-1/2}, \quad a_{\mathrm{B}} = 0.0529177\,\mathrm{nm}$$

References

[l] M.I. Guseva, ES. Ivanova and Yu.V. Martynenko, IAE preprint IAE- 3225 (1979).
[2] Yu.L. Igitkhanov, V.I. Pistunovich and V.A. Pozharov, IAE preprint IAE-4217/8 (1985).
[3] D.L. Smith et al. Proc.9thSymp. on Engineering Problems in Fusion Research, Chicago,IL,USA, 1981.
[4] Yu.V. Martynenko, Itogi nauki i tekniki [Science and Technology Results] 3 (1982) 119.
[5] J. Bohdansky et al. Nucl. Fusion Special issue (1984) 61.
[6] Y. Yamamura, Y. Itikawa and N. Itoh, Institute of Plasma Physics, Nagoya University, Report IPPJ-AM-26 (1983).

Appendix II Efficiency of Water and Helium collant

The proper choice of coolant is important for a Fusion Power Plant. The coolants usualy considered are 1) water in different operational temperature intervals (low(~100-200°C), in Power Work Reactor range (PWR) (~280°C-320°C) and in supercritical stage (>374°C), Helium gas and liquid metals (like fluid Li or the eutectic PbLi) and Molten salts (like FLiBe or Flinabe) that usualy also accomplish the breeding function. Water allows to reach high **heat transfer coefficients,** $h \equiv q[W/m^2] / \Delta T°K$ and presents high thermal capacity and sufficiently high density that allow the transport of heat with low difference of temperatures and using relatively small volumes of coolant. Water heat capacity is under normal conditions c_p=4200 J/(kg·K). Water is, however, limited in temperatures: to avoid vapor transition the the high pressure is required for with the selected temperature level (at PWR temperature level up to 15MPa). Beyond the preasure of ~ 22MPa and temperature ~ 374°C, water exists as supercritical fluid (**see Fig. 1.II**).

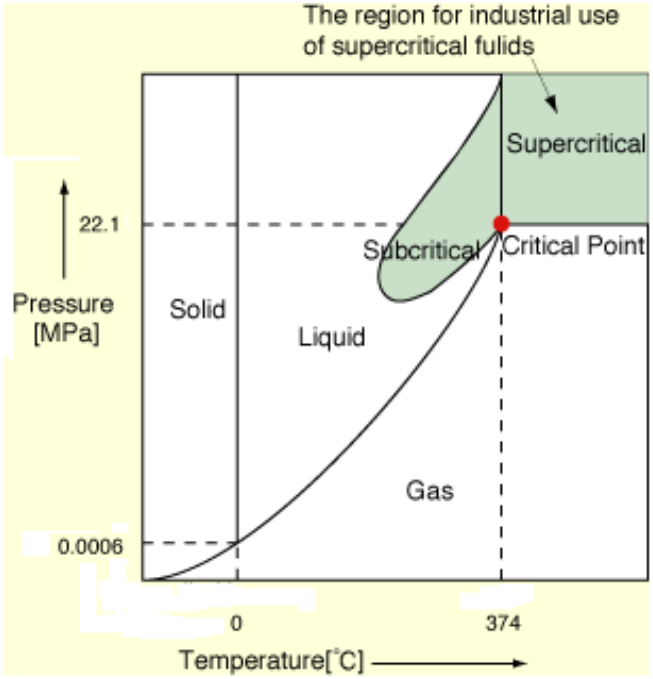

Water can be used as a coolant in divertors, blankets and the completely related manifold region.

The disadvantages are mostly in the poor compatibility with other materials used in the fusion reactor, e.g. chemical compatibility with usual breeders/multipliers like Li, PbLi and Be. Reaction with Li is violent, less dangerous with PbLi. With Be at temperature higher than~600°C the reaction with steam is exothermic, with H production; this constitutes a serious safety issue for a reactor. Water reacts at high temperature also with other metals that could be used in the reactor (like steam with tungsten [1]) causing H release, too.Water is also responsible of corrosion with steel and this is particularly enhanced if supercritical water is used.

Fig. 1.II Phase diagram for water

Other issue is the mismatch of temperature windows with structural materials used in fusion, like the ferritic, ferritic-marthensitic steels. The max temperature of water (in PWR conditions) (~280°C-320°C, is too low related to the lower range suitable for these materials. Tungsten has a body-centred cubic lattice structure and exhibits very low ductility at room temperature. In fact, the DBTT tends to increase under irradiation up to temperatures related to PWR water conditions. The ductile to-brittle transition temperature can be reduced by alloying. In any case, to exploit the exceptional coolant properties of water (feature that could be very favorable for the divertor, in which huge heat fluxes strike to the target plates) a combination with suitable structural/heat materials has to be selected. Of the few possible materials with exceptional thermal properties that maybe be used for divertor application, CuCrZr could be used only at low temperature level (if capable to withstand 30 dpa that is questionable) and W/W-alloys (questionable under irradiation) are not compatible with water. New classes of suitable structural materials are requested that can withstand heat fluxes >10MW/m^2 and neutron damage at least of 30 dpa.

Water plays an important role also in the neutronic balance of the FPP. It moderates the neutrons and contributes to the parasitical absorption of neutron. It should be considered carefully in the neutronic analysis, but possible working points exist and concept of breeding blanket have been proposed (both with PbLi and ceramic/Be).

Water has also issues with T. Permeation and isotopical exchange of T in water can cause issues to decontaminate the coolant water in the fusion reactor.

Considering all these arguments, it can be understand why only few concepts of fusion reactors with water cooling are considered. The only "under development" concept is the Japan Demo [2], a solid breeder blanket with water cooling; the conditions are at supercritical water technology, namely 25 MPa at 380°C, for the blanket and low pressure/temperature, namely 4 MPa at 200°C; in divertor. In EU a water cooled concepts, the Model A combining the Water Cooled Lithium Lead blanket with a water cooled divertor [3], was proposed at the beginning of the PPCS and successively dropped in favor of a Helium Cooled Lithium Lead; the coolant conditions were 15.5 MPa, 285-325°C in blanket, and 4.2 MPa, 140-167°C in divertor.

Helium gas has the best compatibility with all the materials used in the fusion reactor. Furthermore, it can be adapted to a wide range of temperature windows to cope with almost all the materials; in addition is suitable for very high coolant temperature increasing the efficiency of the power generation cycle. Howewer, as a gas its cooling properties are poor if compared with water. The low density can be partially compensated by using it at high pressure (usually 8-10 MPa). To achieve **higher heat transfer** required for cooling plasma surface component, high velocity should be achieved with increasing of pressure drops. A big issue is the huge pumping power necessary to circulate it in the system. This reduces the efficiency of the power conversions, partially nullifying the advantage of higher coolant temperature. Still suitable working points can be found, if it is possible to design blanket for pumping power lower than 5% (of the extracted heat) accepting also <10% in the divertor cooling.

From a neutron point of view Helium is ideal as it is does not interact with neutrons, however large void fraction can be produced in the breeding zone for helium circulation increasing the volume (and so the radial thickness) of the in-vessel components (i.e. manifolds). This void fraction makes difficult also to accomplish an effective shielding function with the in-vessel components; e.g. the pipes are transparent for neutron and special design is required (i.e. dog legs) to avoid neutron streaming. Again, this results to an increase of radial-built thickness of in-vessel components.

Extraction of tritium from He is not difficult, however the safety risk related to the T permeation in components like steam generators, can require very strict requirements on the max T partial pressure in the coolant that could penalize largely the system under an economical point of view and maybe jeopardise feasibility of necessary coolant purification systems or anti-permeation barriers.
Helium cooled divertors has been proposed mainly in order:
a) to use the same coolant as the blanket in FPP concepts with helium cooled blankets;
b) to avoid the presence of water that is not compatible with some breeders (see above);
c) to reach high temperature in order to integrate with high efficiency~17% of the fusion power collected in the divertor area in the plant power generation system.

Helium can achieve easily these plant requirements. Issues are, like for water coolant, the absence of materials suitable to achieve the structural and heat requirements of the divertor, namely high pressure coolant containment, with >10 MW/m^2 heat removal at a neutron damage of at least 30 dpa.

The big disadvantage of helium coolant is the relatively low **heat transfer coefficient** that can be achieved by conventional pipe cooling. It is necessary to develop special cooling technology based on parallel cooling, with turbulence promoters like pin/fins or surface impingement through small holes. All these technologies causes high pressure drops (i.e. large pumping power) and complicate geometries (hence complicate manufacturing). Examples of development of this component can be found in [4] and [5].

The availability of Helium remains unclear. In spite of all the issues listed here, almost the half of the worldly proposed FPP concepts makes use of Helium as coolant: in EU the Model A (HCPB blanket with an High Temperature Helium Cooled, HTHC, divertor) [6] and AB (HCLL blanket with HTHC divertor) [7] are candidate for ITER TBM and DEMO. Another EU (and US) concept,

the Dual Coolant Lithium Lead [8, 9], uses Helium for cooling the steel structures (~50% of the total cooling).

Summarize, one can say, that Water remains the best coolant, but issued in compatibility with other fusion materials, make is use in a FPP very challenging. Helium has worst cooling capability, requires large volumes and causes high power pumping; however, his compatibility with all the reactor materials and adaptability to any operational temperature makes it very suitable for fusion application.

References

[1] G.R. Smolik, K.A. McCarthy, D.A. Petti, K. Coates, Hydrogen generation from steam reaction with tungsten, Journal of Nuclear Materials 258-263 (1998) 1979-1984.
[2] S. Suzuki, K. Ezato, T. Hirose, K. Sato, H. Yoshida, M. Enoeda, M. Akiba, First wall and divertor engineering research for power plant in JAERI, Fusion Engineering and Design 81 (2006) 93-103
[3] P. Sardain, B. Michel, L. Giancarli, A. Li Puma, Y. Poitevin, J. Szczepanski, D. Maisonnier, D. Ward, U. Fischer, P. Pereslavtsev, A. Natalizio, J. Collen, A. Orden Martinez: Power plant conceptual study WCLL concept, Fusion Engineering and Design 69 (2003) 769-774.
[4] P. Norajitra, R. Giniyatulin, V. Kuznetsov, I.V. Mazul, G. Ritz, He-cooled divertor for DEMO: Status of development and HHF tests, Fusion Engineering and Design 85 (2010) 2251–2256
[5] M.S. Tillack, A.R. Raffray, X.R. Wang, S. Malang, S. Abdel-Khalik, M. Yoda, D. Youchison, Recent US activities on advanced He-cooled W-alloy divertor concepts for fusion power plants, Fusion Engineering and Design 86 (2011) 71–98
[6] S. Hermsmeyer, S. Malang, U. Fischer, S. Gordeev, Lay-out of the He-cooled solid breeder model B in the European power plant conceptual study, Fusion Engineering and Design 69 (2003) 281-287
[7] A. Li Puma, J.L. Berton, B. Brañas, L. Bühler, J. Doncel, U. Fischer, W. Farabolini, L. Giancarli, D. Maisonnier, P. Pereslavtsev, S. Raboin, J.-F. Salavy, P. Sardain, J. Szczepanski, D. Ward: Breeding blanket design and systems integration for a helium-cooled lithium–lead fusion power plant, Fusion Engineering and Design 81 (2006) 469–476
[8] P. Norajitra, L. Bühler, U. Fischer, S. Gordeev, S. Malang, G. Reimann: Conceptual design of the dual-coolant blanket in the frame of the EU power plant conceptual study, Fusion Engineering and Design 69 (2003) 669-673
[9] S. Malang, A.R. Raffray, N.B. Morley, An example pathway to a fusion power plant system based on lead–lithium breeder: Comparison of the dual-coolant lead–lithium (DCLL) blanket with the helium-cooled lead–lithium (HCLL) Fusion Engineering and Design 84 (2009) 2145–2157

ISSN 1869-9669